

Cite this: DOI: 00.0000/xxxxxxxxxx

Stable thin clathrate layers

Eva Pospíšilová^{a,b,*}

Received Date

Accepted Date

DOI: 00.0000/xxxxxxxxxx

We explore *elemental* Si, Ge and Sn free-standing slabs in diamond, clathrate and other competing structures and evaluate their stability by comparing Kohn-Sham total energies at the same atoms/area coverage ρ . We find that within 3-6 ML range (in units of diamond monolayer), the surface energy stabilizes *clathrates* against the bulk-stable diamond structure or other competitors, for all three elements. At 1.3-1.6 ML coverages, Si and Ge stable layers are adatomic decorations of the puckered honeycomb lattice, forming a dumbbell-decorated pattern with rectangular unit cell. Analogical Sn layer is unstable to a web-like net of interconnected Sn_9 clusters. The zoo of stable thin-layer non-diamond structures is completed by a Sn metallic bilayer at 2.3 ML coverage.

1 Introduction

For bulk Sn, Ge and Si, cubic diamond (cF8) phase is the ground state structure (GS), lying 23, 27 and 54 meV/at. below its energetically closest sp^3 adversary – type-II clathrate – according to the basic PAW GGA DFT setup. The main question of the presented fundamental theoretical DFT study is, whether opening a surface could grant clathrates an overall energetic advantage over diamond, resulting in *stable* free-standing clathrate thin films.

The inquiry is not restricted to clathrates, but spans wide area of known sp^3 Column-XIV allotropes and thanks to long Molecular Dynamics (MD) annealing sped up by Machine Learning Force Fields (MLFF) innumerable other candidates for the stable films as well, including metallic even-layers of Sn.

Free-standing thin films minimizing per-atom-energy for the given thickness (coverage) $\rho \equiv N/S$ can be imposed by structure-neutral substrate such as amorphous or electronically-balanced oxide (ZrO_2) or graphite wafer. Further stabilization of the most stable – *elemental* – clathrate slabs could be achieved by lattice-matching substrate, e.g. via *coherent* clathrate-diamond interface¹.

In the focus here are several-ML (diamond monolayers) thick films, no longer linked to their parent bulk phases by the physical properties. As for the thinnest ones, even interaction between slab's faces comes into play, hence new – yet unexplored – features are expected.

The paper is organized as follows. In addition to the basic

DFT setup applied, the crucial aspects of energy-minimization of a thin film such as the choice of proper termination, surface reconstruction when cut from the mother bulk phase together with MD-related approaches starting from random atomic positions or from the melt are described in Section 2. Section 3 introducing known parent bulk phases for thin-film production ensues. Section 4 reveals realm of stability of clathrate films for each of the elements Sn, Ge, Si and compares the associated terminations and reconstructions of the per-atom-energy minimizing slabs. We go on to discuss the possibility of spontaneous clathrate crystallization from the melt in Section 5 and the impact of van der Waals dispersion interaction in its last Subsection 5.4. The most important outputs of our work are summarized in the final Section 6. Additional Figures and xyz-files* of all stable films are included in the Supplemental Material (SM) and are referenced as SX.Y from the main text, where integers X and Y index particular SM Section and Figure, respectively.

2 Methods & Definitions

2.1 DFT

For atomic relaxations as well as for Molecular Dynamics (MD) simulations Vienna *ab initio* Simulation Package (VASP)² implementation of the plane-wave Density Functional Theory was employed powered by the Projector Augmented-Wave potentials (PAW)³ in PW91 Generalized Gradient Approximation (GGA)⁴.

As a default setup, we used VASP “Accurate” setting and default values of energy cutoff (ENCUT), and converged energy on K-point mesh density to 1 meV/atom precision. Simulated films infinite in two dimensions were separated by at least 15 Å vacuum layers

^a Institute of Materials and Machine Mechanics, Slovak Academy of Sciences, v.v.i., Dúbravská cesta 9, Bratislava, 84513, Slovakia

^b Institute of Physics, Slovak Academy of Sciences, v.v.i., Dúbravská cesta 11, Bratislava, 84511, Slovakia

* Corresponding author at: Institute of Materials and Machine Mechanics, Slovak Academy of Sciences, v.v.i., Dúbravská cesta 9, Bratislava, 84513, Slovakia. E-mail address: e.pospisilova@savba.sk (E. Pospíšilová).

* xyz-file contains three lattice vectors whose component unit is Å (first three lines), number of atoms (4th line) and fractional coordinates of each atom followed by the atomic number and two times the order number

in the third dimension to prevent mutual interactions of the periodic copies.

In study⁵ it has been demonstrated that despite the spin-orbit coupling does have a measurable effect on the formation energy, the energy shift is nearly constant for all 2D Sn structures (55 – 59 meV/at.) and as such can be neglected. Another DFT extension, van der Waals dispersion interaction (PBE-D3 correction to DFT), is discussed in Subsection 5.4.

2.2 Ab Initio Molecular Dynamics (AIMD)

By ab initio Molecular Dynamics (AIMD) we mean long MD runs – (tens of) millions of \sim fs-steps – markedly accelerated by Machine Learning Force Fields (MLFF) as implemented in VASP.

AIMD was used within the present work on three occasions. Firstly, AIMD is the simplest way to amorphous bulk and thin films, described in Subsection 3.5, avoiding ingenious construction. Unfortunately, there is no such an automated ab initio way to clathrates, see Section 5, where an attempt has been made to recrystallize clathrate slabs from the melt, either in a free-standing slab form or as a Ge slab on an appropriate InN substrate.

The third instance was the thin-film configurational-space search. Despite the clathrate-slab notation suggested in Table 1, Subsubsection 3.3.1, several-atom-thick layers have actually no relation to *any* bulk phase: they are unique identities themselves. Long AIMD runs thus attest to the completeness of our thinnest-film enumeration, mainly specific Sn metallic even-layers rediscovered this way in Subsection 3.4. AIMD confirms that there are not any other low-energy thin-film atomic arrangements.

Namely, for the Sn, Ge and Si thinnest-film production in the range of coverages $\rho \in [0.85; 4.0]$ ML with the basic step $\Delta\rho \approx 0.5$ ML, 4×10^5 steps 5 fs each in the temperature range $T \in [300; 500]$ K were performed, leading to *no* new phases. As concerns Sn, due to the close competition of square and triangle even-layers in this temperature range and owing to the plethora of Sn phases, Subsection 3.4, we have gradually increased coverage from 2 ML to 2.5 ML via random single-atom addition to the $(23.9\text{\AA})^3$ supercell, witnessing a coexistence of the two at approximately 2.29 ML (for 137 – 138 atoms in the cell).

Extra, we have executed several Replica Exchange (RE) simulations 20-50 thousand 5 fs-step long starting from random atomic configurations with all three elements, in the temperature range from room up to the respective melting point, again, with *no* new unexpected results. These were either simulations with fixed boundary conditions (coverage) or complemented by energy cost function scaling either linearly with surface (surface energy) or quadratically with the departure of a *coverage* from its initial value, emulating through the stiffness constant some kind of elastic penalty for the sample thickening, which we would like to artificially suppress.

RE is a particular example of a delicate trade-off between precision and computational cost, since several simulations are running at once, calling for as moderate KPOINTS, ENCUT and POTIM, as possible. In the Sn case, we ended with (3 3 1) KPOINTS, while Si and Ge demanded at least 3 specially chosen KPOINTS and even

those may not be enough, since Si slabs melted below 1030 K at default value of ENCUT and 5 fs time-step. It is indeed surprising that even single Ba atom addition to our several-dozen-atom periodic cells of free-standing thin-film samples, does not lead to a *solo* clathrate cage. We hope that the present work stimulates further research (with enhanced values of all the parameters) towards this goal.

2.3 Atomic Structure, Termination, Thickness, Reconstruction: Definitions

2.3.1 Atomic structure.

Vast majority of the slabs were carved out from the known bulk phases, described in Section 3, by planar sections. The second way to Column-XIV thin films led through the *ab initio* Molecular Dynamics introduced in Subsection 2.2. Except for Sn – a borderline case between metal and semiconductor – the work deals exclusively with sp^3 allotropes where all atoms exhibit more or less tetrahedral environment with quartet of nearest neighbours forming average bond angle around 109.5°.

All the known high-pressure allotropes more than 50 meV/at. above the respective cubic diamond (cF8) phase, such as BC8, R8, ST12, BT8⁶, mC16, bct-5⁷, obtained chiefly by (de)compression, were avoided [see Table S1.1, SM, for phases that were taken into account], since the main goal is to predict stable slabs with *lower* internal energy per atom compared to the corresponding diamond slabs of the same thickness. The only exception will be the amorphous phases, due to the intention to crystallize stable clathrate slabs from the melt and owing to their inherent indifference to the structure of a substrate, in contradistinction to diamond or clathrates.

Extra, atomic configurations directly related to diamond, such as hexagonal diamond (lonsdaleite), so called diamond polytypes, were also excluded from the competition, as *brand new* materials bearing novel properties are in the sights.

2.3.2 Termination.

From now on, termination is a particular *orientation and position* of a cutting plane with respect to a bulk crystal, producing planar slab of constant thickness:

2.3.3 Thickness.

of a slab is measured by the *coverage* ρ defined by:

$$\rho \equiv N/S \quad (1)$$

where N stands for the number of atoms per surface area S of a periodic cell. Individual cases of planar terminations suitable for each bulk phase are listed in the next Section 3.

For the sake of simple element comparison, coverage ρ will be measured in dimensionless “monolayer” (ML) unit, one ML corresponding to ρ value of a single (111) layer of cubic α -phase (cF8, diamond) of either Si, Ge or Sn.

2.3.4 Reconstruction.

Hereafter, by *reconstruction* we mean addition of atoms of the same kind, *adatoms*, (i.e. Sn atoms in the Sn-slab case) to the

film's surface followed by DFT relaxation of the atomic positions, while in-plane lattice parameters held fixed. We did not attempt any hydrogenation, whereas "bare" surfaces after relaxation of atomic positions will be called anyway "unreconstructed".

Particular instances of surface reconstruction shall be specified for each parent bulk phase and for every termination thereof in the next Section 3.

2.4 Slab Stability Assessment

Due to the intrinsic positivity of the **surface energy** γ there is a general trend of decreasing per-atom energy with slab thickness. At the same time, flat slabs occur at discrete, characteristic values of **coverage** ρ and energy per atom. Hence, we seek after energy-minimizing slab structures for a given **coverage** ρ , corresponding to certain slab thickness.

Let's consider two directly constructed points $E(\rho)$, e.g. a couple of (111)-diamond slabs with distinct thicknesses $\rho_1 \equiv N_1/S_1$, $\rho_2 \equiv N_2/S_2$ with energies per atom E_1, E_2 , respectively, which may differ in type of surface reconstruction, hence in the value of **surface energy** $\gamma_1 \neq \gamma_2$. An *interpolation* between the points has a meaning of a *terrace* of energy E such that $E_1 > E > E_2$ and coverage ρ such that $\rho_1 < \rho < \rho_2$ between the two slabs, whose contribution to the overall energy-per-atom of the whole system tends to zero for periodic boundary conditions (PBC) tending to infinity. Because energy, surface and number of atoms per periodic cell are additive quantities satisfying ($p_i \equiv N_i/N$, $i \in \{1, 2\}$):

$$p_1 + p_2 = \frac{N_1}{N} + \frac{N_2}{N} = 1 = \frac{S_1}{S} + \frac{S_2}{S} = \frac{E_1}{E} \frac{N_1}{N} + \frac{E_2}{E} \frac{N_2}{N} \quad (2)$$

the *linear interpolation* on the graph $E_{\text{atom}}(\rho^{-1})$ follows:

$$\frac{S}{N} = p_1 \left(\frac{S_1}{N_1} \right) + p_2 \left(\frac{S_2}{N_2} \right) \Leftrightarrow (\rho)^{-1} = p_1(\rho_1)^{-1} + p_2(\rho_2)^{-1} \quad (3)$$

corresponding to this particular interpolation in the graphs $E_{\text{atom}}(\rho)$:

$$E = E_2 + \frac{\rho_2 - \rho}{\rho_2 - \rho_1} \frac{\rho_1}{\rho} (E_1 - E_2) \quad (4)$$

The aim of this sort of graphs is to compare thin-film energy per atom, E_{atom} , of different atomic configurations, terminations and reconstructions for the common intermediate coverage ρ , not associated with any planar slab structure already measured.

In the simplest case of a constant surface energy γ , hyperbolic trends (4) of the curves $E_{\text{atom}}(\rho)$ for each structural family of slabs, cf. Figure 6, can be derived directly from the definition of the **surface energy**:

$$\gamma \stackrel{\text{def.}}{=} \frac{E_{\text{cell}} - E_{\text{bulk}}N}{2S} \Rightarrow E_{\text{atom}}(\rho) = \frac{E_{\text{cell}}}{N} = 2 \frac{\gamma}{\rho} + E_{\text{bulk}} \quad (5)$$

where E_{atom} is energy per slab's atom, E_{cell} is overall energy per periodic cell with the total of N atoms, E_{bulk} is energy per one atom of the respective bulk phase and ρ is thin-film **coverage** possessing two faces, hence the factor "2" in Equation 5).

In the case of *layered* growth mode with *constant* surface

energy γ of a thin film and/or in the close vicinity of the scattered points in Figure 6, the hyperbolic dependence (5) describes slabs with (non-)integer number of layers. Each point of the hyperbolic convex hull can be thus assigned an (in)complete slab; incompleteness meaning a slab with a *terrace*.

The free-standing slab setup with PBC (periodic cell extended vertically in the z direction to include vacuum gap between periodic images of a slab) introduces specific constraints: for systems with lattice parameters up to few tens of Å, it effectively hampers formation of non-planar bulky morphologies (e.g. nanowires, nanoparticles). Importantly, all the slabs in current simulations are only *metastable* – stabilized by artificial effect of *finite* PBC – whose increase would progressively lead to spontaneous transformation to nanowires and nanoparticles, respectively, owing to the $\gamma > 0$ of G4 sp³ elements.

While this phenomenon actually helps studying slabs as templates for adlayers that might form on an appropriate substrate by wetting it, we have to keep in mind that our simulations do not fairly assess the tendencies to possible island formation⁸, once the material is deposited on a substrate. Questions related to *dewetting* are actually highly relevant for sp³-type adlayers⁹, e.g. silicon on an insulator.

3 Competing allotropes

3.1 Monolayers

Stabilizing reconstruction evidently depends on the layer thickness. Singular point are monolayers, displaying just one atomic layer to reconstruct. However, there are infinitely many ways to do so.

As for Sn, Ge and Si, clear choice^{10–12} are various reconstructions of (111)-diamond monolayer, so called stanene, germanene and silicene, see Figure 1. Because the basic reconstruction unit is *dumbbell*, we will call them hereafter db-monolayers¹².

Even though each dumbbell constructed on germanene (silicene) lowers per-atom-energy, MoS₂ configuration, corresponding to the full coverage, has branches with imaginary frequencies in *ab-initio* phonon spectra indicating mechanical instability¹². The ground state of (Sn, Ge, Si) db-monolayer is therefore non-trivial and requires systematic investigation.

For every admissible dumbbell density per unit area in the given supercell – from minimal zero stanene density up to the maximal MoS₂ dumbbell density – *all* dumbbell configurations were tested for the resulting internal energy per atom and plotted as a function of **coverage** ρ , see Subsection 2.4. We have chosen 2×2 oP10 supercell with originally 32 stanene atoms (without adatoms). Adatoms were placed just on one sublattice of the bipartite stanene lattice followed by the systematic elimination of the symmetrically equivalent adatomic configurations.

For both germanene and silicene, oP10 minimizes internal energy per slab's atom, cf. Figure 6. On the contrary, all the candidate db-monolayers, succumbed in the course of AIMD simulations, starting from random atomic positions and from hP10 db-stanene as well, to a web-like net of interconnected Sn₉ clusters, Sn₉-web, (Figure 2) in the Sn case for the given **coverage**,

Figure 6.

As it shall be explicitly illustrated by an example of bilayers, Subsection 3.4, Sn due to its metallic temper favours 6-coordinated atoms resulting in genuine G4 bond-angles equal to 60° (Figure 4, typical of a-Ge and a-Si surface¹³) and 109.5° dominant in a Sn9-web to purely sp^3 -like coordination of 4, accompanied by “factitious” bond angles 54° , 66° , 72° , 129° , enforced by the arrangements depicted in Figure 1.

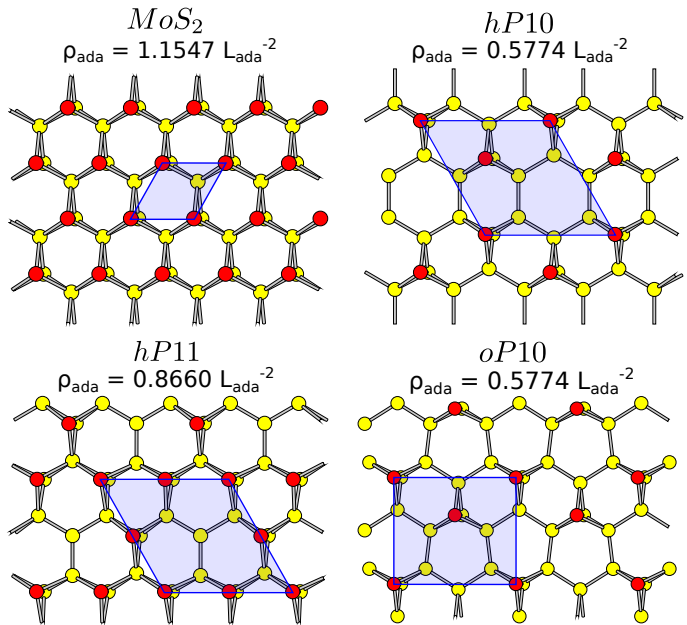


Fig. 1 Various reconstructions of (111)-diamond Sn, Ge and Si monolayers. Blue shaded objects delimit periodic cell. Red balls designate adatoms. ρ_{ada} under Pearson symbol stands for the area-density of adatoms expressed through typical length unit L_{ada} : the distance between nearest neighbours on a sublattice of a bipartite (111)-diamond lattice.

3.2 Diamond

As a reference for elemental Sn, Ge and Si diamond slabs (no mention of carbon in this work!), we have chosen (111)-terminated ones. It has been shown by numerous experimental and theoretical groups that (111)-diamond section of Sn¹⁶, Ge and Si^{17–22} is a cleavage face possessing the lowest **surface energy** γ among all the cubic-diamond (cF8) bulk sections. Note that this statement is valid just after proper *bulk* surface reconstruction^{17, 22}.

Several reconstructions of (111)-diamond surface have been compared: $\sqrt{3} \times \sqrt{3}$, 2×2 , $c(2 \times 4)$, $c(2 \times 8)$ ^{23, 24}, 3×3 DAS, 7×7 DAS²⁵, but the variation of the per-atom energies turned out to be negligible with respect to the clathrate-diamond differences above 3 ML slab’s thickness, cf. Figure 6. Mind that below, say, 10ML surface states or surface atoms cannot be distinguished since practically all atoms belong to the surface¹⁷, so the notion of the **surface energy** γ is not relevant here.

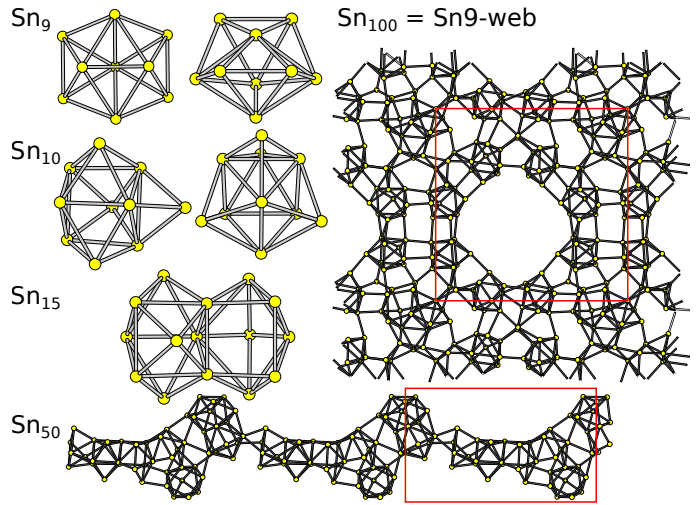


Fig. 2 Sn₉ and Sn₁₀ clusters (from two different view angles) are fundamental units of threadlike tin structures that form spontaneously for low coverages ρ (discontinuous layers with holes)^{14, 15}. Sn₁₅ subunit also frequent in Sn clusters comprises two Sn₉ basic units sharing a common triangle. Sn₅₀ and Sn₁₀₀ are examples of our long DFT annealings at room temperatures with 50 and 100 Sn atoms, respectively, enclosed in fixed $24 \times 24 \times 24 \text{ \AA}^3$ cubic container. Sn₁₀₀ is composed of 8 Sn₉ clusters in a ring. Red borderline delimits periodic motif.

3.3 Clathrates

3.3.1 Clathrate Terminations.

We have investigated all planar sections of clathrate types I–IV, leading to equilateral-/isosceles-triangle, square and rectangle in-plane tilings and combinations thereof, Table 1. To every such orientation of a section plane with respect to a bulk clathrate there are four distinct terminations⁸, e.g.:

$$T_h \rightarrow T'_c \rightarrow T'_h \rightarrow T_c \quad (6)$$

schematically depicts the 4-layer Triangular-tiling period in the “z” direction perpendicular to the section plane (shared by both isosceles and equilateral triangle, likewise for the square and rectangle tiles) of puckered terminal planes with characteristic “holes” – T_h , T'_h – alternating with flat terminal planes displaying “caps” around the tile vertices: T'_c , T_c , consult Figures S2.1 and S3.1 (SM) for decagonal (iso-tri, rectangle) and dodecagonal tiles (equi-tri, square), respectively.

Note that the only exception from the rule (6) comprises trio of (111)-terminations of type-II clathrate where T_c planes are missing. These very missing flat planes of clathrate-III 6-caps, Figure S2.1 in SM, act as a bridge between type-II and type-III clathrates, representing the only difference between the two.

Explicit clathrate construction, i.e. atomic decorations of clathrate tiles mentioned above, was achieved via symmetry-preserving dual transformation^{26, 27} of the respective Frank-Kasper (FK) phases. Equally, orientation of section planes was inspired by the well-known FK atomic planes, linked by dual transformation to the planes of clathrate-cage centers. It turns out that these are the section orientations yielding planar clathrate slabs containing at least 3-coordinated surface atoms, completely with-

out terraces or cages sticking out from the surface.

This, however, is not the whole story about sensible clathrate terminations, since each clathrate cage itself represents an object with at least 3-coordinated surface atoms, even when entirely isolated. Adding 5-caps or 6-caps onto puckered T_h and T'_h planes does not change the surface density of unsaturated (so called dangling) bonds. Therefore, we expect that the growth mode of a clathrate will be either pure island or mixed island-layer type, depending on the energy scales related to the processes of (1) completion of a surface cage and (2) coalescing cages together⁸.

type	Pearson	sect.	tile	notation
I	cP46	(100)	square	Si.square-I-N
II	cF136	(110)	iso-tri	Si.iso-II-N
II	cF136	(111)	equi-tri	Si.equi-II-N
III	hP40	(001)	equi-tri	Si.equi-III-N
III	hP40	(100)	rectangle	Si.rect-III-N
IV	tP172	(001)	equi-tri + square	Si.dodeca-IV-N
-	oP148	-	iso-tri + rect.	Si.deca-N

Table 1 designation of an N -monolayer-thick planar slab cut from the parent bulk clathrate, for which Pearson symbol is stated, by planar section with the respective clathrate tile information. Decagonal R2T4 approximant⁸ (oP148) does not belong to any canonical clathrate I-IV type

3.3.2 Clathrate Nomenclature.

We shall designate clathrate slabs according to the element, the associated clathrate tile corresponding to particular orientation of a section plane with respect to a bulk clathrate phase and the thickness measured by number of (111)-diamond monolayers N , Table 1. For the sake of concise and uncluttered notation, unless otherwise stated, the respective N will be rounded to the nearest integer value except for half-integers and optimal surface terminations with energy-minimizing reconstruction, detailed in Section 4, for the given coverage ρ are meant.

3.3.3 Clathrate Reconstruction.

Here we describe, for the first time, the optimal surface-energy minimizing reconstructions of planar clathrate sections listed in Table 1 for each of the four terminations from Equation (6).

The basic reconstruction element is again *dumbbell*, but unlike (111)-diamond surface termination, surface adatom S is located *beneath* some group of 3-coordinated surface atoms, whose dangling bonds it should saturate.

There are three basic positions⁸ of a clathrate-surface adatom S (Figures S2.1, S3.1 in SM):

1. Under cage faces aka “caps”:

1a. Under 5-gonal cage facets: T_c, R_c, T'_c, R'_c .

1b. Under 6-gonal cage facets: T_c, T'_c, S_c .

2. Dumbbell under the 3-coordinated atom with:

2a. all neighbours 4-coordinated: T'_c, R'_c, R_c, S_c .

2b. two neighbours 3-coordinated: R_h, R'_h, S_h .

2c. three neighbours 3-coordinated: T'_h .

3. Midedge position: under the bond of 3-coordinated atoms: T_h, R_h, S_h .

3.4 Tin-Specific Phases

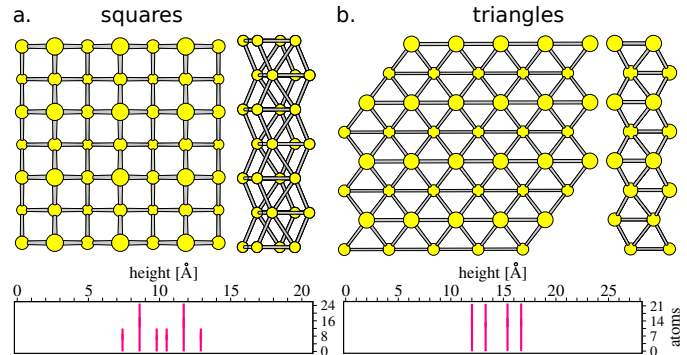


Fig. 3 Two Sn thin-film metallic phases: square and hexagonal. Left: Square Sn bilayer: front view and side view, firstly published in⁵. Right: Hexagonal Sn bilayer: front and side view, yet unpublished, discovered via long MD DFT room-temperature runs in our work. Bottom panel: histograms of number of atoms per unit cell per given z coordinate perpendicular to the bilayer plane. Both phases have the front atoms exactly above the bottom atoms of a bilayer in the z direction.

Unlike Ge and Si, tin owing to its position at the bottom of Column-XIV lies on the borderline between semiconductors (C, Ge, Si) and metals (Pb), clearly exhibiting metallic properties at ambient conditions. At the level of (111)-diamond bilayer ($\rho \approx 2$) square and hexagonal metallic Sn films are competing with one another, Figure 3. The couple of metallic phases are designated as “squares” and “triangles” in result Figure 6.

Whereas square Sn-I phase constitutes the ground state of Sn bilayer⁵, hexagonal counterpart emerges during long MD or Replica Exchange (RE) annealings at room temperature. These observations suggest that hexagonal phase is favoured by (vibrational) entropy, corroborated by numerous defects of hexagonal polymorphs compared to the relatively perfect square one. All the metallic atomically-thin Sn films showed strong tendency towards the formation of even-layers.

Interestingly, both types of metallic bilayers can be viewed as two planar sections of γ -Sn phase^{28, 29} in mutually perpendicular directions after symmetry breaking (slight displacement of a couple of atoms). Besides Sn9-web, Figure 2, hexagonal Sn even-layers, are the second discovery of our DFT RE runs.

Despite being presented as stanene 4-layer, in the central Figure 1a³⁰ presumably is depicted triangular Sn 4-layer with hexagon centers *filled* with Sn atoms, experimentally prepared by non-equilibrium process: pulsed laser ablation of β -Sn target floating on liquid hexane.

3.5 Amorphous Phases

3.5.1 Amorphous Tin.

As opposed to Ge and Si, in the case of bulk Sn there is no such a local minimum of the potential energy landscape deserving the title *amorphous*. More precisely, the aforementioned minima - even more than one mechanically stable structure - can be readily visited in the DFT universe; the real obstacle, however, resides in their experimental accessibility.

So as to observe a bulk-like amorphous Sn layer by quenched condensation on a cold substrate, it requires at least 8 atomic % of some other metal, e.g. Cu, and even then the resulting alloy crystallizes above approximately 20 K^{31–33}. Another method – quenched simultaneous condensation of Sn and H on a substrate on nitrogen temperature – produces bulk-like amorphous semiconducting Sn, stable up to 180 K³⁴. The other procedures include for example ion implantation of radioactive Sn isotopes³⁵, or intense electrolytic chemical reaction able to extract selected elements from the common precursor, such as sulphur from SnS₂ crystal³⁶.

Possible realization through decompression of high-pressure intermediate obtained by compression of type-II clathrate³⁷ or α -tin^{7, 38} seems impracticable for tin, compared to Si and Ge, since analogically DFT-generated metallic Sn disordered liquid (90 meV/at. above α -Sn) possesses by 10 meV/at. lower internal energy than sp³-amorphous Sn gained by a-Ge rescaling to the typical Sn-Sn distances, Table S1.1, SM. This metallic liquid then readily transforms to various metallic *crystalline* phases of Sn. The phase space of Sn is much more complicated than that of Si and Ge, and may well hide yet unexplored and even unexpected allotropes³⁹, though.

3.5.2 Amorphous Silicon.

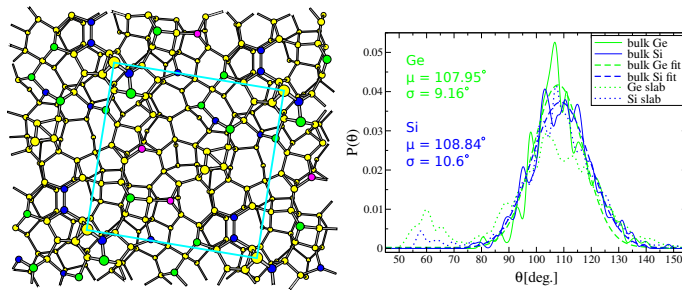


Fig. 4 Left: Typical surface of a-Si: most of the atoms are 4-coordinated yellow balls, blue balls are sp²-bonded atoms, green balls are p³-bonded and magenta atoms possess two bond angles $\approx 100^\circ$ and one $\approx 120^\circ$. There are two atoms with even sharper pyramidal bonding geometry of $\theta_{\text{ave}} < 80^\circ$. Periodic cell is delimited by cyan line. Size of a ball is proportional to its distance from the observer. Right: Bond-angle distributions of the best bulk a-Si and a-Ge without defects, produced by DFT on-the-fly trained VASP MLFF, fitted by gaussians, compared with thick slabs of the same material.

Surprisingly, bulk a-Si can be prepared completely faultless without any coordination defects showing perfect gaussian bond-angle distribution⁴⁰, Figure 4, around (almost ideal) tetrahedral bond-angle 108.6° with the standard deviation from the narrow

interval 9 – 11°^{41–46}. This was also the case of our samples generated using VASP MLFF suite trained on-the-fly during ab initio heating from 300 K to 900 K of the quenched melt (10^4 5 fs-steps at 3000 K) followed by annealing at 900 K^{47–49} (2×10^5 MLFF 5 fs-steps) and slow cooling (3×10^6 MLFF 5 fs-steps) back to room temperature within the standard DFT setup, Subsection 2.1. The density of thus prepared bulk a-Si, Figure 4, was 98.1% of α -Si (cF8) value, its internal energy being 158 meV/at. above Si.cF8, Table S1.1 (SM), falling into the interval 0.09 – 0.17 eV/at. stated in the literature^{43, 50–52}.

The effect of thorough ab initio annealing and relaxation of a-Si surface has been validated in solo paper¹³. It has been proven that DFT treatment leads to the significant relaxation, namely to the p³ and sp² hybridizations of 3-coordinated surface atoms, with average bond angles θ_{ave} of 99.4° and 119.1°, respectively, quite distinct from 108° θ_{ave} of 3-fold bulk atoms. This effect is sizable, since 3-fold atoms comprise $\sim 22\%$ of the surface; the rest consisting of $\sim 74\%$ sp³- and 4% 5-coordination. Besides characteristic hybridizations, another intrinsic surface feature are 3-member rings accompanied by small 50° – 60° bond-angle peak, not found in the bulk a-Si distribution¹³, approved by our DFT results, Figure 4.

The a-Si surface energy is supposed to be $\gamma = 1.05 \pm 0.14 \text{ J/m}^2$ ¹³, or 1.34 J/m^2 ⁴⁸. The latter paper⁴⁸ states somewhat large γ – even larger than quoted experimental values 1.14 J/m^2 ⁵³, 1.23 J/m^2 ⁵⁴, 1.24 J/m^2 ⁵⁵, of ideal (111) diamond termination – but *without* proper annealing after a tearing test. ($1 \text{ erg/cm}^2 = \text{mJ/m}^2$ and $1 \text{ eV}/\text{\AA}^2 = 16.02176634 \text{ J/m}^2$) According to Materials Project²², the surface energy of reconstructed (111) Si.cF8 surface is 1.30 J/m^2 .

Our DFT computed (111) Si.cF8 unreconstructed surface has energy 1.57 J/m^2 , its c(2 × 4) reconstruction²³ has surface energy $\gamma = 1.27 \text{ J/m}^2$, in good agreement with literature. Our a-Si slabs with coverages ranging from 0.27 – 0.77 at./ \AA^2 (for unit conversion: 1 ML = 0.15469 at./ \AA^2 is the coverage of one Si diamond monolayer, 1 ML) possess energies from the interval $0.77 – 0.87 \text{ J/m}^2$ or $48 – 54 \text{ meV}/\text{\AA}^2$: as expected lower than (111)-cF8 termination; γ of partially crystallized (to cF8) a-Si samples attacking lower bound. Mind that *computed* value of a-Si γ strongly depends on the *bulk* a-Si energy via Equation 5 (E_{bulk} term), which, according to the literature, is from the relatively **broad interval**, see above. For further comparison, surface energy of the best reconstructed Si clath-II slabs, Figure 7, is 0.865 J/m^2 , on the a-Si γ *upper limit*.

3.5.3 Amorphous Germanium.

Despite structural properties of bulk a-Ge being the same as those of a-Si, cf. Figure 4, and despite bulk a-Ge constructed directly via a-Si rescaling to the characteristic Ge-Ge distances succeeded by atomic relaxation, we have observed for the first time that a-Ge *surface* features are completely different, Figure 5. Note that elemental Ge thin films were in fashion in 1970s and 1980s, when DFT was still in its infancy, hence all we know about structural units of a-Ge (thin film) surface comes from DFT simulations of our own.

The density of bulk a-Ge comprises 96.68% of the Ge.cF8 value

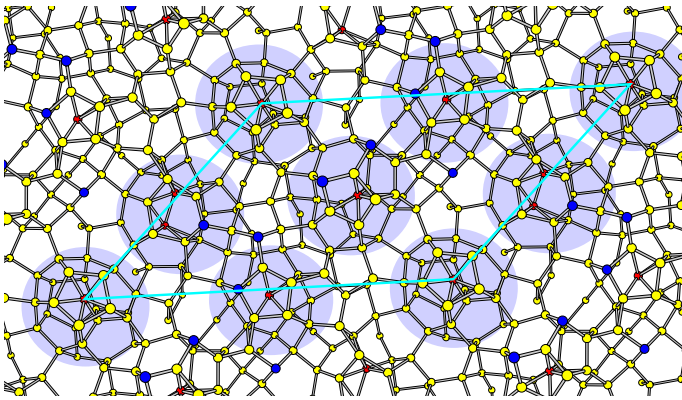


Fig. 5 Typical a-Ge surface obtained by VASP on-the-fly MLFF from the melt by repeated annealing at 646K and slow quench to 300K. Periodic cell is delimited by cyan line. Most of the surface atoms are (approx. sp^3) 4-coordinated: yellow balls. Red balls: over-coordinated adatoms. Blue balls: dangling bonds, mainly associated with 5- and 6-caps.

and is by 128 meV/at. unstable at 0 K to diamond, Table S1.1, SM. a-Ge slabs were prepared by long annealing slightly below $T_c = 650$ K, just as bulk a-Ge.

The surface energy of a-Ge slabs with characteristic 5-caps and 6-caps on the surface, Figure 5, lies in the interval (0.45 – 0.55) J/m² or equivalently (28 – 34) meV/Å², approximately one half of unreconstructed (111) diamond, 1.07 J/m² (Materials Project states the value 1.11 J/m²²²). These a-Ge clathrate-surface elements manifest themselves in the bond-angle distribution as a strong peak around 60°, Figure 4, even stronger than that of a-Si surface of different origin.

For further comparison, surface energy of (111) diamond can be lowered to 0.865 J/m² by $\sqrt{3} \times \sqrt{3}$ reconstruction, which is still much higher than a-Ge values. Surface energy of the best clathrate reconstructions, 5-caps and 6-caps with one adatom, consult Figures S2.1 and S3.1 (SM) and Figure 7, are 0.734 J/m² and 0.559 J/m², respectively, again attacking upper threshold of a-Ge range, like in the a-Si case (but substantially lower than γ of reconstructed Ge diamond surface).

3.6 Chiral Framework Structures

To the best of our knowledge, the only sp^3 G4 allotropes possessing *lower* internal energy per atom than type-II clathrate *not* structurally related to diamond are Chiral Framework Structures, CFS, or spirals: CFS-5⁵⁶, CFS-6⁵⁷ or NGS⁵⁸, T12⁵⁹, see also Table S1.1, SM.

All three structures are fully sp^3 -hybridized, displaying main peak of the bond-angle distribution around 109.5° and do not contain any imaginary frequencies supporting dynamical stability of these allotropes at ambient pressure^{56, 59}.

Lattice Gas Monte Carlo (LGMC) algorithm was deployed to seek after the best planar terminations for thin films. An attractive toy potential was applied that favored two CN=3 surface atoms over a couple of CN=2, CN=4 atoms: thus simulations tend to produce surfaces similar to the unreconstructed (111)-diamond (or clathrate). Simulation itself was a multiply repeated cooling while recording the lowest-energy configurations (by our

own program).

LGMC research of CFS-6 ended in two surface terminations normal to (120) and (001) directions [(001) is the axis of the main spiral with hexagonal cross section], subjected to subsequent reconstructions for several Si, Ge and Sn film thicknesses.

For both sections two surface reconstructions were attempted: **adatoms** were firstly placed below each bond joining a couple of unsaturated atoms – (001)-1, (120)-1 – and secondly to the valley between them – (001)-2, (120)-2. As concerns thicknesses above 0.54 at./Å², relaxations have just effect on the slab's surface; the interior remains spiral-like and does not change its phase upon relaxation.

Atomic and cell relaxations left (120) (un)reconstructed surface intact, while surface of (001) termination has changed substantially and manifested 3- and 4-coordinated atoms only. As for (001)-1 and (001)-2 reconstructions, adatoms move towards the spiral's main axis, saturating as many dangling bonds of the surrounding spiral as possible.

As expected from the already probed clathrate-surface reconstructions, Subsubsection 3.3.3, the only successful attempt was (120)-1 for Ge and Sn, resembling midedge reconstruction of clath-II T_h tiles, cf. Figure S2.1, S3.1 (SM), which was forbidden for Si, Figure 6. Si CFS-6, which is energetically degenerated with clath-II bulk, can not be cut and reconstructed effectively, therefore only unreconstructed Si.CFS surfaces were included in Figure 6 summarizing the chief results.

(120) termination is clearly better than (001) owing to the smaller area-density of the coordination defects (dangling bonds) and the absence of 2-coordinated atoms, but both are worse compared to the best clath-II planar sections, Figure 7. Clathrates exhibit lower per-atom energy and lower **surface energy** γ for all three elements and thicknesses under question.

As for CFS-5, there are two equivalent sections in directions (100) and (010), with just 3- and 4-coordinated atoms. In this case, 3-fold atoms are arranged in 4-atom chains per periodic box, exhibiting highest area-density of coordination defects among all CFS sections already mentioned. Several solo-adatom reconstructions were attempted, none of them being successful at lowering energy-per-atom or even surface energy γ , so compositions of several such adatoms seem to be also useless (absent in Figure 6).

Finally, natural planar termination of T12 normal to (001) direction with exclusively 3- and 4-coordinated surface atoms is the same as (120) cut of CFS-6, since both structures are stackings of equal 3-atom thick layers, having almost the same bulk energy per atom, wherefore the reconstructions of T12 were not executed.

4 Results

Our principal results are **coverage** ranges for which clathrate slabs are the ground state with $\Delta E(\rho) \equiv E_{clath}(\rho) - E_{ref}(\rho) < 0$; where $E_{ref}(\rho)$ is energy of the closest competing structure, usually diamond. They are summarized in Table 2, Figure 6 (see also Figures S4.1, S4.2 and S4.3 in SM) and the surface reconstruction of per-atom-energy minimizing clathrate slabs corresponding

element	clath-II surface	ρ_0	ρ_{\max} ML	ρ_1	ΔE_{\max} meV/atom
Sn	(111)	3.2	3.2	10.0	-35
Ge	(111)&(110)	2.5	3.4	7.4	-34
Si	(110)	2.5	3.3	5.3	-44

Table 2 *coverage intervals at which the ground-state slab is a clathrate (always type-II): columns ρ_0 and ρ_1 are endpoints of the clathrate stability intervals expressed in (111)-diamond-monolayer units (ML). ΔE_{\max} is the “maximum energy gain” relative to competitors at ρ_{\max}*

to ρ_{\max} , where ΔE is maximal, are depicted in Figure 7. xyz-files of all stable thin films except for diamond are given in Section S9 (SM). Finally, in Subsection 4.4 a possible mechanism of electronic stabilization of clathrate thin films with respect to diamond ones is advocated.

4.1 Tin

For the lowest coverages below 2 ML, discontinuous structures are formed, depending on the size of a supercell. At $\rho \approx 1.7$ ML, thread-like arrangements of Sn₉, Sn₁₀ and Sn₁₅ units^{14, 15} turn into a Sn₉-web, Figures 2, 6. These small Sn “houses” seem to be the energy-minimizing interface between metallic Sn bilayers with surrounding vacuum.

Around $\rho \approx 2$ ML, uneven match among hexagonal and square metallic bilayers happens, Figure 3, designated as “triangles” and “squares” in Figure 6, respectively, squares being the clear winner by ≈ 30 meV/at., Subsection 3.4.

Finally, above $\rho \approx 3$ ML up to $\rho \approx 10$ ML, clathrate slabs get a word in, Table 2, Figure 6. For more than $\rho \approx 10.4$ ML, approaching the bulk limit, thin-film clathrates are surpassed by reconstructed thick diamond layers.

Internal-energy-minimizing clathrate films are (111)-cut of type-II bulk showing equilateral-triangle T_h tiling in the section plane, Subsubsection 3.3.1, reconstructed equally by adatoms at the midedge positions (in the middle of each tile’s side), samples Sn.equi-II-N, $N \in \{3; 5; 7.5; 10\}$, Section S9.1 (SM) and Figure 7. Owing to its metallic behaviour, Sn favours the highest area-density of adatoms from amid Group IV; this particular reconstruction presenting such an example, cf. Figure S3.1 (SM), resulting in 1.5 adatom per triangle tile – the largest admissible clathrate adatomic surface density.

As concerns CFS, Subsection 3.6, the best reconstructed surface, CFS-6 (120)-1, possesses both higher area-density of defects (in the form of 3-coordinated atoms) as well as greater bulk per-atom-energy, thus dropping out of the game, Figure 6.

4.2 Germanium

The most stable Si and Ge monolayer is oP10-reconstructed germanene and silicene, Subsection 3.1, Figure 6. Unlike metallic Sn, there is no known (meta)stable Ge or Si bilayer. Above $\rho \approx 2.5$ ML clathrates clearly reign stable-thin-film configurational space, starting with Ge.iso-II-2.5 (S9.2.2 in SM) one-cage thick isosceles-triangle (110)-cut of type-II bulk composed of combined $T_h + T'_h$ tiles, Figure S2.1 of SM, reconstructed by solo adatom per T_h tile (i.e. without midedge adatoms in T'_h tiles).

Next, in the thickness range $\rho \in [2.5; 7.4]$ ML, Table 2, just as in the case of Sn, (111)-cut clath-II films designated as Ge.equi-II-N, $N \in \{3; 3.5; 6\}$, Section S9.2 (SM), are by far most stable. This time, however, the best termination are markedly *deformed* T'_h 6-caps, Subsubsection 3.3.1, with one adatom each. The net result of thorough AIMD annealing and subsequent relaxation is transition of 6-cap to effectively 5-cap plus one atom, Figure 7, for all the Ge.equi-II-N samples. The configurational space above $\rho \approx 7$ ML is obviously a bulk limit, where diamond films become dominant, regardless of reconstruction, Figure 6.

As CFS layers are concerned, the concluding remark from the preceding Subsection 4.1 holds, the best CFS-6 (120)-1 moving even further away from the convex hull compared to Sn.CFS-6.

4.3 Silicon

The area-density of adatoms gradually decreases in the sequence $Sn \rightarrow Ge \rightarrow Si$. From the G4, Si is most sensitive to adatom addition, unequivocally favouring isosceles-triangle (110)-cut of type-II bulk composed of combined $T_h + T'_h$ tiles, Figure S2.1 of SM, in the whole range of Si clathrate-film stability: $\rho \in [2.5; 5]$ ML, Table 2, resulting in samples labeled Si.iso-II-N at discrete thicknesses $N \in \{2.5; 4; 5\}$, Section S9.3 (SM). Like in the Ge case, they are reconstructed by solo adatom in the middle of T_h tile (i.e. without adatoms at midedge T'_h positions).

According to Figures S4.1, S4.2, S4.3 (SM), clathrate films are already winning by cheaper surface termination *before* surface reconstruction, but proper reconstructions render them another important advantage over the diamond slabs.

As expected, for Si, the best CFS surface is *unreconstructed*, Figure 6, almost overlaying high-energy amorphous $E(\rho)$ curve far from the overall convex envelope.

Note that despite the lower surface energy γ for both a-Ge and a-Si, Subsubsections 3.5.3 and 3.5.2, respectively, the stability of clathrate (and even diamond) slabs over amorphous ones, Table 6, is secured by their *bulk* energy, Table S1.1 (SM).

4.4 Electronic Stabilization of Clathrate Films

Electronic densities of states (eDOS) of the most stable Sn, Ge and Si clathrate slabs are displayed in Figure S8.2 (SM). Clathrates definitely enhance the tendency of the sp³ elements towards bandgap formation – this is clearly visible already in the bulk, see Figure S8.1 (SM).

Trends are evident both with respect to clathrate/diamond competition and as a function of *coverage*, because the thinnest 2.5 ML-slabs (samples Sn.equi-II-2.5, Ge.iso-II-2.5, Si.iso-II-2.5) exhibit distinct eDOS as well as ~ 3.5 ML-thick ones (samples Ge.equi-II-3.5, Si.equi-III-3.5), whereas eDOS of thicker slabs approaches the bulk limit.

Comparing clathrate vs. diamond, ultrathin slabs confirm and enhance clathrate tendency for the gap formation, while the reconstructed diamond slabs tend to fill the electronic states just above or even across the Fermi energy. This trend must be the substantial reason for the enhanced clathrate stability.

Looking at the slab width variation, it is obvious that 2.5 ML-slab eDOS stand out loosing any correspondence with the bulk.

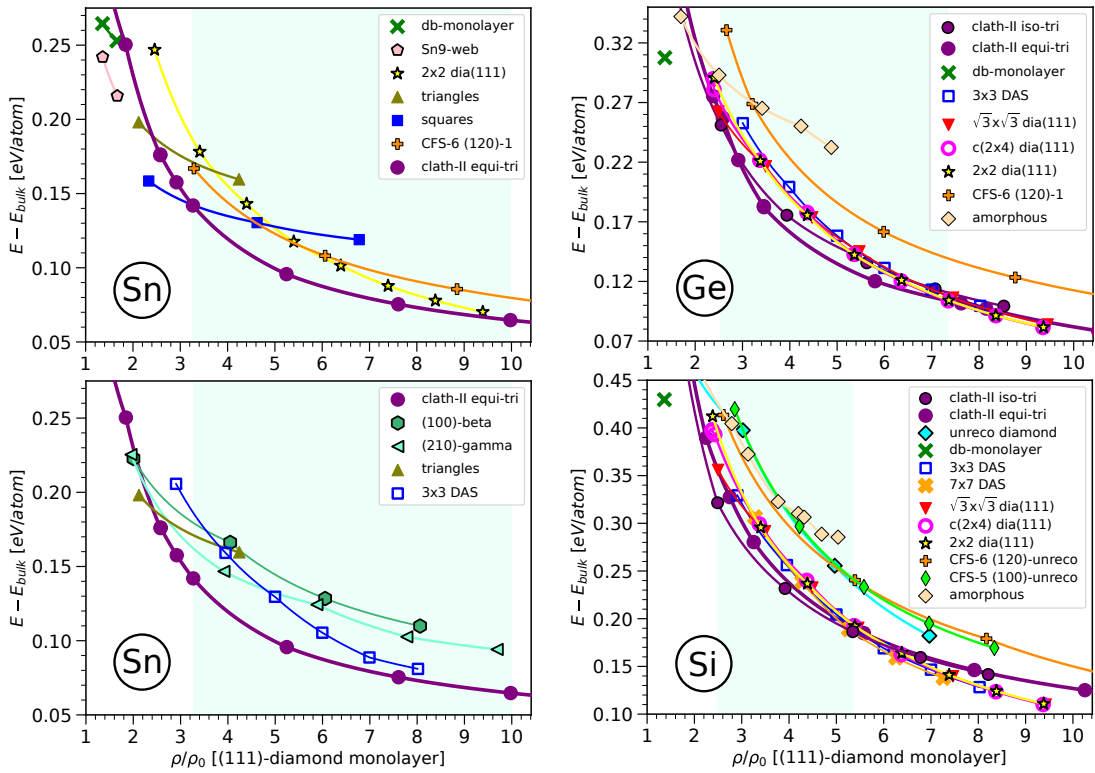


Fig. 6 Shaded green area: stability region of Sn, Ge, Si clathrate thin films. DFT internal energy with respect to the cF8 bulk phase as a function of coverage is plotted in each case.

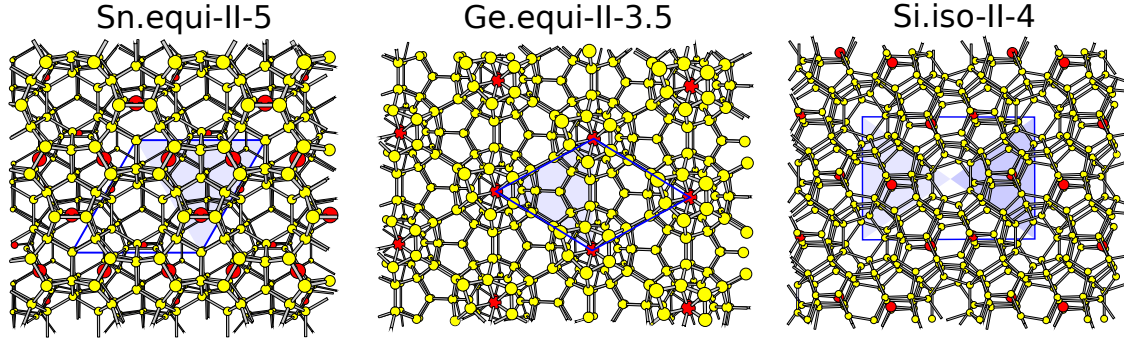


Fig. 7 The structure of the most stable free-standing Sn, Ge, Si clathrate type-II thin films: their termination and reconstruction as a function of a chemical element. Shaded areas correspond to elementary-triangle clathrate tiles (isosceles for Si, equilateral for Ge and Sn). Periodic cell is highlighted by solid blue line. Surface adatoms are bigger red balls. The integer in the sample's label designates number of (111)-diamond ML in thickness (coverage ρ).

3.5 ML-thick Ge and Si slabs are distinguished by their bandgaps reaching the bulk-bandgap width, and are broader than bandgaps of thicker slabs of the same kind.

5 Discussion

Here we attempt to crystallize the most stable clathrate thin films from the melt to directly prove the chief results of our work, Figures 6 and 7. The highest expectations are from the a-Ge slabs, owing to the promising spontaneously reconstructed surface – 5-caps and 6-caps with one or two **adatoms**, Figure 5 – that might serve as a condensation centers for clathrate cages.

5.1 Crystallization of Free-Standing Molten Si Slab

a-Si slabs, energetically unstable at 0 K with respect to both diamond and clathrate slabs for any **coverage** ρ , Figure 6, crystallize *exothermically* into diamond after annealing at $T_c \in [900 - 1100]$ K; the thicker slab the higher annealing temperature (due to the higher cohesive energy; $T_c = 1100$ K constituting the bulk limit). All of our a-Si slabs were prepared either by long **DFT MD** (on-the-fly VASP MLFF) annealing slightly below T_c or by **Replica Exchange** method covering the temperature range [400 K; T_c].

In particular, partial crystallization of 0.496 Å/Å²-thick a-Si slab into cF8 was accompanied by 36 meV/at. energy release while annealing at 900 K and cooling down to 300 K. a-Si slabs of cov-

erages $\rho = 0.602 \text{ at./\AA}^2$ and 0.688 at./\AA^2 lowered their internal energies by 28 meV/at. and 30 meV/at. during the same procedure, respectively. Crystallization of 0.779 at./\AA^2 -thick slab required annealing temperature at least 1000 K. The exothermic change of a-Si phase is an evidence that amorphous slabs can not compete with more stable diamond ones at 0 K at any coverage.

5.2 Crystallization of Free-Standing Molten Ge Slab

Unlike a-Si bulk surface containing exclusively p^3 -, sp^2 - and sp^3 -bonded atoms, Figure 4, a-Ge surface displays characteristic 5-caps and 6-caps with one or two **adatoms**, Figure 5, which can be regarded as nuclei of clathrate cages. Therefore we attempted to crystallize one of the most stable free-standing clathrate films – Ge.equi-II-3.5 – from the melt in fixed-volume simulation, Figure S6.1 (SM). Initial atomic configuration *before* melting can be found in Subsubsection S9.2.4 (SM).

Slow cooling down of 3000 K-melt to room temperature in 2×10^4 MD $\Delta t = 5 \text{ fs}$ -steps produced (from both faces) symmetrical disordered slab composed mainly of eclipsed hexagons and pentagons, 120 meV/at. above original clathrate Ge.equi-II-3.5 48-atom sample.

Subsequent annealing $520 \text{ K} \rightarrow 350 \text{ K}$ in 4×10^6 MLFF $\Delta t = 5 \text{ fs}$ -steps resulted in asymmetrical diamond film with dumbbell reconstruction from one side and kind of warts from the other, Figure S6.1 (SM). This diamond slab, not surprisingly, was still 45 meV/at. above initial clathrate Ge.equi-II-3.5 sample.

A couple of long zero-pressure MLFF annealings at 450 K (or 400 K) and subsequent slow cooling to room temperature – $\sim 10^6$ steps 5 fs each – of 192-atom sample [$2 \times 2 \times 1$ supercell of 48-atom Ge.equi-II-3.5 slab] in fixed periodic cell produced several characteristic 5-, 6- and even 7-cap features on the slab's surface like in Figure 5, but with no vital signs of a clathrate cage. Phase transition to the original clathrate slab (before melting) was prohibited by a kinetic barrier, as the slab got stuck in amorphous configuration. The same holds for 240-atom sample shown in Figure 5, starting from random atomic positions, annealed millions of 1 fs-steps at fixed 650 K temperature (of bulk a-Ge to cF8-Ge transition) and cooled to room temperature during $\sim 10^4$ steps (ought to be longer).

There was just one purely MD simulation (before the advent of MLFF in VASP) with 150-atom slab at fixed temperature 400 K, half million of 5 fs-steps long, starting from random atomic positions, that produced single reconstructed clathrate cage.

Since transformation of the-best-clathrate-slab melt into a diamond one (cubic, not lonsdaleite) was well reproducible in many Si and Ge cases of distinct thicknesses, we assume that clathrates are kinetically forbidden. Next we shall try to crystallize them on specially designed clathrate-matching substrates¹.

5.3 Crystallization of Molten Ge Slab on InN

Even more interesting is the (re)crystallization of the same molten Ge.equi-II-3.5 layer on coherent InN binary-diamond substrate. The coherency of such an interface was the objective of article¹, where it has been shown that InN wafer gives Ge type-II or type-III clathrate growth fundamental advantage: its bulk-lattice

misfit equals 2.3% instead of 12.6% misfit of Ge diamond film on the same InN substrate.

Recrystallization of Ge.equi-II-3.5 on InN led unexpectedly to a thin disordered Ge film connected with InN via a crystalline layer of regular 5-gons, Figure S6.2 (SM) [see Subsection S9.4.1 for initial xyz-file], 54 meV/at. above the original clathrate-diamond interface. The final result is probably due to the very 5-gonal buffer layer, which, as opposed to the coherent clathrate-diamond interface, saturates *all* the sp^3 bonds from the diamond side. As has been already pointed out¹, clathrate is able to saturate at most 6 out of 9 dangling bonds on the diamond surface, Figure S6.3. Even more can be observed: not just all bonds of the substrate are saturated, but all bond angles with vertices at the substrate atoms are around the ideal tetrahedral angle ($\approx 109.5^\circ$), Figures S6.5, S6.8. Ge melt constitutes an intermediate situation between Ge clathrate and recrystallized Ge layer from the point of view of bond angles; all N bonds are saturated even by the melt, Figures S6.4, S6.7.

The statement above holds for the nitrogen termination of InN substrate (from both sides), the more reactive element from the couple (In, N). If the substrate were terminated by In, it would not grant any benefit to an overlaying Ge clathrate at all. The same would be perhaps true for other electronically balanced substrates such as graphite or ZrO_2 , were it not for the covalent bonds e.g. between graphite and Ge-clathrate-film adatoms, already witnessed in DFT relaxations of our own.

When exactly the same experiment was carried out with thicker Ge layer, Ge.equi-II-6, the same 5-gonal buffer monolayer linked InN substrate with adjacent cubic-diamond Ge thin film, Figure S6.6 (SM), with some disordered mess on its outer surface. Thus it can be concluded that it is the very Ge buffer layer playing first fiddle on a N-terminated substrate. Mind, on the other hand, that the final diamond layer is by 38 meV/at. worse compared to the original clathrate-diamond setup, see Subsubsection S9.4.2 for the initial xyz-file, so the reason for diamond Ge output is kinetic, as well.

5.4 van der Waals Dispersion Correction

Karttunen et al. demonstrated that for silicon the dispersion interaction neglected in original PBE functional not only adds notable binding contribution of $\sim 0.3 \text{ eV/at.}$ to the bulk systems, but also impacts considerably on energy differences due to the approximately linear dependence of the dispersion energy on the *atomic density*⁶⁰. The same picture emerges also for germanium⁶¹. Both cited sources point out effectiveness of the Grimme's et al. dispersion correction implemented along PBE functional ("PBE-D3") in VASP^{62–64} in comparison with other ways of treating dispersion within the DFT framework. Thus the dispersion correction practically doubles ΔE between bulk clathrate and cubic diamond structure, from 50 to 100 meV/at. for Si, and from 30 to 90 meV/at. for Ge, concerning cubic type-II clathrate (Pearson cF136), owing to the somewhat higher density of the diamond phase⁶⁰.

However, the situation is different in the case of tin. According to references^{61, 65} binding energy of cubic-diamond α -Sn is

described accurately by PBE *without* dispersion correction, while PBE-D3 leads to overbinding by a clear margin. Added to this, PBE-D3 overestimates dramatically dispersion energy of the metallic β -Sn *reverting* ΔE between α and β from 42 meV/at. in favour of α to 43 meV/at. in favour of β (!). Since vibrational free energy privileges β (and we checked that the dispersion correction does not shift the phonon frequencies markedly), PBE-D3 contradicts the experimental fact the stable low-temperature phase being α up to approximately room temperature.

In Figure S7.1 (SM), the effect of PBE-D3 correction on our results for Si and Ge is displayed (IVDW=12 in VASP), but we refrain from doing the same for Sn.

Effect of a long-range dispersion interaction in general increases with the thickness of the slab culminating in bulk, so the thinnest films in the focus of the present study are afflicted to much lesser extent. Nevertheless – as expected, the range of clathrate-film stability has been considerably retrenched by dispersion correction for both Ge and Si.

The original interval of Ge clath-II stability, $\rho \in (2.5; 7.4)$ ML, Figure 6, reduced to $\rho \in (3; 5.5)$ ML, Figure S7.1, leaving single (out of 4 stable slabs without vdW) directly constructed thin film Ge.equi-II-3.5 of thickness (coverage) $\rho \approx 3.5$ ML on the overall convex hull: its energetic advantage over the diamond slab of the same coverage diminished from 34 meV/at. to 24 meV/at. (both below the diamond slab).

The original interval of Si clath-II stability, $\rho \in (2.5; 5.3)$ ML, Figure 6, reduced to $\rho \in (2.5; 4.0)$ ML, Figure S7.1, leaving solo (out of 3 stable slabs without vdW) directly constructed thin film Si.iso-II-2.5 of thickness (coverage) $\rho \approx 2.5$ ML on the overall convex envelope: its energetic benefit over the diamond slab of the same coverage lessened from 44 meV/at. to 23 meV/at. (both with respect to the diamond slab) as well.

6 Conclusions

This work exposes intervals of stability of several-ML thick clathrate layers, namely [2.5; 7.4] ML for Ge, [2.5; 5.3] ML for Si and [3.4; 10.0] ML for Sn, where ML stands for the unit thickness of (111)-diamond monolayer of the given element. Column-XIV slabs are stabilized by means of the surface energy in two respects: cheaper terminations and higher energy gain by reconstructions compared to the diamond films.

Natural planar clathrate terminations, as well as the recipe for their reconstructions have been described for the first time, being superior to their diamond counterparts from the point of view of the surface energy.

Combined (do)decagonal rectangle(square)-triangle clathrate tilings were not efficient in lowering internal energy per atom, with respect to the pure triangular ones.

Apart from clathrate thin films, we have discovered several Sn nanolayer phases during long MD runs at room temperature (200 – 400 K), namely Sn₉-web phase and hexagonal even-layers. In the latter case, the effect of entropy is playing decisive role in the layer stabilization since strongly defective triangular phase emerged at finite temperature and was presumably prepared during non-equilibrium processes³⁰, clearly far away (30 meV/at.)

from the ground-state.

Conflicts of interest

The author declares that she has no known competing financial interests or personal relationships that could have appeared to influence the work reported in this paper.

Data availability

The data supporting this article have been included as part of the Supplementary Information.

Acknowledgements

I acknowledge support from grants VEGA 2/0144/21, APVV-19-0369 and APVV-20-0124. I also acknowledge opportunity to write this article and finish the calculations after the defense of my dissertation thesis entitled “Search for Stable Clathrate Films within Elements from Column XIV of the Periodic Table” under supervisor Dr. Marek Mihalkovič, containing vast majority of material for this article, at the Institute of Materials and Machine Mechanics in Bratislava. Calculations were performed at the Computing Center of the Slovak Academy of Sciences using the supercomputing infrastructure acquired under Projects ITMS 26230120002 and 26210120002 and EuroHPC grant no. 101101903 (supercomputer Devana). Part of the research results was obtained using the computational resources procured in the national project National competence centre for high performance computing (project code: 311070AKF2) funded by European Regional Development Fund, EU Structural Funds Informatization of society, Operational Program Integrated Infrastructure.

References

- E. Pospišilová, M. Mihalkovič: Prediction of Coherent Interfaces between Diamond and Clathrate Structures, *Computational Materials Science*, **VOLUME 226**, 112228, <https://doi.org/10.1016/j.commatsci.2023.112228> (2023).
- G. Kresse and J. Furthmüller: Efficient iterative schemes for ab initio total-energy calculations using a plane-wave basis set, *PHYSICAL REVIEW B*, **VOLUME 54, ISSUE 16**, 11169, <https://link.aps.org/doi/10.1103/PhysRevB.54.11169> (1996).
- G. Kresse and D. Joubert: From ultrasoft pseudopotentials to the projector augmented-wave method, *PHYSICAL REVIEW B*, **VOLUME 59, ISSUE 3**, 1758, <https://link.aps.org/doi/10.1103/PhysRevB.59.1758> (1999).
- J. P. Perdew, J. A. Chevary, S. H. Vosko, K. A. Jackson, M. R. Pederson, D. J. Singh, and C. Fiolhais: Atoms, molecules, solids, and surfaces: Applications of the generalized gradient approximation for exchange and correlation, *PHYSICAL REVIEW B*, **VOLUME 46**, 6671, <https://link.aps.org/doi/10.1103/PhysRevB.46.6671> (1992).

- 5 P. Borlido et al.: Structural prediction of stabilized atomically thin tin layers, *npj 2D Materials and Applications*, **VOLUME 3, ISSUE 21**, <https://doi.org/10.1038/s41699> (2019).
- 6 B. Haberl, T. A. Strobel, and J. E. Bradby: Pathways to exotic metastable silicon allotropes, *Applied Physics Reviews* **VOLUME 3, ISSUE 4**, 040808, <https://doi.org/10.1063/1.4962984> (2016).
- 7 D. Sellı, I. A. Baburin, R. Martoňák: Novel metastable metallic and semiconducting germaniums, *Scientific Reports*, **VOLUME 3**, 1466, <https://doi.org/10.1038/srep01466> (2013).
- 8 V. Kumar Singh, E. Pospíšilová, M. Mihalkovič, S. R. Barman et al.: Decagonal Sn clathrate on *d*-Al-Ni-Co, *Physical Review B*, **VOLUME 107, ISSUE 4**, 045410, <https://link.aps.org/doi/10.1103/PhysRevB.107.045410> (2023).
- 9 K. Sudoh, M. Naito: Interfacial reaction during dewetting of ultrathin silicon on insulator, *Comptes Rendus Physique*, **VOLUME 14, ISSUE 7**, 601, <https://doi.org/10.1016/j.crhy.2013.06.008> (2013).
- 10 Peizhe Tang et al.: Stable two-dimensional dumbbell stanene: A quantum spin Hall insulator, *Physical Review B* **VOLUME 90, ISSUE 12**, 121408, <https://link.aps.org/doi/10.1103/PhysRevB.90.121408> (2014).
- 11 Ya-ping Wang et al.: Large-gap quantum spin Hall state in functionalized dumbbell stanene, *Applied Physics Letters* **VOLUME 108, ISSUE 7**, 073104, <https://doi.org/10.1063/1.4942380> (2016).
- 12 V. O. Özçelik, E. Durgun, and S. Ciraci: New Phases of Germanene, *The Journal of Physical Chemistry Letters* **VOLUME 5, ISSUE 15**, 2694, <https://doi.org/10.1021/jz500977v> (2014).
- 13 S. Hara, S. Izumi, T. Kumagai, S. Sakai: Surface energy, stress and structure of well-relaxed amorphous silicon: A combination approach of ab initio and classical molecular dynamics, *Surface Science*, **VOLUME 585, NUMBER 1**, 17, <https://doi.org/10.1016/j.susc.2005.03.061> (2005).
- 14 Haisheng Li et al.: Threadlike Tin Clusters with High Thermal Stability Based on Fundamental Units, *The Journal of Physical Chemistry C*, **VOLUME 116, ISSUE 1**, <https://doi.org/10.1021/jp208121s>, pg. 231 (2012).
- 15 Haisheng Li et al.: Tin Clusters Formed by Fundamental Units: A Potential Way to Assemble Tin Nanowires, *Physical Chemistry Chemical Physics*, **VOLUME 15, ISSUE 6**, <https://doi.org/10.1039/C2CP42948A>, pg. 1831 (2013).
- 16 J.-Y. Lee et al.: The surface energy and stress of metals, *Surface Science* **VOLUME 674**, 51, <https://doi.org/10.1016/j.susc.2018.03.008> (2018).
- 17 A. A. Stekolnikov, J. Furthmüller, and F. Bechstedt: Absolute surface energies of group-IV semiconductors: Dependence on orientation and reconstruction, *Physical Review B* **VOLUME 65, ISSUE 11**, 115318, <https://link.aps.org/doi/10.1103/PhysRevB.65.115318> (2002).
- 18 A. A. Stekolnikov and F. Bechstedt: Shape of free and constrained group-IV crystallites: Influence of surface energies, *Physical Review B* **VOLUME 72, ISSUE 12**, 125326, <https://link.aps.org/doi/10.1103/PhysRevB.72.125326> (2005).
- 19 G.-H. Lu, M. Huang, M. Cuma, F. Liu: Relative stability of Si surfaces: A first-principles study, *Surface Science* **VOLUME 588, ISSUE 1-3**, 61, <https://doi.org/10.1016/j.susc.2005.05.028> (2005).
- 20 G. V. Gadiyak, Yu. N. Morokov, A. S. Kushkova, S. M. Repinskii, and A. A. Shklyaev: Calculation of Wulff's diagram for germanium, *Physics, Chemistry and Mechanics of Surfaces* **VOLUME 3, NUMBER 7**, 1978 (1985).
- 21 G. V. Gadiyak, A. A. Karpushin, A. S. Kushkova, Yu. N. Morokov, S. M. Repinsky, A. A. Shklyaev: Wulff's Diagram for the Surfaces of Silicon and Germanium. Quantum Chemical Calculation, *Physics, Chemistry and Mechanics of Surfaces* **VOLUME 3** (1988).
- 22 "Materials Project, Materials Virtual Lab," <http://crystalium.materialsvirtuallab.org/>, accessed: 2024-08-08.
- 23 R. Zhachuk, S. Teys, J. Coutinho: Strain-induced structure transformations on Si(111) and Ge(111) surfaces: a combined density-functional and scanning tunneling microscopy report, *The Journal of Chemical Physics* **VOLUME 138, ISSUE 22**, 224702, <https://doi.org/10.1063/1.4808356> (2013).
- 24 R. Zhachuk, J. Coutinho, A. Dolbak, V. Cherepanov, and B. Voigtländer: Si(111) strained layers on Ge(111): Evidence for c(2×4) domains, *Physical Review B* **VOLUME 96, ISSUE 8**, 085401, <https://link.aps.org/doi/10.1103/PhysRevB.96.085401> (2017).
- 25 R. A. Zhachuk, and J. Coutinho: Crucial role of vibrational entropy in the Si(111)-7 × 7 surface structure stability, *Physical Review B* **VOLUME 105, ISSUE 24**, 245306, <https://link.aps.org/doi/10.1103/PhysRevB.105.245306> (2022).
- 26 F. C. Frank, J. S. Kasper: Complex Alloy Structures Regarded as Sphere Packings. I. Definitions and Basic Principles, *Acta Crystallographica*, **VOLUME 11**, 184, <https://doi.org/10.1107/S0365110X58000487> (1958).
- 27 F. C. Frank, J. S. Kasper: Complex Alloy Structures Regarded as Sphere Packings. II. Analysis and Classification of Representative Structures, *Acta Crystallographica*, **VOLUME 12**, 483, <https://doi.org/10.1107/S0365110X59001499> (1959).
- 28 B. Wehinger et al.: Diffuse scattering in metallic tin polymorphs, *Journal of Physics: Condensed Matter*, **VOLUME 26, ISSUE 11**, 115401, <https://iopscience.iop.org/article/10.1088/0953> (2014).
- 29 R. Kubiak: Evidence for the Existence of the γ Form of Tin, *Journal of the Less-Common Metals*, **VOLUME 116, ISSUE 2**, 307, <https://doi.org/10.1016/0022> (1986).
- 30 S. Saxena, R. P. Chaudhary & S. Shukla: Stanene: Atomically Thick Free-standing Layer of 2D Hexagonal Tin, *Scientific Reports*, **VOLUME 6**, 31073,

- <https://doi.org/10.1038/srep31073>, (2016).
- 31 G. Bergmann: Upper Critical Field and the Density of States in Amorphous Superconductors, *Physical Review B*, **VOLUME 7, ISSUE 11**, 4850, https://doi.org/10.1007/978-1-4612-6530-7_11 (1973).
 - 32 K. Knorr, N. Barth: Investigation of disordered Sn-films by superconducting tunneling, *Solid State Communications*, **VOLUME 6, ISSUE 11**, 791, [https://doi.org/10.1016/0038-1098\(68\)90011-7](https://doi.org/10.1016/0038-1098(68)90011-7) (1968).
 - 33 W. Buckel: Superconductivity and Metastable Phases in Thin Films, *Journal of Vacuum Science & Technology*, **VOLUME 10, ISSUE 5**, 599, <https://doi.org/10.1116/1.1318397> (1973).
 - 34 M. Vergnat, G. Marchal, and Ph. Mangin: Preparation and structure of amorphous semiconductor hydrogenated tin, *Applied Physics Letters*, **VOLUME 57, ISSUE 22**, 2300, <https://doi.org/10.1063/1.103893> (1990).
 - 35 L. K. Nanver, G. Weyer, and B. I. Deutch: Experimental Study of the Amorphous Phases of Group-IV Semiconductors by the 119m Sn Mössbauer Probe, *Zeitschrift für Physik B Condensed Matter*, **VOLUME 47, ISSUE 2**, 103, <https://doi.org/10.1007/BF01441292> (1982).
 - 36 P. Li, W. Fu, P. Zhuang, Y. Cao, C. Tang, A. B. Watson, P. Dong, J. Shen, M. Ye: Amorphous Sn/Crystalline SnS₂ Nanosheets via In Situ Electrochemical Reduction Methodology for Highly Efficient Ambient N₂ Fixation, *Small*, **VOLUME 15, ISSUE 40**, 1902535, <https://doi.org/10.1002/smll.201902535> (2019).
 - 37 M. Ryník, S. Leoni, and R. Martoňák: Pressure-induced structural transformation of clathrate Ge₁₃₆ via an ultrafast recrystallization of an amorphous intermediate, *Physical Review B*, **VOLUME 105, ISSUE 13**, 134107, <https://link.aps.org/doi/10.1103/PhysRevB.105.134107> (2022).
 - 38 V. V. Brazhkin, A. G. Lyapin, S. V. Popova, and R. N. Voloshin: Nonequilibrium phase transitions and amorphization in Si, Si/GaAs, Ge, and Ge/Gash at the decompression of high-pressure phases, *Physical Review B*, **VOLUME 51, ISSUE 12**, 7549, <https://link.aps.org/doi/10.1103/PhysRevB.51.7549> (1995).
 - 39 Liang Xu et al.: Folded network and structural transition in molten tin, *Nature Communications*, **VOLUME 13**, 126, <https://doi.org/10.1038/s41467> (2022).
 - 40 P. Biswas, R. Atta-Fynn, and D. A. Drabold: Reverse Monte Carlo modeling of amorphous silicon, *Physical Review B*, **VOLUME 69, ISSUE 19**, 195207, <https://link.aps.org/doi/10.1103/PhysRevB.69.195207> (2004).
 - 41 J. Fortner and J. S. Lannin: Radial distribution functions of amorphous silicon, *Physical Review B*, **VOLUME 39, NUMBER 8**, 5527, <https://link.aps.org/doi/10.1103/PhysRevB.39.5527> (1989).
 - 42 E. Guerrero, and D. A. Strubbe: Structural changes and void generation in low-density amorphous silicon: a computational study, *arXiv preprint arXiv:1907.01327*, <https://escholarship.org/content/qt4mz432s1/qt4mz432s1>
 - 43 A. Pedersen, L. Pizzagalli and H. Jónsson: Optimal atomic structure of amorphous silicon obtained from density functional theory calculations, *New Journal of Physics*, **VOLUME 19, NUMBER 6**, 063018, <https://iopscience.iop.org/article/10.1088/1367-2630/aa5b4f> (2017).
 - 44 R. V. Meidanshahi, S. Bowden and S. M. Goodnick: Electronic structure and localized states in amorphous Si and hydrogenated amorphous Si, *Physical Chemistry Chemical Physics*, **VOLUME 21, ISSUE 24**, 13248, <https://doi.org/10.1039/C9CP01121H> (2019).
 - 45 I. Štich, R. Car, M. Parrinello: Amorphous silicon studied by ab initio molecular dynamics: Preparation, structure, and properties, *Physical Review B*, **VOLUME 44, NUMBER 20**, 11092, <https://link.aps.org/doi/10.1103/PhysRevB.44.11092> (1991).
 - 46 D. Choudhary and P. Clancy: Characterizing the nature of virtual amorphous silicon, *The Journal of Chemical Physics* **VOLUME 122, ISSUE 17**, 174509 (2005).
 - 47 R. Li, E. Lee, T. Luo: A unified deep neural network potential capable of predicting thermal conductivity of silicon in different phases, *Materials Today Physics*, **VOLUME 12**, 100181, <https://doi.org/10.1016/j.mtphys.2020.100181> (2020).
 - 48 H. M. Shodja, M. Tabatabaei and K. Esfarjani: First principles molecular dynamics studies of elastic constants, ideal tensile strength, chemistry of crack initiation, and surface and cohesive energies in amorphous silicon, *Philosophical Magazine*, **VOLUME 94, NUMBER 25**, 2913, <https://doi.org/10.1080/14786435.2014.939735> (2014).
 - 49 I. Santos , M. Aboy, L. A. Marqués, P. López, L. Pelaz: Generation of amorphous Si structurally compatible with experimental samples through the quenching process: A systematic molecular dynamics simulation study, *Journal of Non-Crystalline Solids*, **VOLUMES 503-504**, 20, <https://doi.org/10.1016/j.jnoncrysol.2018.09.024> (2019).
 - 50 A. Pedersen, L. Pizzagalli, and H. Jónsson: Atomic and electronic structures of a vacancy in amorphous silicon, *Physical Review B*, **VOLUME 101, ISSUE 5**, 054204, <https://link.aps.org/doi/10.1103/PhysRevB.101.054204> (2020).
 - 51 Y. Furukawa and Y. Matsushita: First-Principles Prediction of Densities of Amorphous Materials: The Case of Amorphous Silicon, *Journal of the Physical Society of Japan*, **VOLUME 87, NUMBER 2**, 024701, <https://doi.org/10.48550/arXiv.1704.06107> (2017).
 - 52 J. S. Custer et al.: Density of amorphous Si, *Applied Physics Letters*, **VOLUME 64, ISSUE 4**, 437, <https://doi.org/10.1063/1.111121> (1994).
 - 53 C. Messmer, J. C. Bilello: The surface energy of Si, GaAs, and GaP, *Journal of Applied Physics*, **VOLUME 52, ISSUE 7**, 4623, <https://doi.org/10.1063/1.329342> (1981).
 - 54 R. J. Jaccodine: Surface Energy of Germanium and Silicon, *Journal of The Electrochemical Society*, **VOLUME 110, NUMBER 6**, 524,

- <https://iopscience.iop.org/article/10.1149/1.2425806> (1963).
- 55 J. J. Gilman: Direct Measurements of the Surface Energies of Crystals, *Journal of Applied Physics*, **VOLUME 31, ISSUE 12**, 2208, <https://doi.org/10.1063/1.1735524> (1960).
- 56 A. Mujica, C. J. Pickard, R. J. Needs: Low-energy tetrahedral polymorphs of carbon, silicon, and germanium, *Physical Review B*, **VOLUME 91, ISSUE 21**, 214104, <https://link.aps.org/doi/10.1103/PhysRevB.91.214104> (2015).
- 57 C. J. Pickard, R. J. Needs: Hypothetical low-energy chiral framework structure of group 14 elements, *Physical Review B*, **VOLUME 81, ISSUE 1**, 014106, <https://link.aps.org/doi/10.1103/PhysRevB.81.014106> (2010).
- 58 J. Conesa: Computer Modeling of allo-Si and allo-Ge Polymorphs, *The Journal of Physical Chemistry B* **VOLUME 106, ISSUE 13**, 3402, <https://doi.org/10.1021/jp014115g> (2002).
- 59 Z. Zhao et al.: Tetragonal Allotrope of Group 14 Elements, *Journal of the American Chemical Society*, **VOLUME 134, NUMBER 30**, 12362, <https://doi.org/10.1021/ja304380p> (2012).
- 60 A. J. Karttunen, D. Usvyat, M. Schütz and L. Maschio: Dispersion interactions in silicon allotropes, *Physical Chemistry Chemical Physics* **VOLUME 19, ISSUE 11**, 7699, <https://doi.org/10.1039/C6CP08873B> (2017).
- 61 F. Tran, J. Stelzl, P. Blaha: Rungs 1 to 4 of DFT Jacob's ladder: Extensive test on the lattice constant, bulk modulus, and cohesive energy of solids, *The Journal of Chemical Physics* **VOLUME 144, ISSUE 20**, 204120, <https://doi.org/10.1063/1.4948636> (2016).
- 62 S. Grimme, J. Antony, S. Ehrlich, H. Krieg: A consistent and accurate ab initio parametrization of density functional dispersion correction (DFT-D) for the 94 elements H-Pu, *The Journal of Chemical Physics* **VOLUME 132, ISSUE 15**, 154104, <https://doi.org/10.1063/1.3382344> (2010).
- 63 S. Grimme, S. Ehrlich, L. Goerigk: Effect of the damping function in dispersion corrected density functional theory, *Journal of Computational Chemistry* **VOLUME 32**, 1456, <https://doi.org/10.1002/jcc.21759> (2011).
- 64 S. Grimme: Density functional theory with London dispersion corrections, *WIREs Computational Molecular Science* **VOLUME 1**, 211, <https://doi.org/10.1002/wcms.30> (2011).
- 65 “P. Blaha and F. Tran: DFT approximations: Which one to use?” <https://dokumen.tips/documents/dft-approximations-which-one-to-use-p-blaha-and-f-tran.html>, institute of Materials Chemistry, TU Wien, lecture, pg. 8.

Supplemental Material

Table of Contents

- S1. Comparison of Column-XIV Bulk Energies**
- S2. Surface Reconstruction of Decagonal Clathrate Tiles**
- S3. Surface Reconstruction of Dodecagonal Clathrate Tiles**
- S4. Reconstructed vs. Unreconstructed Surfaces**
- S5. Energy-Comparison of Various Types of Clathrate Slabs**
- S6. Crystallization of Clathrate Slabs from the Melt**
- S7. van der Waals Dispersion Correction of G4 Slabs**
- S8. Electronic Density of States: Clathrate Slabs & Bulk**
- S9. xyz Files**
 - S9.1 Tin-Slab xyz Files**
 - S9.1.1 Sn9-web**
 - S9.1.2 triangles**
 - S9.1.3 squares**
 - S9.1.4 Sn.equi-II-3**
 - S9.1.5 Sn.equi-II-5**
 - S9.1.6 Sn.equi-II-7.5**
 - S9.1.7 Sn.equi-II-10**
 - S9.2 Germanium-Slab xyz Files**
 - S9.2.1 Ge.db-monolayer (oP10)**
 - S9.2.2 Ge.iso-II-2.5**

S9.2.3 Ge.equi-II-3

S9.2.4 Ge.equi-II-3.5

S9.2.5 Ge.iso-II-4

S9.2.6 Ge.equi-II-6

S9.3 Silicon-Slab xyz Files

S9.3.1 Si.db-monolayer (oP10)

S9.3.2 Si.iso-II-2.5

S9.3.3 Si.equi-II-3

S9.3.4 Si.iso-II-4

S9.3.5 Si.iso-II-5

S9.4 Ge-Clathrate/InN

S9.4.1 Thinner Ge Clathrate Film on InN

S9.4.2 Thicker Ge Clathrate Film on InN

S1. Comparison of Column-XIV Bulk Energies

Config.	C	Si	Ge	Sn	Pb
fcc	4573	608	331	75	-3.598
bcc	4367	587	341	86	42
graphite	-9.231	640	602	570	719
hP1	971	352	243	45	96
tI4	cF8	328	228	46	128
cF8	131	-5.420	-4.516	-3.863	251
lonsdaleite	155	11	18	16	292
clathI	239	64	33	28	279
clathII	205	54	27	23	280
clathIII	260	81	48	40	288
clathIV	243	69	38	31	276*
deca	241	71	41	35	299*
icosa	288	92	59	49	274*
CFS-6	241	55	35	30	286
CFS-5	263	41	39	36	289
T12	238	45	36	32	278
amorph	–	158	128	91–101	–

Table S1.1: Bulk energies of famous Column-XIV allotropes, that were taken into slab internal-energy competition, see Section 3 in the main text. Internal energies of 17 bulk configurations of G4 elements after cell and atomic relaxations starting from sound initial atomic positions and lattice parameters. cF8 stands for the cubic diamond phase; lonsdaleite (wurtzite) is the hexagonal diamond polytype with eclipsed bond conformations. “deca” stands for “decagonal clathrate approximant”, *Pearson symbol* oP392. “icosa” means “icosahedral clathrate approximant”, cI920. „clathI” (cP46), “clathII” (cF136), “clathIII” (hP40) and “clathIV” (tP172) denotes type I, II, III and IV clathrate, respectively. “CFS” means Chiral Framework Structures (including T12), see Subsection 3.6 (of the main text). “amorph” denotes sp^3 -amorphous phases of Ge and Si, visit Subsection 3.5; for Sn the lower bound corresponds to a-metal, whereas upper bound to an abstract a- sp^3 Sn obtained by a-Ge rescaling to the typical Sn interatomic distances. Kohn-Sham energies in eV/atom of the most stable (GS) structures are **highlighted by red**. GS energies have been subtracted from the remaining energies and the corresponding differences $E - E_{GS}$ are stated in units of meV/atom for easier comparison of *distinct* elements. * – amorphized or strongly deformed during relaxation process. Without former annealing or external strain. Converged on K-points with default VASP DFT PAW GGA (PW91) ENCUT-s.

S2. Surface Reconstruction of Decagonal Tiles

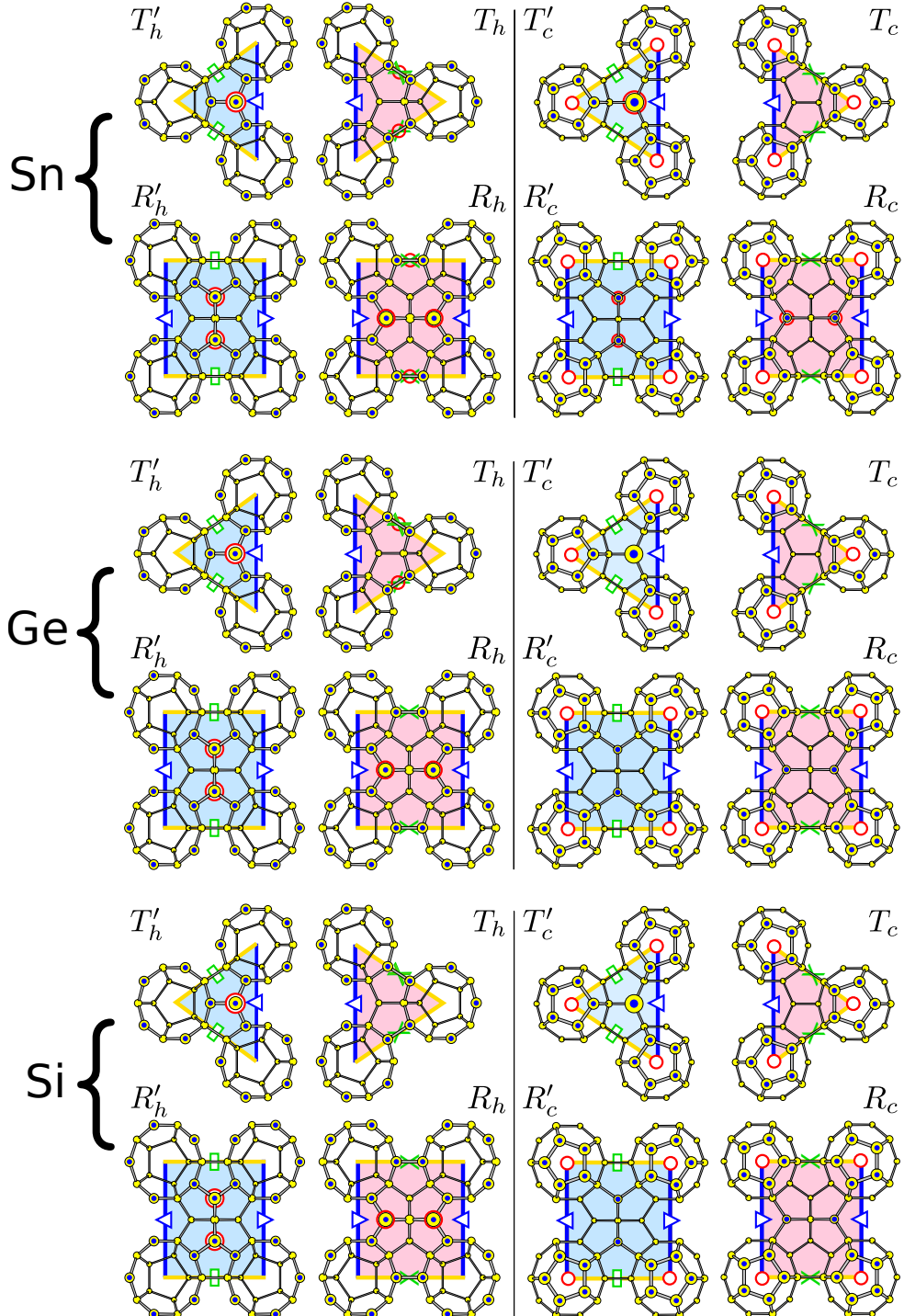


Figure S2.1: Reconstruction of *decagonal* Sn, Ge, Si clathrate tiles: isosceles triangle (T) and rectangle (R) terminated by cage “caps” (c) and “holes” (h). Adatoms (beneath the original atoms, inside the film) highlighted by red rings. 3-coord. atoms before the reconstruction marked with central blue dots, the rest are 4-coord. atoms. Side lengths distinguished by blue (longer) and yellow (shorter) color. Sides that fit together marked with green crosses, rectangles.

S3. Surface Reconstruction of Dodecagonal Tiles

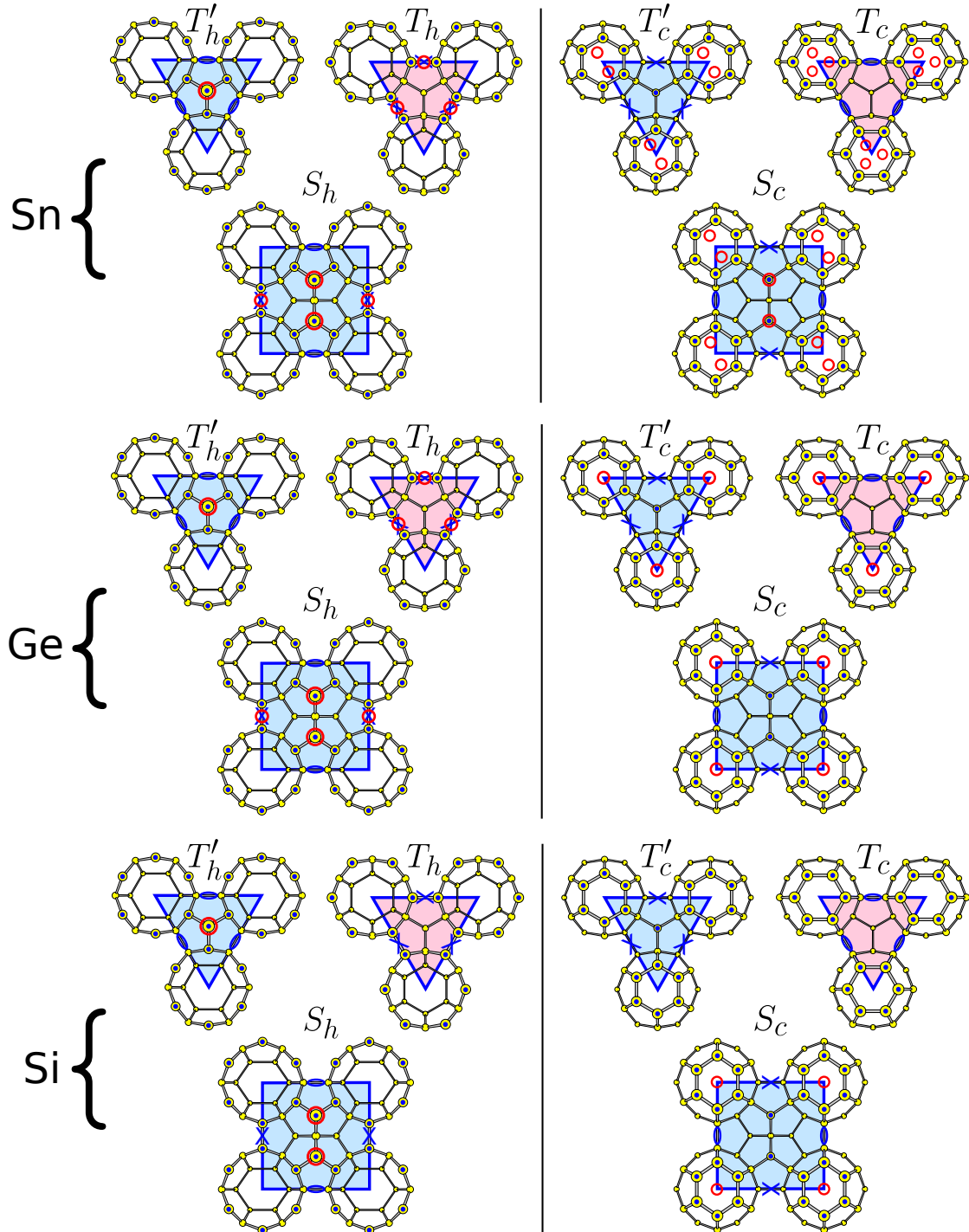


Figure S3.1: Optimal reconstruction of *dodecagonal* Sn, Ge and Si clathrate tiles: equilateral triangle (T) and square (S) terminated by cage “caps” (c) and “holes” (h). For the explanation of the symbols and color scheme, consult Figure S2.1. Note that placing the “caps” on the top of the “holes” does not change the number of unsaturated 3-coordinated atoms (distinguished by blue central dots); this holds also for the decagonal cases, see Figure S2.1.

S4. Reconstructed vs. Unreconstructed Surfaces

Figures S4.1 and S4.3 below implies that Sn and Si clathrate slabs possess clear energetic advantage over the corresponding (111)-diamond films of the same coverage already *before* surface reconstruction (addition of Si atoms to the slab's surface followed by atomic-position DFT relaxation). However, the appropriate surface reconstruction is responsible for further energy decrease of clathrates with respect to the diamond rivals.

Notably, as can be observed in Figure S4.2, the opposite situation happens for Ge, where clathrate's internal-energy advantage over diamond is markedly more pronounced for the *unreconstructed* slabs.

In all the graphs below, the region of clathrate film stability is highlighted by green shadow, compare with Figure 6 of the main text. Reconstructed slabs correspond to the unreconstructed structures (“reconstructed” = “unreconstructed” + adatoms) in each case. As for the reconstructed ones, the most stable clathrate and diamond films for each coverage ρ from Figure 6 of the main text were chosen for comparison, confer Results section.

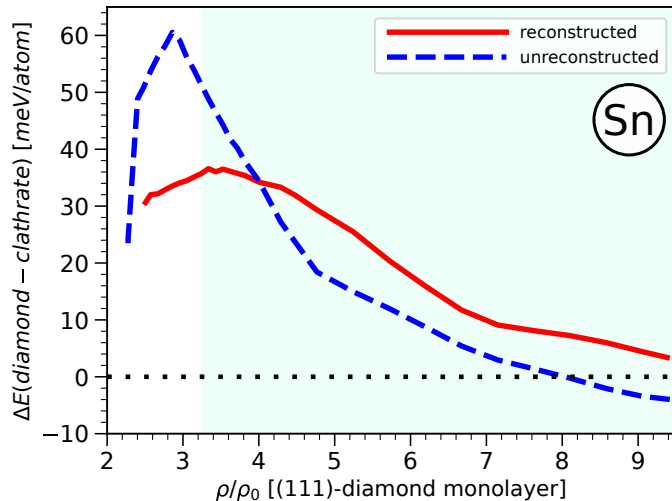


Figure S4.1: Comparison of per-atom energy difference between the most stable Sn clathrate slabs and Sn (111)-diamond ones for reconstructed and unreconstructed case.

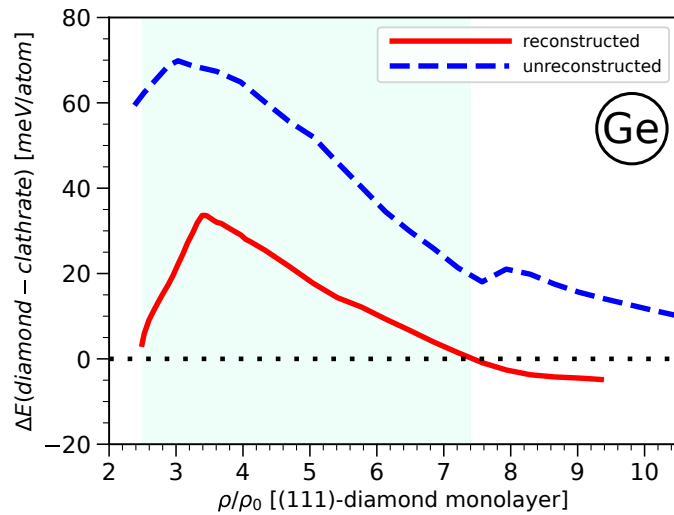


Figure S4.2: Comparison of per-atom energy difference between the most stable Ge clathrate slabs and Ge (111)-diamond ones for reconstructed and unreconstructed case.

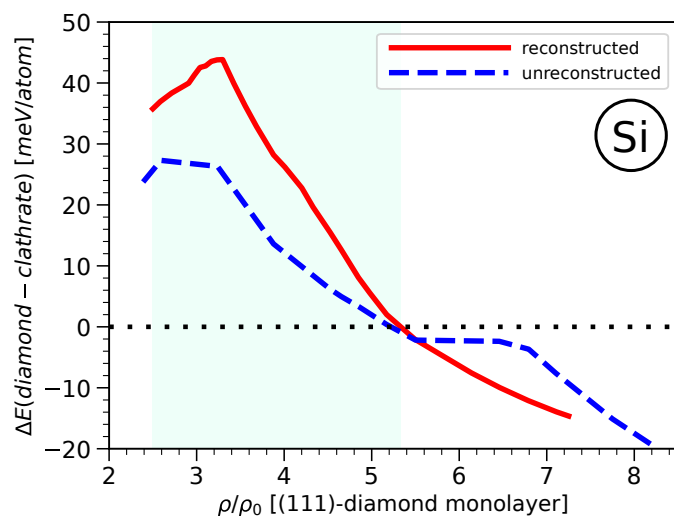


Figure S4.3: Comparison of per-atom energy difference between the most stable Si clathrate slabs and Si (111)-diamond ones for reconstructed and unreconstructed case.

S5. Comparison of Various Types of Clathrate Slabs

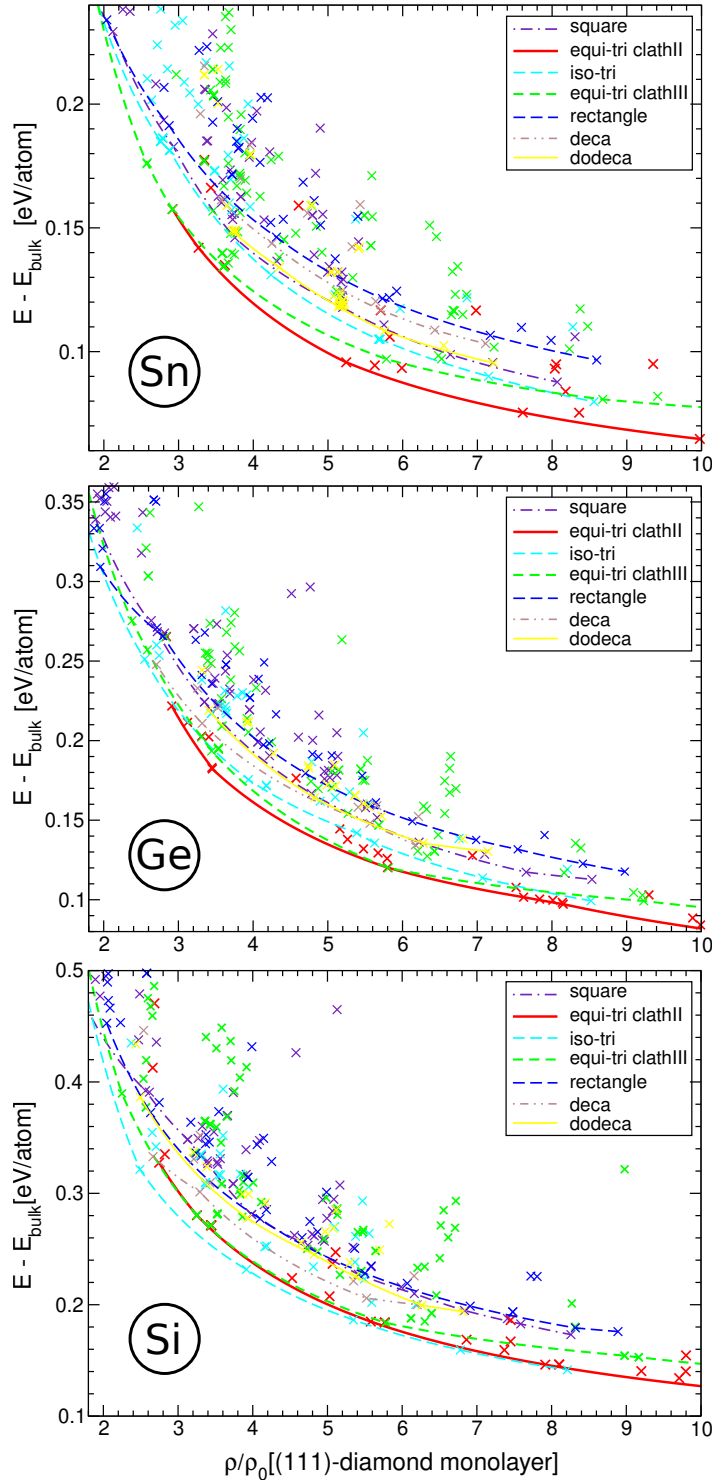


Figure S5.1: Stability comparison (DFT energy per atom at 0K) of seven types of Sn, Ge and Si clathrate thin films: clath-I square, clath-II equilateral triangle, clath-II isosceles triangle, clath-III equilateral triangle and rectangle, decagonal and clath-IV dodecagonal tiling reconstructed according to Figures S2.1, S3.1. Each cross represents one attempt for clath-tile reconstruction.

S6. Crystallization of Clathrate Slabs from the Melt

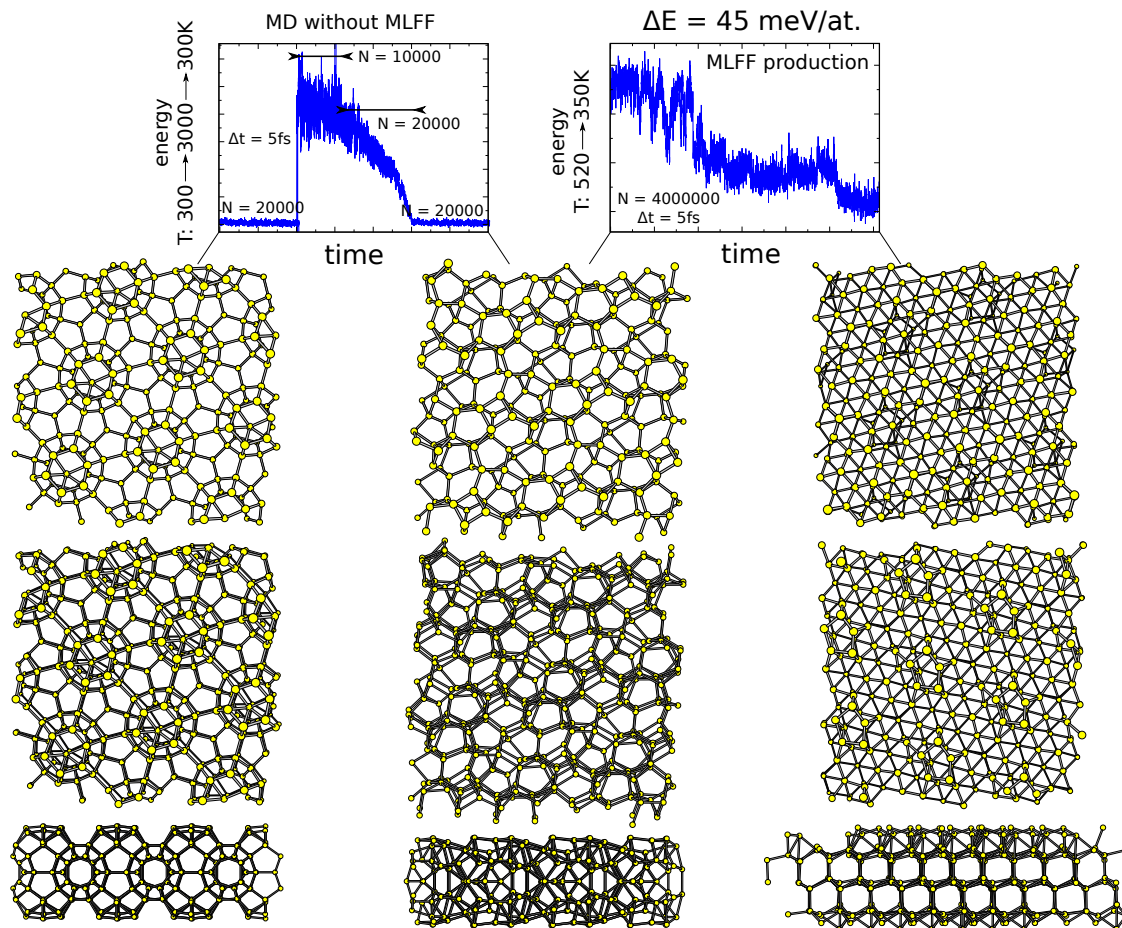


Figure S6.1: Spontaneous re-crystallization of free-standing initially symmetrical Ge film, sample designated as Ge.equi-II-3.5 in the main text, see Subsubsection S9.2.4 for the atomic coordinates.

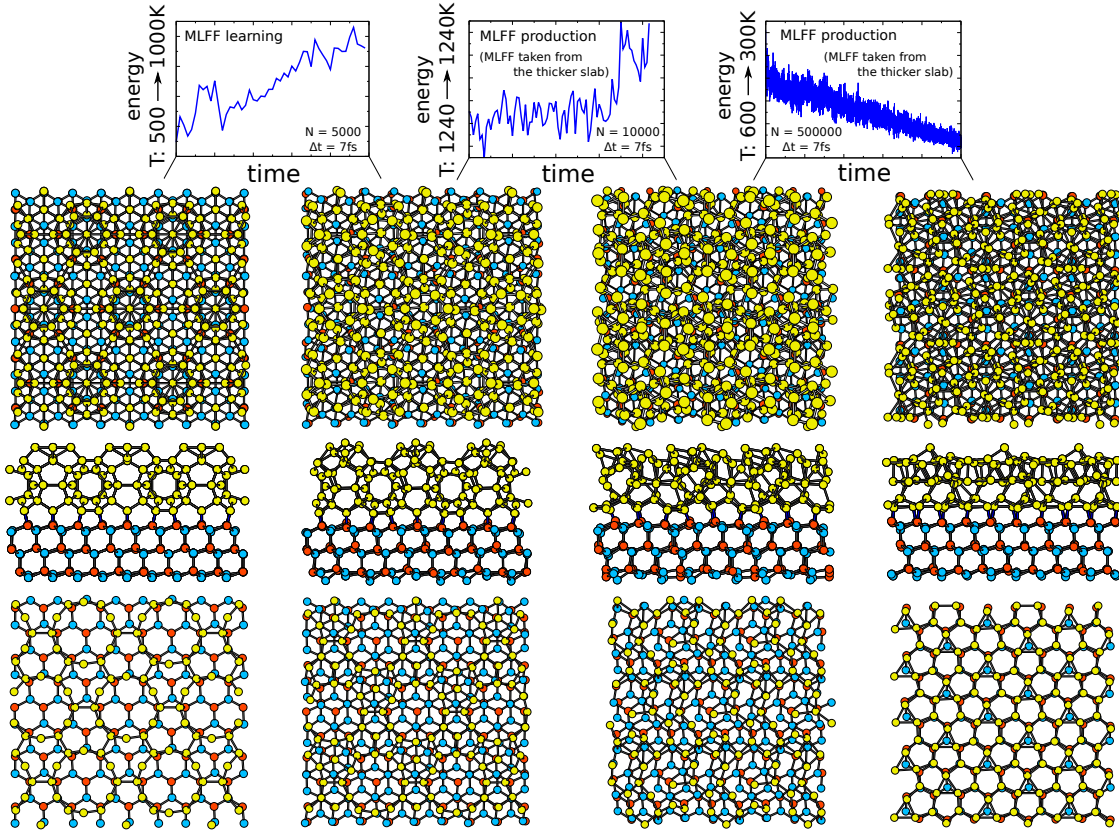


Figure S6.2: Spontaneous re-crystallization of Ge films on InN. Starting from the thinnest clathrate film with 6-caps, see Subsubsection S9.4.1 for the atomic coordinates.

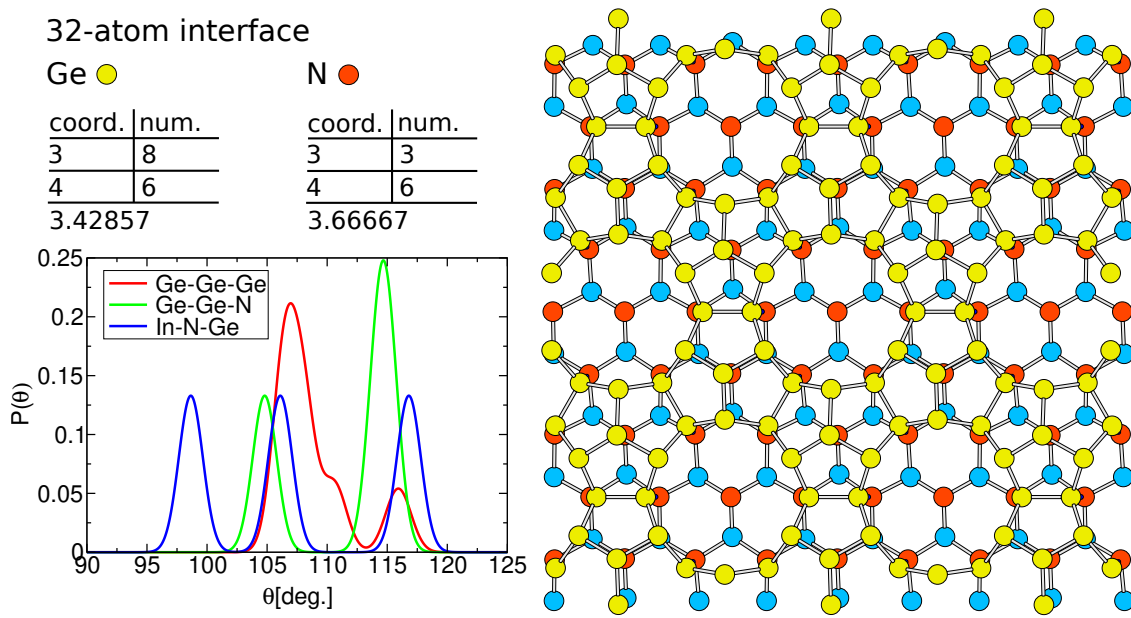


Figure S6.3: Coherent clathrate/diamond interface made up of Ge/InN.

32-atom interface

Ge	coord.	num.
2	4	
3	2	
4	7	
6	1	
3.42857		

N	coord.	num.
4	9	
4.0		

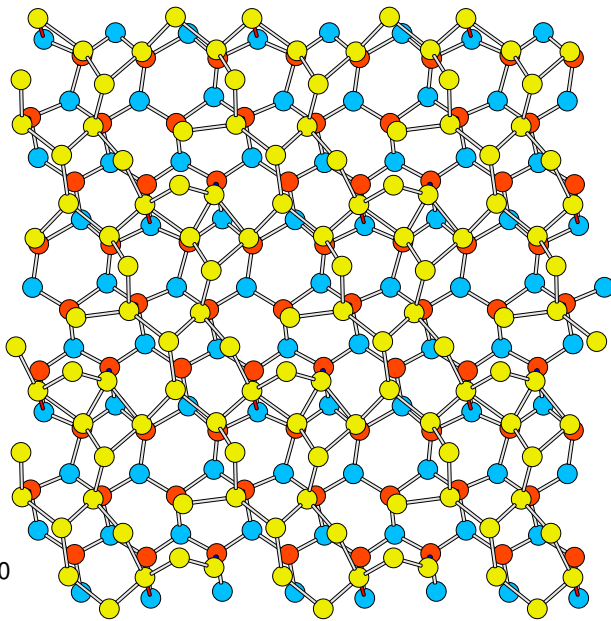
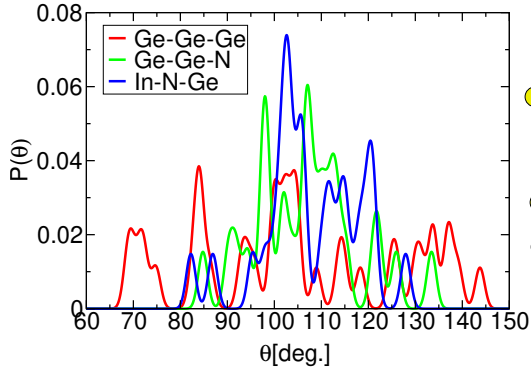


Figure S6.4: Interface between diamond and clathrate melt after $N = 10000$ $dt = 7$ fs-steps at 1240 K, according to roadmap S6.2.

33-atom interface

Ge	coord.	num.
3	6	
5	9	
4.2		

N	coord.	num.
4	9	
4.0		

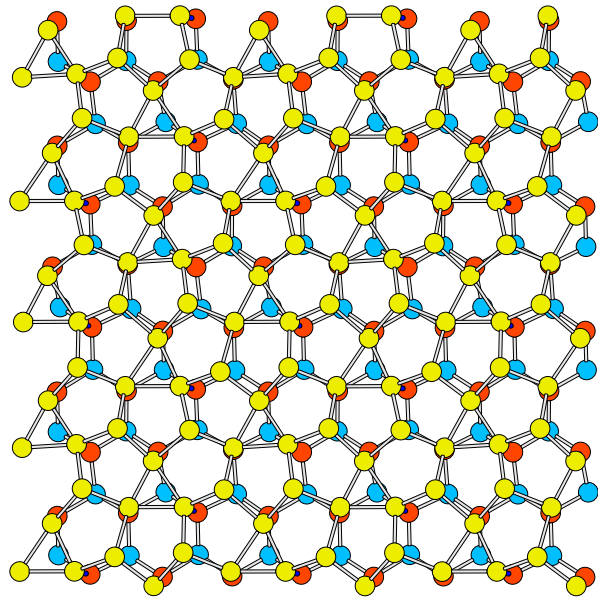
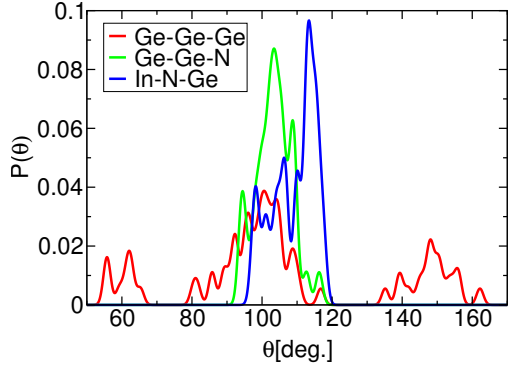


Figure S6.5: Interface between diamond and re-crystallized clathrate melt according to Figure S6.2.

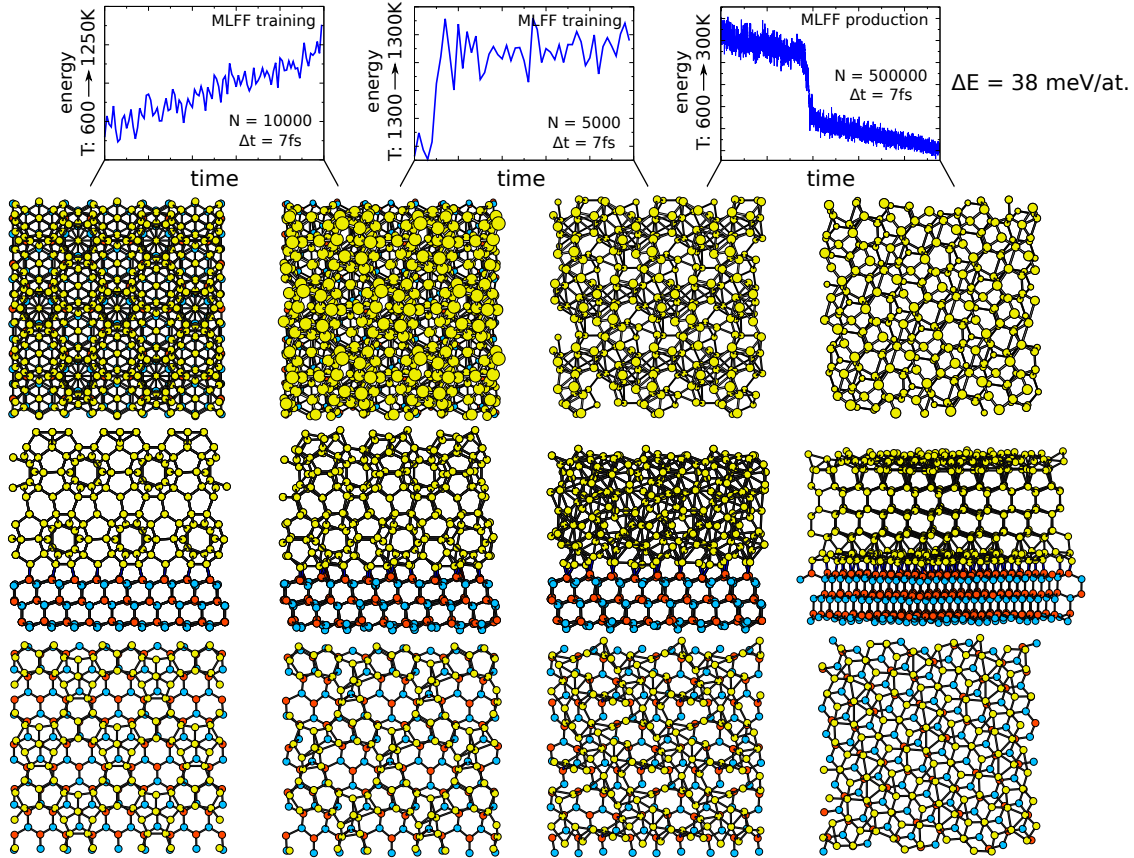


Figure S6.6: Spontaneous re-crystallization of Ge films on InN. Starting from thicker clathrate film with 6-caps, see Subsubsection S9.4.2 for the atomic coordinates.

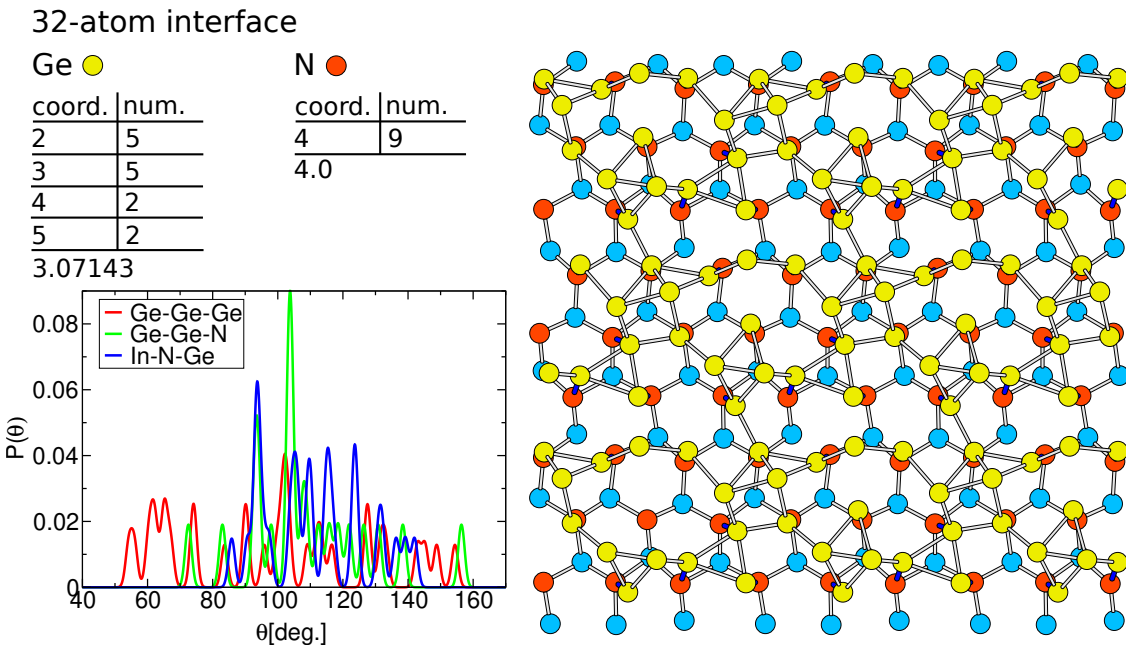


Figure S6.7: Interface between diamond and clathrate melt after $N = 5000$ $dt = 7$ fs-steps at 1300 K, according to Figure S6.6.

33-atom interface

Ge ●

coord.	num.
3	6
4	6
5	3

N ●

coord.	num.
4	9

4.0

3.8

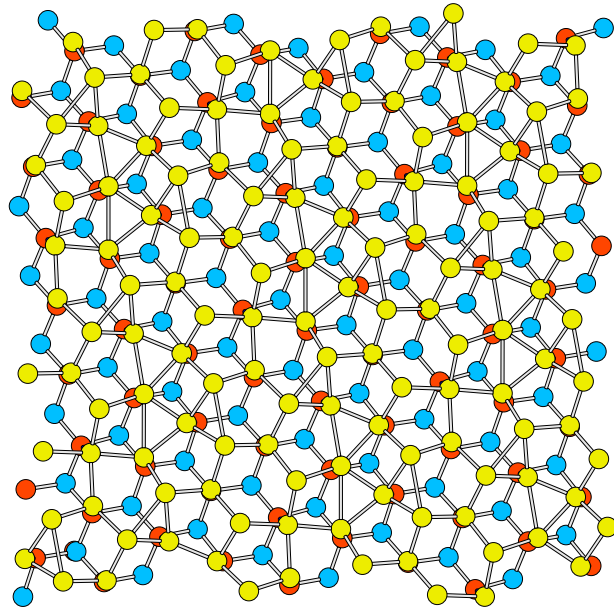
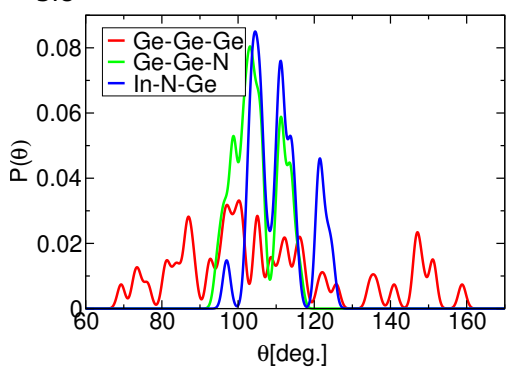


Figure S6.8: Interface between diamond and re-crystallized clathrate melt according to Figure S6.6.

S7. van der Waals Dispersion Correction of G4 Slabs

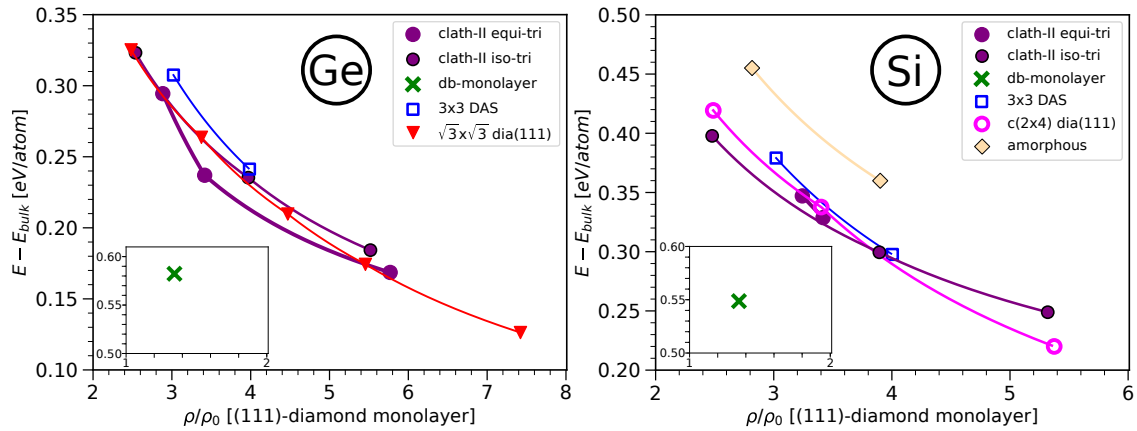


Figure S7.1: Change of the diamond-clathrate stability competition in response to the van der Waals dispersion correction PBE-D3 (ivdw=12), visit Subsection 5.4 in the main text.

S8. Electronic Density of States: Clathrate Slabs & Bulk

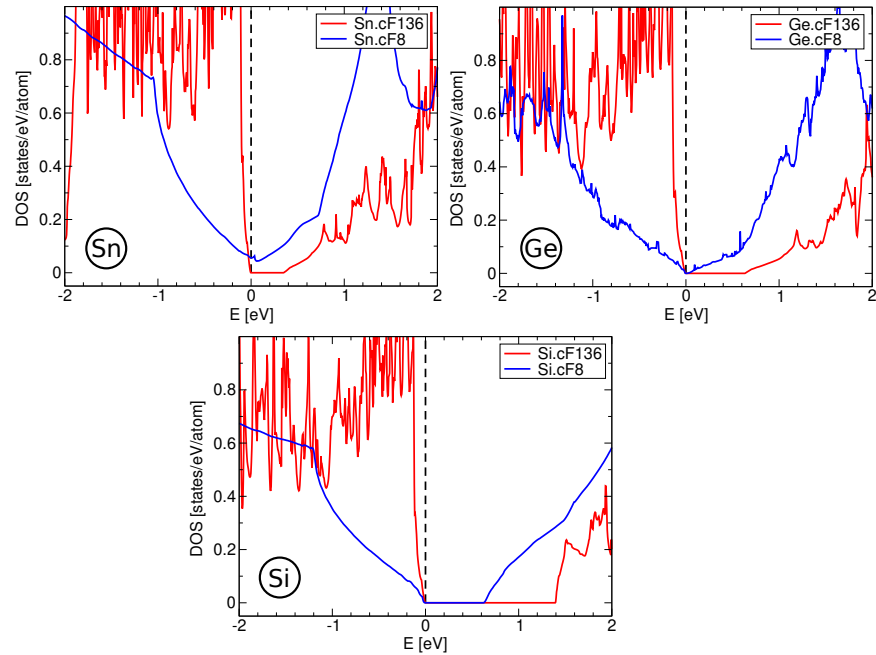


Figure S8.1: Electronic Density of States, eDOS, of the bulk type-II clathrates (cF136) compared with bulk diamond (cF8) for Sn, Ge and Si. Fermi energy, E_F , is designated by the vertical thick dashed line.

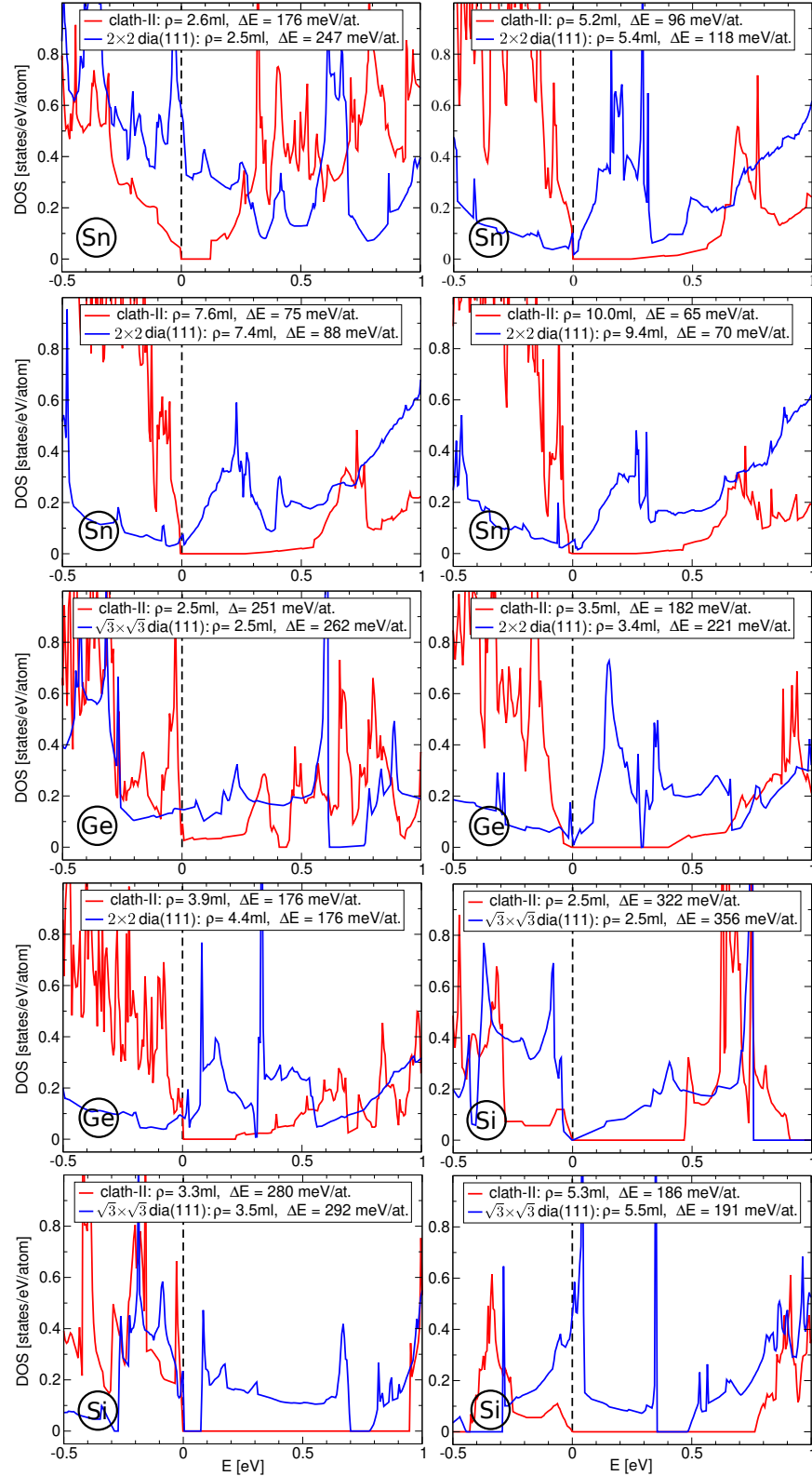


Figure S8.2: Electronic Density of States, eDOS, of the most stable clathrate slabs, compared with that of the competitive diamond slabs of approximately the same thickness ρ . Fermi energy, E_F , is designated by vertical thick dashed line. Visit Subsection 4.4 in the main text.

S9. xyz Files

S9.1 Tin-Slab xyz Files

S9.1.1 Sn9-web

$\rho = 0.1749 \text{ \AA}^{-2} = 1.667 \text{ ML}$, $E - E_{\text{bulk}} = 216 \text{ meV/at.}$

23.9138	0.00000	0.00000				
0.00000	23.9138	0.00000				
0.00000	0.00000	23.9138				
100 atoms						
0.96713	0.89507	0.02979	50	1	1	
0.18163	0.30665	0.95156	50	2	2	
0.00243	0.36734	0.04387	50	3	3	
0.11868	0.91534	0.92111	50	4	4	
0.18669	0.44073	0.96766	50	5	5	
0.12692	0.38930	0.86865	50	6	6	
0.81752	0.94640	0.91512	50	7	7	
0.22004	0.78823	0.05703	50	8	8	
0.88308	0.80335	0.06302	50	9	9	
0.94704	0.92053	0.90656	50	10	10	
0.08813	0.54847	0.12274	50	11	11	
0.30671	0.70521	0.98685	50	12	12	
0.04241	0.44174	0.94857	50	13	13	
0.19810	0.35715	0.06952	50	14	14	
0.86364	0.84115	0.85282	50	15	15	
0.19066	0.17224	0.99467	50	16	16	
0.42224	0.74919	0.03300	50	17	17	
0.70438	0.93414	0.08492	50	18	18	
0.54387	0.91304	0.98796	50	19	19	
0.90148	0.00005	0.99533	50	20	20	
0.44552	0.17554	0.93494	50	21	21	
0.89188	0.65382	0.08673	50	22	22	
0.08124	0.15403	0.07424	50	23	23	
0.64025	0.85720	0.16452	50	24	24	
0.93849	0.79543	0.94609	50	25	25	
0.68329	0.64525	0.96937	50	26	26	
0.98708	0.10118	0.00128	50	27	27	
0.88829	0.53527	0.14043	50	28	28	
0.07818	0.01873	0.03478	50	29	29	
0.42503	0.29041	0.08684	50	30	30	
0.24033	0.95059	0.90392	50	31	31	
0.62870	0.00321	0.00457	50	32	32	
0.18179	0.07626	0.08287	50	33	33	
0.36438	0.36431	0.89509	50	34	34	
0.98208	0.56142	0.06184	50	35	35	

0.69423	0.89719	0.96087	50	36	36
0.50253	0.38736	0.05731	50	37	37
0.45773	0.04332	0.91417	50	38	38
0.82545	0.91695	0.04931	50	39	39
0.55073	0.81738	0.08054	50	40	40
0.06642	0.18467	0.94560	50	41	41
0.34977	0.85690	0.04637	50	42	42
0.10212	0.43689	0.07187	50	43	43
0.16142	0.63510	0.06777	50	44	44
0.80136	0.82302	0.96140	50	45	45
0.61960	0.67539	0.07927	50	46	46
0.10048	0.74935	0.06073	50	47	47
0.35541	0.10422	0.87435	50	48	48
0.77326	0.70727	0.90756	50	49	49
0.35139	0.54493	0.98922	50	50	50
0.44485	0.62899	0.97813	50	51	51
0.68230	0.80690	0.05652	50	52	52
0.60103	0.80739	0.95993	50	53	53
0.83374	0.50991	0.93448	50	54	54
0.09770	0.28042	0.05107	50	55	55
0.25804	0.82722	0.93791	50	56	56
0.23032	0.91394	0.03167	50	57	57
0.97614	0.66315	0.98586	50	58	58
0.45375	0.91336	0.09431	50	59	59
0.85835	0.63266	0.95822	50	60	60
0.32438	0.36599	0.10798	50	61	61
0.38238	0.80974	0.92592	50	62	62
0.31187	0.42331	0.99262	50	63	63
0.04016	0.95712	0.83578	50	64	64
0.42334	0.92829	0.96173	50	65	65
0.06181	0.05552	0.90817	50	66	66
0.77760	0.71842	0.03918	50	67	67
0.10963	0.54441	0.98974	50	68	68
0.23181	0.60240	0.95877	50	69	69
0.68340	0.56369	0.06703	50	70	70
0.17041	0.71722	0.95411	50	71	71
0.52931	0.10250	0.00184	50	72	72
0.28299	0.61421	0.08203	50	73	73
0.18144	0.04656	0.96071	50	74	74
0.09489	0.89037	0.04486	50	75	75
0.16146	0.80502	0.86034	50	76	76
0.90454	0.46266	0.03091	50	77	77
0.57583	0.95224	0.11153	50	78	78
0.44658	0.44157	0.95606	50	79	79
0.56200	0.68418	0.96535	50	80	80
0.95951	0.54163	0.93519	50	81	81
0.33026	0.08375	0.08606	50	82	82
0.44012	0.03100	0.05198	50	83	83
0.80761	0.55570	0.04933	50	84	84
0.32017	0.73529	0.11244	50	85	85

0.33400	0.29204	0.99652	50	86	86
0.67111	0.52100	0.93956	50	87	87
0.41257	0.58602	0.10125	50	88	88
0.06569	0.80185	0.94906	50	89	89
0.04873	0.31091	0.93358	50	90	90
0.33098	0.02608	0.97160	50	91	91
0.40518	0.46092	0.08388	50	92	92
0.45882	0.30776	0.96075	50	93	93
0.43056	0.16401	0.06316	50	94	94
0.61008	0.61374	0.87023	50	95	95
0.32467	0.16033	0.98493	50	96	96
0.53509	0.53990	0.93945	50	97	97
0.53490	0.58237	0.06596	50	98	98
0.15668	0.13509	0.87445	50	99	99
0.59489	0.47624	0.03422	50	100	100

S9.1.2 triangles

$\rho = 0.2225 \text{ \AA}^{-2} = 2.121 \text{ ML}$, $E - E_{\text{bulk}} = 198 \text{ meV/at.}$

3.55789	-0.00806	0.00000
-3.56552	4.68674	0.00000
0.00000	0.00000	28.0000
4 atoms		
0	0.25	0.07803 50 1 1
0	0.75	0.92197 50 2 2
0	0.25	0.96739 50 3 3
0	0.75	0.03261 50 4 4

S9.1.3 squares

$\rho = 0.2448 \text{ \AA}^{-2} = 2.333 \text{ ML}$, $E - E_{\text{bulk}} = 158 \text{ meV/at.}$

5.72637	0.00000	0.00000
0.00000	5.72637	0.00000
0.00000	0.00000	20.5771
8 atoms		
0	0	0.56989 50 1 1
0.5	0.5	0.56989 50 2 2
0	0	0.41700 50 3 3
0.5	0.5	0.41700 50 4 4
0	0.5	0.62798 50 5 5
0.5	0	0.35890 50 6 6
0	0.5	0.47756 50 7 7
0.5	0	0.50932 50 8 8

S9.1.4 Sn.equi-II-3

$\rho = 0.3428 \text{ \AA}^{-2} = 3.268 \text{ ML}$, $E - E_{\text{bulk}} = 142 \text{ meV/at.}$

12.44832	-0.00000	-0.00008			
-6.22416	10.78059	-0.00011			
-0.00022	-0.00049	34.25425			
46 atoms					
0.33338	0.05896	0.26941	50	1	1
0.94107	0.27436	0.26942	50	2	2
0.72567	0.66667	0.26941	50	3	3
0.70092	0.03421	0.26532	50	4	4
0.33337	0.29911	0.26533	50	5	5
0.96582	0.66667	0.26533	50	6	6
0.95506	0.28834	0.02648	50	7	7
0.33331	0.04491	0.02648	50	8	8
0.71162	0.66659	0.02648	50	9	9
0.33332	0.28934	0.02653	50	10	10
0.71067	0.04395	0.02652	50	11	11
0.95605	0.66661	0.02653	50	12	12
0.53980	0.46057	0.07974	50	13	13
0.53938	0.07916	0.07972	50	14	14
0.92083	0.46015	0.07974	50	15	15
0.75269	0.87046	0.21963	50	16	16
0.11783	0.24731	0.21964	50	17	17
0.12956	0.88219	0.21964	50	18	18
1.00000	0.99995	0.10916	50	19	19
0.66670	0.33332	0.19192	50	20	20
0.54890	0.46285	0.21964	50	21	21
0.53716	0.08599	0.21963	50	22	22
0.91402	0.45112	0.21965	50	23	23
0.74587	0.87267	0.07972	50	24	24
0.12686	0.25411	0.07975	50	25	25
0.12729	0.87309	0.07974	50	26	26
0.00003	0.99999	0.19192	50	27	27
0.66667	0.33329	0.10916	50	28	28
0.46594	0.53418	0.15057	50	29	29
0.46583	0.93171	0.15056	50	30	30
0.06830	0.53407	0.15058	50	31	31
0.59842	0.79912	0.15056	50	32	32
0.20077	0.40159	0.15058	50	33	33
0.20089	0.79923	0.15057	50	34	34
0.07730	0.41060	0.34526	50	35	35
0.12885	0.66668	0.32593	50	36	36
0.33338	0.46215	0.32593	50	37	37
0.33339	0.92276	0.34525	50	38	38
0.58947	0.66668	0.34525	50	39	39
0.53791	0.87120	0.32592	50	40	40
0.19051	0.52380	0.26067	50	41	41
0.33337	0.80952	0.26066	50	42	42
0.47623	0.66666	0.26066	50	43	43
0.83399	0.66656	0.10590	50	44	44
0.83265	0.16593	0.10590	50	45	45
0.33327	0.16728	0.10590	50	46	46

S9.1.5 Sn.equi-II-5 $\rho = 0.5501 \text{ \AA}^{-2} = 5.244 \text{ ML}$, $E - E_{\text{bulk}} = 96 \text{ meV/at.}$

12.46276	0.00004	0.00003				
-6.23135	10.79309	-0.00004				
0.00009	-0.00009	41.74180				
74 atoms						
0.33759	0.05312	0.21120	50	1	1	
0.94690	0.28451	0.21120	50	2	2	
0.71549	0.66242	0.21120	50	3	3	
0.71549	0.05310	0.21120	50	4	4	
0.33758	0.28451	0.21120	50	5	5	
0.94688	0.66241	0.21120	50	6	6	
0.95688	0.28649	0.01775	50	7	7	
0.32957	0.04308	0.01775	50	8	8	
0.71350	0.67043	0.01775	50	9	9	
0.32957	0.28649	0.01775	50	10	10	
0.71350	0.04311	0.01775	50	11	11	
0.95692	0.67043	0.01775	50	12	12	
0.61782	0.61360	0.27509	50	13	13	
0.99573	0.38219	0.27509	50	14	14	
0.38642	0.00428	0.27509	50	15	15	
0.99572	0.61358	0.27509	50	16	16	
0.38640	0.38218	0.27509	50	17	17	
0.61781	0.00427	0.27509	50	18	18	
0.53981	0.46019	0.06000	50	19	19	
0.53981	0.07966	0.06000	50	20	20	
0.92034	0.46019	0.06000	50	21	21	
0.20780	0.79221	0.30980	50	22	22	
0.20780	0.41564	0.30981	50	23	23	
0.58436	0.79220	0.30981	50	24	24	
0.74895	0.87449	0.17649	50	25	25	
0.12551	0.25105	0.17649	50	26	26	
0.12551	0.87449	0.17649	50	27	27	
0.99999	0.00001	0.08775	50	28	28	
0.66665	0.33335	0.33446	50	29	29	
0.66665	0.33334	0.15183	50	30	30	
0.54290	0.45710	0.17347	50	31	31	
0.54290	0.08584	0.17347	50	32	32	
0.91416	0.45710	0.17347	50	33	33	
0.74857	0.87430	0.06230	50	34	34	
0.12570	0.25143	0.06230	50	35	35	
0.12570	0.87430	0.06230	50	36	36	
0.41914	0.20960	0.31282	50	37	37	
0.79040	0.58086	0.31282	50	38	38	
0.79041	0.20960	0.31282	50	39	39	
0.99999	0.00001	0.15577	50	40	40	

0.66665	0.33335	0.08417	50	41	41
0.33332	0.66668	0.33051	50	42	42
0.46549	0.53451	0.11781	50	43	43
0.46549	0.93101	0.11781	50	44	44
0.06899	0.53451	0.11781	50	45	45
0.13203	0.86797	0.36675	50	46	46
0.13204	0.26412	0.36675	50	47	47
0.73588	0.86797	0.36675	50	48	48
0.59743	0.79873	0.11954	50	49	49
0.20127	0.40256	0.11954	50	50	50
0.20127	0.79873	0.11955	50	51	51
0.00375	0.38021	0.46855	50	52	52
0.61980	0.62359	0.46855	50	53	53
0.37638	0.99625	0.46855	50	54	54
0.37641	0.38021	0.46855	50	55	55
0.00375	0.62362	0.46855	50	56	56
0.61980	0.99625	0.46855	50	57	57
0.41297	0.20651	0.42629	50	58	58
0.79349	0.58703	0.42629	50	59	59
0.79349	0.20651	0.42630	50	60	60
0.33332	0.66668	0.39854	50	61	61
0.20761	0.79239	0.42399	50	62	62
0.20762	0.41528	0.42399	50	63	63
0.58472	0.79238	0.42399	50	64	64
0.66666	0.33335	0.40212	50	65	65
0.26433	0.13219	0.36849	50	66	66
0.86781	0.73567	0.36849	50	67	67
0.86781	0.13219	0.36849	50	68	68
0.33339	0.16671	0.08294	50	69	69
0.83328	0.16672	0.08294	50	70	70
0.83329	0.66661	0.08294	50	71	71
0.50003	0.49997	0.40335	50	72	72
0.99991	0.49998	0.40336	50	73	73
0.50002	0.00010	0.40336	50	74	74

S9.1.6 Sn.equi-II-7.5

$\rho = 0.7981 \text{ \AA}^{-2} = 7.608 \text{ ML}$, $E - E_{\text{bulk}} = 75 \text{ meV/at.}$

12.50059	-0.00001	0.00007
-6.25030	10.82582	-0.00009
0.00033	-0.00026	52.72611
108 atoms		
0.33844	0.05386	0.16954
0.94615	0.28458	0.16954
0.71543	0.66156	0.16954
0.29003	0.95257	0.82048
0.66258	0.70993	0.82048
		50 1 1
		50 2 2
		50 3 3
		50 4 4
		50 5 5

0.04743	0.33741	0.82048	50	6	6
0.66258	0.95257	0.82048	50	7	7
0.04742	0.70996	0.82048	50	8	8
0.29006	0.33742	0.82048	50	9	9
0.71542	0.05385	0.16954	50	10	10
0.33844	0.28458	0.16954	50	11	11
0.94614	0.66156	0.16954	50	12	12
0.95126	0.27947	0.02386	50	13	13
0.32823	0.04874	0.02386	50	14	14
0.72054	0.67177	0.02386	50	15	15
0.32823	0.27945	0.02386	50	16	16
0.72053	0.04874	0.02386	50	17	17
0.95125	0.67177	0.02386	50	18	18
0.67146	0.72021	0.97325	50	19	19
0.27980	0.95121	0.97325	50	20	20
0.04879	0.32854	0.97325	50	21	21
0.61790	0.61313	0.22015	50	22	22
0.99522	0.38211	0.22015	50	23	23
0.38689	0.00478	0.22015	50	24	24
0.99522	0.61311	0.22015	50	25	25
0.38688	0.38210	0.22015	50	26	26
0.61789	0.00478	0.22015	50	27	27
0.04878	0.72020	0.97325	50	28	28
0.67145	0.95120	0.97325	50	29	29
0.27978	0.32854	0.97325	50	30	30
0.54130	0.45870	0.05090	50	31	31
0.54130	0.08258	0.05090	50	32	32
0.91742	0.45870	0.05090	50	33	33
0.08230	0.54113	0.94596	50	34	34
0.45887	0.91770	0.94596	50	35	35
0.45887	0.54113	0.94596	50	36	36
0.20781	0.79220	0.24744	50	37	37
0.20780	0.41562	0.24744	50	38	38
0.58439	0.79220	0.24744	50	39	39
0.74926	0.87463	0.14250	50	40	40
0.12538	0.25074	0.14250	50	41	41
0.12538	0.87462	0.14250	50	42	42
0.87338	0.12662	0.85368	50	43	43
0.87338	0.74671	0.85368	50	44	44
0.25328	0.12662	0.85368	50	45	45
0.00001	0.99999	0.07199	50	46	46
0.00001	0.99998	0.92623	50	47	47
0.66666	0.33334	0.26717	50	48	48
0.66667	0.33333	0.12142	50	49	49
0.33335	0.66665	0.87583	50	50	50
0.54361	0.45639	0.13955	50	51	51
0.54361	0.08720	0.13955	50	52	52
0.91280	0.45640	0.13955	50	53	53
0.08246	0.54121	0.85570	50	54	54
0.45879	0.91754	0.85570	50	55	55

0.45879	0.54120	0.85571	50	56	56
0.75388	0.87693	0.05385	50	57	57
0.12307	0.24612	0.05385	50	58	58
0.12307	0.87693	0.05385	50	59	59
0.87645	0.12355	0.94334	50	60	60
0.87645	0.75286	0.94334	50	61	61
0.24714	0.12355	0.94334	50	62	62
0.41952	0.20977	0.25007	50	63	63
0.79024	0.58048	0.25007	50	64	64
0.79024	0.20977	0.25007	50	65	65
0.00001	1.00000	0.12575	50	66	66
0.00001	0.99999	0.87267	50	67	67
0.66667	0.33333	0.06766	50	68	68
0.33335	0.66665	0.92969	50	69	69
0.33333	0.66667	0.26371	50	70	70
0.46514	0.53486	0.09582	50	71	71
0.46514	0.93025	0.09582	50	72	72
0.06975	0.53487	0.09582	50	73	73
0.93045	0.46520	0.90088	50	74	74
0.53480	0.06955	0.90088	50	75	75
0.53480	0.46520	0.90088	50	76	76
0.13187	0.86813	0.29252	50	77	77
0.13187	0.26376	0.29252	50	78	78
0.73625	0.86813	0.29252	50	79	79
0.59693	0.79846	0.09758	50	80	80
0.20154	0.40307	0.09758	50	81	81
0.20154	0.79846	0.09758	50	82	82
0.79876	0.20123	0.89937	50	83	83
0.79876	0.59748	0.89937	50	84	84
0.40252	0.20123	0.89937	50	85	85
0.00414	0.38078	0.37293	50	86	86
0.61923	0.62337	0.37292	50	87	87
0.37660	0.99587	0.37292	50	88	88
0.37663	0.38077	0.37292	50	89	89
0.00414	0.62340	0.37293	50	90	90
0.61923	0.99587	0.37293	50	91	91
0.41341	0.20671	0.33973	50	92	92
0.79330	0.58660	0.33973	50	93	93
0.79329	0.20671	0.33973	50	94	94
0.33333	0.66667	0.31756	50	95	95
0.20789	0.79212	0.33769	50	96	96
0.20789	0.41579	0.33769	50	97	97
0.58421	0.79212	0.33769	50	98	98
0.66667	0.33334	0.32073	50	99	99
0.26417	0.13209	0.29404	50	100	100
0.86791	0.73584	0.29404	50	101	101
0.86791	0.13209	0.29405	50	102	102
0.16674	0.33343	0.87209	50	103	103
0.66656	0.83325	0.87209	50	104	104
0.16673	0.83327	0.87209	50	105	105

0.49994	0.50006	0.32131	50	106	106
0.00013	0.50007	0.32132	50	107	107
0.49993	0.99988	0.32132	50	108	108

S9.1.7 Sn.equi-II-10

$\rho = 1.047 \text{ \AA}^{-2} = 9.978 \text{ ML}$, $E - E_{\text{bulk}} = 65 \text{ meV/at.}$

12.51618	0.00000	0.00000			
-6.25809	10.83933	0.00000			
0.00000	0.00000	62.18220			
142 atoms					
0.33865	0.05400	0.14502	50	1	1
0.94600	0.28466	0.14502	50	2	2
0.71534	0.66135	0.14502	50	3	3
0.28466	0.94600	0.85498	50	4	4
0.66135	0.71534	0.85498	50	5	5
0.05400	0.33865	0.85498	50	6	6
0.66135	0.94600	0.85498	50	7	7
0.05400	0.71534	0.85498	50	8	8
0.28466	0.33865	0.85498	50	9	9
0.71534	0.05400	0.14502	50	10	10
0.33865	0.28466	0.14502	50	11	11
0.94600	0.66135	0.14502	50	12	12
0.00492	0.38702	0.81203	50	13	13
0.61298	0.61791	0.81203	50	14	14
0.38209	0.99508	0.81203	50	15	15
0.95141	0.27916	0.02146	50	16	16
0.32776	0.04859	0.02146	50	17	17
0.72084	0.67224	0.02146	50	18	18
0.32776	0.27916	0.02146	50	19	19
0.72084	0.04859	0.02146	50	20	20
0.95141	0.67224	0.02146	50	21	21
0.38209	0.38702	0.81203	50	22	22
0.00492	0.61791	0.81203	50	23	23
0.61298	0.99508	0.81203	50	24	24
0.67224	0.72084	0.97854	50	25	25
0.27916	0.95141	0.97854	50	26	26
0.04859	0.32776	0.97854	50	27	27
0.61791	0.61298	0.18797	50	28	28
0.99508	0.38209	0.18797	50	29	29
0.38702	0.00492	0.18797	50	30	30
0.99508	0.61298	0.18797	50	31	31
0.38702	0.38209	0.18797	50	32	32
0.61791	0.00492	0.18797	50	33	33
0.04859	0.72084	0.97854	50	34	34
0.67224	0.95141	0.97854	50	35	35

0.27916	0.32776	0.97854	50	36	36
0.54119	0.45881	0.04431	50	37	37
0.54119	0.08239	0.04431	50	38	38
0.91761	0.45881	0.04431	50	39	39
0.08239	0.54119	0.95569	50	40	40
0.45881	0.91761	0.95569	50	41	41
0.45881	0.54119	0.95569	50	42	42
0.20780	0.79220	0.21105	50	43	43
0.20780	0.41560	0.21105	50	44	44
0.58440	0.79220	0.21105	50	45	45
0.74926	0.87463	0.12216	50	46	46
0.12537	0.25074	0.12216	50	47	47
0.12537	0.87463	0.12216	50	48	48
0.87463	0.12537	0.87784	50	49	49
0.87463	0.74926	0.87784	50	50	50
0.25074	0.12537	0.87784	50	51	51
0.41560	0.20780	0.78895	50	52	52
0.79220	0.58440	0.78895	50	53	53
0.79220	0.20780	0.78895	50	54	54
0.00000	0.00000	0.06239	50	55	55
0.00000	0.00000	0.93761	50	56	56
0.66667	0.33333	0.22778	50	57	57
0.66667	0.33333	0.10411	50	58	58
0.33333	0.66667	0.89589	50	59	59
0.33333	0.66667	0.77222	50	60	60
0.54366	0.45634	0.11954	50	61	61
0.54366	0.08731	0.11954	50	62	62
0.91268	0.45634	0.11954	50	63	63
0.08731	0.54366	0.88045	50	64	64
0.45634	0.91268	0.88045	50	65	65
0.45634	0.54366	0.88045	50	66	66
0.20976	0.79024	0.78666	50	67	67
0.20976	0.41951	0.78666	50	68	68
0.58049	0.79024	0.78666	50	69	69
0.75402	0.87701	0.04699	50	70	70
0.12299	0.24598	0.04699	50	71	71
0.12299	0.87701	0.04699	50	72	72
0.87701	0.12299	0.95301	50	73	73
0.87701	0.75402	0.95301	50	74	74
0.24598	0.12299	0.95301	50	75	75
0.41951	0.20976	0.21334	50	76	76
0.79024	0.58049	0.21334	50	77	77
0.79024	0.20976	0.21334	50	78	78
0.00000	0.00000	0.10800	50	79	79
0.00000	0.00000	0.89200	50	80	80
0.66667	0.33333	0.77518	50	81	81
0.66667	0.33333	0.05849	50	82	82
0.33333	0.66667	0.94151	50	83	83
0.33333	0.66667	0.22482	50	84	84
0.46511	0.53489	0.08246	50	85	85

0.46511	0.93022	0.08246	50	86	86
0.06978	0.53489	0.08246	50	87	87
0.93022	0.46511	0.91754	50	88	88
0.53489	0.06978	0.91754	50	89	89
0.53489	0.46511	0.91754	50	90	90
0.13189	0.86811	0.24930	50	91	91
0.13189	0.26378	0.24930	50	92	92
0.73622	0.86811	0.24930	50	93	93
0.59695	0.79847	0.08405	50	94	94
0.20153	0.40305	0.08405	50	95	95
0.20153	0.79847	0.08405	50	96	96
0.79847	0.20153	0.91595	50	97	97
0.79847	0.59695	0.91595	50	98	98
0.40305	0.20153	0.91595	50	99	99
0.26378	0.13189	0.75070	50	100	100
0.86811	0.73622	0.75070	50	101	101
0.86811	0.13189	0.75070	50	102	102
0.00411	0.38075	0.31748	50	103	103
0.61925	0.62335	0.31748	50	104	104
0.37665	0.99589	0.31748	50	105	105
0.37665	0.38075	0.31748	50	106	106
0.00411	0.62335	0.31748	50	107	107
0.61925	0.99589	0.31748	50	108	108
0.41340	0.20670	0.28932	50	109	109
0.79330	0.58660	0.28932	50	110	110
0.79330	0.20670	0.28932	50	111	111
0.33333	0.66667	0.27051	50	112	112
0.20793	0.79207	0.28760	50	113	113
0.20793	0.41586	0.28760	50	114	114
0.58414	0.79207	0.28760	50	115	115
0.66667	0.33333	0.27322	50	116	116
0.26395	0.13198	0.25060	50	117	117
0.86802	0.73604	0.25060	50	118	118
0.86802	0.13198	0.25060	50	119	119
0.62335	0.61925	0.68252	50	120	120
0.99589	0.37665	0.68252	50	121	121
0.38075	0.00411	0.68252	50	122	122
0.99589	0.61925	0.68252	50	123	123
0.38075	0.37665	0.68252	50	124	124
0.62335	0.00411	0.68252	50	125	125
0.20670	0.79330	0.71068	50	126	126
0.20670	0.41340	0.71068	50	127	127
0.58660	0.79330	0.71068	50	128	128
0.66667	0.33333	0.72949	50	129	129
0.41586	0.20793	0.71240	50	130	130
0.79207	0.58414	0.71240	50	131	131
0.79207	0.20793	0.71240	50	132	132
0.33333	0.66667	0.72678	50	133	133
0.13198	0.86802	0.74940	50	134	134
0.13198	0.26395	0.74940	50	135	135

0.73604	0.86802	0.74940	50	136	136
0.50005	0.49995	0.72624	50	137	137
0.99990	0.49995	0.72624	50	138	138
0.50005	0.00010	0.72624	50	139	139
0.49995	0.50005	0.27376	50	140	140
0.00010	0.50005	0.27376	50	141	141
0.49995	0.99990	0.27376	50	142	142

S9.2 Germanium-Slab xyz Files

S9.2.1 Ge.db-monolayer (oP10)

$\rho = 0.1884 \text{ \AA}^{-2} = 1.359 \text{ ML}$, $E - E_{\text{bulk}} = 308 \text{ meV/at.}$

7.84310	0.00000	0.00000				
0.00000	38.86961	0.00000				
0.00000	0.00000	6.76570				
10 atoms						
0.02034	0.00000	0.81941	32	1	1	
0.47966	0.00000	0.81941	32	2	2	
0.52034	0.00000	0.18059	32	3	3	
0.97966	0.00000	0.18059	32	4	4	
0.25000	0.03815	0.67495	32	5	5	
0.25000	0.96185	0.67495	32	6	6	
0.75000	0.96185	0.32505	32	7	7	
0.75000	0.03815	0.32505	32	8	8	
0.25000	0.00000	0.37240	32	9	9	
0.75000	0.00000	0.62760	32	10	10	

S9.2.2 Ge.iso-II-2.5

$\rho = 0.3534 \text{ \AA}^{-2} = 2.548 \text{ ML}$, $E - E_{\text{bulk}} = 251 \text{ meV/at.}$

15.67423	0.00000	0.00000				
0.00000	11.19385	0.00000				
0.00000	0.00000	28.11850				
62 atoms						
0.00001	0.00000	0.00000	32	1	1	
0.36467	0.00000	0.10991	32	2	2	
0.36467	0.00000	0.89009	32	3	3	
0.50130	0.00000	0.15808	32	4	4	
0.50130	0.00000	0.84192	32	5	5	
0.76010	0.00000	0.04475	32	6	6	
0.76010	0.00000	0.95525	32	7	7	
0.91225	0.00000	0.07406	32	8	8	
0.91225	0.00000	0.92595	32	9	9	
0.49329	0.00000	0.05356	32	10	10	
0.49329	0.00000	0.94644	32	11	11	
0.24297	0.11297	0.00000	32	12	12	
0.24297	0.88703	0.00000	32	13	13	
0.55267	0.16644	0.10305	32	14	14	
0.55267	0.83356	0.89694	32	15	15	
0.55267	0.16644	0.89694	32	16	16	
0.55267	0.83356	0.10305	32	17	17	
0.30975	0.18824	0.07465	32	18	18	
0.30975	0.81176	0.92535	32	19	19	
0.30975	0.18824	0.92535	32	20	20	

0.30975	0.81176	0.07465	32	21	21
0.95601	0.17575	0.12814	32	22	22
0.95601	0.82425	0.87186	32	23	23
0.95601	0.17575	0.87186	32	24	24
0.95601	0.82425	0.12814	32	25	25
0.08999	0.18182	0.00000	32	26	26
0.08999	0.81818	0.00000	32	27	27
0.69977	0.19543	0.07184	32	28	28
0.69977	0.80456	0.92816	32	29	29
0.69977	0.19543	0.92816	32	30	30
0.69977	0.80456	0.07184	32	31	31
0.05137	0.29872	0.07307	32	32	32
0.05137	0.70128	0.92693	32	33	33
0.05137	0.29872	0.92693	32	34	34
0.05137	0.70128	0.07307	32	35	35
0.66295	0.31657	0.00000	32	36	36
0.66295	0.68343	0.00000	32	37	37
0.83205	0.29264	0.10315	32	38	38
0.83205	0.70736	0.89685	32	39	39
0.83205	0.29264	0.89685	32	40	40
0.83205	0.70736	0.10315	32	41	41
0.44360	0.31369	0.07471	32	42	42
0.44360	0.68631	0.92529	32	43	43
0.44360	0.31369	0.92529	32	44	44
0.44360	0.68631	0.07471	32	45	45
0.19963	0.33467	0.10130	32	46	46
0.19963	0.66533	0.89870	32	47	47
0.19963	0.33467	0.89870	32	48	48
0.19963	0.66533	0.10130	32	49	49
0.51078	0.38706	0.00000	32	50	50
0.51078	0.61294	0.00000	32	51	51
0.25094	0.50000	0.15702	32	52	52
0.25094	0.50000	0.84298	32	53	53
0.26308	0.50000	0.05291	32	54	54
0.26308	0.50000	0.94709	32	55	55
0.38975	0.50000	0.11150	32	56	56
0.38975	0.50000	0.88850	32	57	57
0.75200	0.50000	0.00000	32	58	58
0.84553	0.50000	0.07091	32	59	59
0.84553	0.50000	0.92909	32	60	60
0.99777	0.50000	0.04467	32	61	61
0.99777	0.50000	0.95533	32	62	62

S9.2.3 Ge.equi-II-3

$\rho = 0.4037 \text{ \AA}^{-2} = 2.911 \text{ ML}$, $E - E_{\text{bulk}} = 222 \text{ meV/at.}$

10.88372	-0.00000	0.00204			
-5.44186	9.33195	-0.00089			
0.00667	0.00048	34.96546			
41 atoms					
0.33470	0.04609	0.25061	50	1	1
0.95527	0.28723	0.25061	50	2	2
0.72578	0.66666	0.24872	50	3	3
0.71201	0.04620	0.25327	50	4	4
0.33247	0.28712	0.25327	50	5	5
0.96033	0.66666	0.25513	50	6	6
0.92142	0.25204	0.07214	50	7	7
0.33606	0.08131	0.07214	50	8	8
0.74943	0.66668	0.07242	50	9	9
0.33610	0.29972	0.04765	50	10	10
0.70306	0.03364	0.04765	50	11	11
0.96650	0.66668	0.04764	50	12	12
0.53293	0.44755	0.09586	50	13	13
0.55305	0.08189	0.09515	50	14	14
0.91793	0.46807	0.09555	50	15	15
0.75604	0.87970	0.21275	50	16	16
0.12609	0.24659	0.21253	50	17	17
0.12317	0.87502	0.21254	50	18	18
0.00216	0.00060	0.11854	50	19	19
0.66819	0.33376	0.18882	50	20	20
0.54300	0.45362	0.21275	50	21	21
0.54616	0.08674	0.21253	50	22	22
0.91481	0.45831	0.21254	50	23	23
0.75205	0.88580	0.09586	50	24	24
0.13783	0.25146	0.09515	50	25	25
0.11654	0.86528	0.09555	50	26	26
0.00110	0.99957	0.18882	50	27	27
0.66823	0.33274	0.11854	50	28	28
0.46653	0.53371	0.15486	50	29	29
0.46666	0.92995	0.15442	50	30	30
0.06985	0.53440	0.15449	50	31	31
0.59949	0.79963	0.15486	50	32	32
0.20338	0.40338	0.15442	50	33	33
0.20212	0.79894	0.15449	50	34	34
0.12584	0.49295	0.29437	50	35	35
0.05444	0.66665	0.32424	50	36	36
0.32321	0.44254	0.30830	50	37	37
0.29955	0.84037	0.29437	50	38	38
0.55285	0.66666	0.29650	50	39	39
0.54732	0.89077	0.30830	50	40	40
0.36303	0.66666	0.24997	50	41	41

S9.2.4 Ge.equi-II-3.5

$\rho = 0.4781 \text{ \AA}^{-2} = 3.448 \text{ ML}$, $E - E_{\text{bulk}} = 183 \text{ meV/at.}$

10.71370	-0.01100	-0.00829			
-5.49272	9.36400	-0.25389			
-0.21007	-0.40637	30.60224			
48 atoms					
0.03938	0.81651	0.19581	32	1	1
0.04665	0.82625	0.27601	32	2	2
0.11219	0.35595	0.23590	32	3	3
0.13361	0.25074	0.05846	32	4	4
0.21634	0.29959	0.39743	32	5	5
0.18713	0.50189	0.07438	32	6	6
0.16572	0.49868	0.41335	32	7	7
0.15609	0.05849	0.16867	32	8	8
0.17348	0.07731	0.30260	32	9	9
0.16140	0.68985	0.16920	32	10	10
0.16828	0.70342	0.30314	32	11	11
0.24190	0.22156	0.23555	32	12	12
0.24199	0.62007	0.23625	32	13	13
0.36033	0.24629	0.07152	32	14	14
0.39287	0.23103	0.43153	32	15	15
0.35751	0.74388	0.04028	32	16	16
0.39007	0.72863	0.40028	32	17	17
0.36533	0.08255	0.12695	32	18	18
0.38570	0.12853	0.35199	32	19	19
0.36468	0.84638	0.11982	32	20	20
0.38505	0.89237	0.34486	32	21	21
0.50849	0.75334	0.23626	32	22	22
0.50840	0.35482	0.23555	32	23	23
0.98625	0.47286	0.12520	32	24	24
0.00594	0.49970	0.34986	32	25	25
0.98530	0.09568	0.12195	32	26	26
0.00628	0.12315	0.34661	32	27	27
0.95036	0.26790	0.16891	32	28	28
0.96249	0.28829	0.30290	32	29	29
0.78790	0.68665	0.16891	32	30	30
0.80003	0.70702	0.30290	32	31	31
0.74445	0.47524	0.12195	32	32	32
0.76413	0.50205	0.34661	32	33	33
0.74412	0.85179	0.12521	32	34	34
0.76510	0.87925	0.34986	32	35	35
0.70374	0.14867	0.19581	32	36	36
0.71101	0.15841	0.27601	32	37	37
0.63820	0.61894	0.23591	32	38	38
0.58467	0.47626	0.05846	32	39	39
0.56325	0.47301	0.39743	32	40	40
0.53406	0.67535	0.07439	32	41	41
0.61677	0.72416	0.41335	32	42	42
0.58211	0.27149	0.16866	32	43	43
0.58897	0.28505	0.30261	32	44	44

0.57690	0.89760	0.16922	32	45	45
0.59430	0.91642	0.30314	32	46	46
0.36517	0.44353	0.12499	32	47	47
0.38523	0.53138	0.34682	32	48	48

S9.2.5 Ge.iso-II-4

$\rho = 0.5461 \text{ \AA}^{-2} = 3.939 \text{ ML}$, $E - E_{\text{bulk}} = 176 \text{ meV/at.}$

-15.82209	15.82209	0.00000			
-0.00007	-0.00007	15.71212			
47.38157	47.38157	-0.00043			
192 atoms					
0.00000	0.88780	0.12974	32	1	1
0.00000	0.50254	0.93508	32	2	2
0.94334	0.00665	0.08217	32	3	3
0.94333	0.24350	0.00107	32	4	4
0.89604	0.92204	0.95858	32	5	5
0.90596	0.94148	0.05038	32	6	6
0.90724	0.94027	0.11385	32	7	7
0.90850	0.09119	0.00154	32	8	8
0.90851	0.15890	0.08174	32	9	9
0.90729	0.30984	0.96935	32	10	10
0.90595	0.30842	0.03291	32	11	11
0.89610	0.32794	0.12476	32	12	12
0.89967	0.70122	0.97045	32	13	13
0.90120	0.69291	0.03171	32	14	14
0.91681	0.69646	0.12495	32	15	15
0.91682	0.55370	0.95830	32	16	16
0.90118	0.55689	0.05163	32	17	17
0.89971	0.54879	0.11290	32	18	18
0.84765	0.05524	0.97125	32	19	19
0.84821	0.05655	0.03191	32	20	20
0.83387	0.04919	0.12574	32	21	21
0.83387	0.20091	0.95740	32	22	22
0.84819	0.19337	0.05138	32	23	23
0.84772	0.19496	0.11203	32	24	24
0.83869	0.79897	0.94772	32	25	25
0.84356	0.80720	0.05037	32	26	26
0.84406	0.80743	0.11390	32	27	27
0.84113	0.66051	0.00105	32	28	28
0.84112	0.58926	0.08229	32	29	29
0.84409	0.44269	0.96935	32	30	30
0.84354	0.44266	0.03297	32	31	31
0.83878	0.45095	0.13564	32	32	32
0.80668	0.74184	0.08225	32	33	33
0.80669	0.50793	0.00105	32	34	34
0.75000	0.99383	0.98263	32	35	35

0.75000	0.99488	0.02032	32	36	36
0.75000	0.99855	0.14880	32	37	37
0.74999	0.84154	0.97019	32	38	38
0.75000	0.84207	0.03112	32	39	39
0.75000	0.86023	0.12929	32	40	40
0.75000	0.75066	0.00081	32	41	41
0.75000	0.49909	0.08258	32	42	42
0.75000	0.25199	0.93431	32	43	43
0.75000	0.25501	0.06302	32	44	44
0.75000	0.25613	0.10069	32	45	45
0.75000	0.39037	0.95384	32	46	46
0.75000	0.40784	0.05223	32	47	47
0.75000	0.40835	0.11322	32	48	48
0.69332	0.74184	0.08225	32	49	49
0.69331	0.50793	0.00106	32	50	50
0.66129	0.79900	0.94773	32	51	51
0.65644	0.80720	0.05037	32	52	52
0.65594	0.80743	0.11390	32	53	53
0.65888	0.66051	0.00106	32	54	54
0.65889	0.58926	0.08229	32	55	55
0.65592	0.44270	0.96935	32	56	56
0.65647	0.44266	0.03297	32	57	57
0.66123	0.45096	0.13564	32	58	58
0.65235	0.05525	0.97125	32	59	59
0.65179	0.05655	0.03191	32	60	60
0.66613	0.04919	0.12574	32	61	61
0.66614	0.20092	0.95740	32	62	62
0.65181	0.19337	0.05138	32	63	63
0.65228	0.19496	0.11203	32	64	64
0.60032	0.70122	0.97045	32	65	65
0.59880	0.69291	0.03172	32	66	66
0.58319	0.69646	0.12495	32	67	67
0.58319	0.55371	0.95829	32	68	68
0.59883	0.55689	0.05163	32	69	69
0.60030	0.54879	0.11290	32	70	70
0.60393	0.92205	0.95860	32	71	71
0.59404	0.94148	0.05038	32	72	72
0.59276	0.94027	0.11385	32	73	73
0.59150	0.09119	0.00154	32	74	74
0.59149	0.15890	0.08174	32	75	75
0.59271	0.30985	0.96935	32	76	76
0.59405	0.30842	0.03291	32	77	77
0.60390	0.32794	0.12476	32	78	78
0.55666	0.00665	0.08217	32	79	79
0.55667	0.24350	0.00107	32	80	80
0.49998	0.90791	0.97172	32	81	81
0.50000	0.90693	0.03132	32	82	82
0.50000	0.88780	0.12974	32	83	83
0.50000	0.75359	0.02030	32	84	84
0.50000	0.00101	0.00159	32	85	85

0.50000	0.24902	0.08172	32	86	86
0.50001	0.36206	0.95334	32	87	87
0.50000	0.34292	0.05197	32	88	88
0.50000	0.49621	0.06306	32	89	89
0.50000	0.49435	0.10075	32	90	90
0.99998	0.90791	0.97172	32	91	91
0.00000	0.90693	0.03132	32	92	92
0.99999	0.75551	0.98260	32	93	93
1.00000	0.75359	0.02030	32	94	94
1.00000	0.74775	0.14810	32	95	95
1.00000	0.00101	0.00159	32	96	96
0.00000	0.24902	0.08172	32	97	97
0.00000	0.36206	0.95334	32	98	98
0.00000	0.34292	0.05197	32	99	99
0.00000	0.34197	0.11162	32	100	100
0.00000	0.49621	0.06306	32	101	101
0.00000	0.49435	0.10075	32	102	102
0.05666	0.00665	0.08217	32	103	103
0.05667	0.24350	0.00107	32	104	104
0.10393	0.92205	0.95860	32	105	105
0.09404	0.94148	0.05038	32	106	106
0.09276	0.94027	0.11385	32	107	107
0.09150	0.09119	0.00154	32	108	108
0.09150	0.15890	0.08174	32	109	109
0.09272	0.30985	0.96935	32	110	110
0.09406	0.30842	0.03291	32	111	111
0.10390	0.32794	0.12476	32	112	112
0.10032	0.70122	0.97045	32	113	113
0.09880	0.69291	0.03172	32	114	114
0.08319	0.69646	0.12495	32	115	115
0.08319	0.55371	0.95829	32	116	116
0.09883	0.55689	0.05163	32	117	117
0.10030	0.54879	0.11290	32	118	118
0.15235	0.05525	0.97125	32	119	119
0.15179	0.05655	0.03191	32	120	120
0.16613	0.04919	0.12574	32	121	121
0.16614	0.20092	0.95740	32	122	122
0.15181	0.19337	0.05138	32	123	123
0.15228	0.19496	0.11203	32	124	124
0.16129	0.79900	0.94773	32	125	125
0.15644	0.80720	0.05037	32	126	126
0.15594	0.80743	0.11390	32	127	127
0.15888	0.66051	0.00106	32	128	128
0.15888	0.58926	0.08229	32	129	129
0.15592	0.44270	0.96935	32	130	130
0.15647	0.44266	0.03297	32	131	131
0.16123	0.45096	0.13564	32	132	132
0.19332	0.74184	0.08225	32	133	133
0.19331	0.50793	0.00106	32	134	134
0.25000	0.99383	0.98263	32	135	135

0.25000	0.99488	0.02032	32	136	136
0.25000	0.99855	0.14880	32	137	137
0.24999	0.84154	0.97019	32	138	138
0.25000	0.84207	0.03112	32	139	139
0.25000	0.86023	0.12929	32	140	140
0.25000	0.75066	0.00081	32	141	141
0.25000	0.49909	0.08258	32	142	142
0.25000	0.25199	0.93431	32	143	143
0.25000	0.25501	0.06302	32	144	144
0.25000	0.25613	0.10069	32	145	145
0.25000	0.39037	0.95384	32	146	146
0.25000	0.40784	0.05223	32	147	147
0.25000	0.40835	0.11322	32	148	148
0.30668	0.74184	0.08225	32	149	149
0.30669	0.50793	0.00105	32	150	150
0.33869	0.79897	0.94772	32	151	151
0.34356	0.80720	0.05037	32	152	152
0.34406	0.80743	0.11390	32	153	153
0.34113	0.66051	0.00105	32	154	154
0.34112	0.58926	0.08229	32	155	155
0.34409	0.44269	0.96935	32	156	156
0.34354	0.44266	0.03297	32	157	157
0.33877	0.45095	0.13564	32	158	158
0.34765	0.05524	0.97125	32	159	159
0.34821	0.05655	0.03191	32	160	160
0.33387	0.04919	0.12574	32	161	161
0.33387	0.20091	0.95740	32	162	162
0.34819	0.19337	0.05138	32	163	163
0.34772	0.19496	0.11203	32	164	164
0.39967	0.70122	0.97045	32	165	165
0.40120	0.69291	0.03171	32	166	166
0.41681	0.69646	0.12495	32	167	167
0.41682	0.55370	0.95830	32	168	168
0.40118	0.55689	0.05163	32	169	169
0.39971	0.54879	0.11290	32	170	170
0.39604	0.92204	0.95858	32	171	171
0.40596	0.94148	0.05038	32	172	172
0.40724	0.94027	0.11385	32	173	173
0.40849	0.09119	0.00154	32	174	174
0.40851	0.15890	0.08174	32	175	175
0.40729	0.30984	0.96935	32	176	176
0.40595	0.30842	0.03291	32	177	177
0.39610	0.32794	0.12476	32	178	178
0.44334	0.00665	0.08217	32	179	179
0.44333	0.24350	0.00107	32	180	180
0.50000	0.75551	0.98260	32	181	181
0.50000	0.74775	0.14810	32	182	182
0.50000	0.34197	0.11162	32	183	183
0.50000	0.50254	0.93508	32	184	184

0.00001	0.48841	0.97807	32	185	185
0.75000	0.26178	0.97745	32	186	186
0.25000	0.26178	0.97745	32	187	187
0.50001	0.48841	0.97807	32	188	188
0.75000	0.98864	0.10562	32	189	189
1.00000	0.76126	0.10506	32	190	190
0.25000	0.98864	0.10562	32	191	191
0.50000	0.76126	0.10506	32	192	192

S9.2.6 Ge.equi-II-6

$\rho = 0.8042 \text{ \AA}^{-2} = 5.800 \text{ ML}$, $E - E_{\text{bulk}} = 120 \text{ meV/at.}$

10.86109	-0.01836	-0.00140			
-5.44644	9.39675	-0.00201			
-0.00506	-0.01138	38.26388			
82 atoms					
0.34308	0.99782	0.20027	32	1	1
0.95338	0.22993	0.20030	32	2	2
0.72149	0.60798	0.20028	32	3	3
0.72123	0.99788	0.20033	32	4	4
0.34308	0.22938	0.20035	32	5	5
0.95299	0.60771	0.20028	32	6	6
0.96265	0.23156	0.02246	32	7	7
0.33972	0.98994	0.02231	32	8	8
0.71411	0.61309	0.02088	32	9	9
0.33792	0.23100	0.02467	32	10	10
0.71970	0.99048	0.02487	32	11	11
0.94899	0.61236	0.02657	32	12	12
0.62392	0.55966	0.26098	32	13	13
0.00197	0.32778	0.26100	32	14	14
0.39179	0.94936	0.26101	32	15	15
0.00168	0.55928	0.26101	32	16	16
0.39187	0.32751	0.26096	32	17	17
0.62336	0.94936	0.26094	32	18	18
0.55050	0.40345	0.05898	32	19	19
0.54819	0.03198	0.05903	32	20	20
0.91888	0.39903	0.05877	32	21	21
0.21366	0.73739	0.29415	32	22	22
0.21406	0.36150	0.29395	32	23	23
0.59000	0.73776	0.29395	32	24	24
0.75507	0.81993	0.16734	32	25	25
0.13133	0.19586	0.16734	32	26	26
0.13097	0.81953	0.16713	32	27	27
0.00616	0.94435	0.08239	32	28	28
0.67271	0.27901	0.31721	32	29	29
0.67247	0.27846	0.14409	32	30	30
0.54885	0.40170	0.16467	32	31	31
0.54892	0.03090	0.16469	32	32	32

0.92028	0.40228	0.16462	32	33	33
0.75975	0.82036	0.06012	32	34	34
0.12706	0.18979	0.06017	32	35	35
0.13048	0.82432	0.05992	32	36	36
0.42506	0.15537	0.29660	32	37	37
0.79642	0.52673	0.29667	32	38	38
0.79584	0.15530	0.29662	32	39	39
0.00578	0.94493	0.14701	32	40	40
0.67283	0.27877	0.08011	32	41	41
0.33916	0.61231	0.31428	32	42	42
0.47142	0.47972	0.11194	32	43	43
0.47075	0.87492	0.11187	32	44	44
0.07566	0.47956	0.11171	32	45	45
0.13824	0.81366	0.34849	32	46	46
0.13788	0.21000	0.34825	32	47	47
0.74200	0.81360	0.34828	32	48	48
0.60333	0.74352	0.11303	32	49	49
0.20693	0.34763	0.11302	32	50	50
0.20700	0.74388	0.11280	32	51	51
0.00788	0.32120	0.44041	32	52	52
0.62631	0.56969	0.43883	32	53	53
0.38469	0.94679	0.43897	32	54	54
0.38521	0.32675	0.43642	32	55	55
0.00710	0.55604	0.43472	32	56	56
0.62574	0.94497	0.43662	32	57	57
0.42658	0.15510	0.40225	32	58	58
0.79363	0.52576	0.40252	32	59	59
0.79807	0.15739	0.40231	32	60	60
0.33886	0.61299	0.37890	32	61	61
0.21890	0.73738	0.40136	32	62	62
0.21495	0.36666	0.40117	32	63	63
0.58439	0.73396	0.40112	32	64	64
0.67328	0.27961	0.38118	32	65	65
0.26929	0.07742	0.34942	32	66	66
0.87392	0.68234	0.34958	32	67	67
0.87409	0.07810	0.34935	32	68	68
0.12613	0.38780	0.97224	32	69	69
0.12048	0.61134	0.98264	32	70	70
0.37306	0.43569	0.98467	32	71	71
0.34993	0.83480	0.97218	32	72	72
0.61879	0.61212	0.95792	32	73	73
0.54857	0.78605	0.98497	32	74	74
0.78277	0.73339	0.48905	32	75	75
0.83059	0.98027	0.47662	32	76	76
0.00628	0.72773	0.47865	32	77	77
0.00715	0.22614	0.50337	32	78	78
0.22977	0.95724	0.48911	32	79	79
0.18093	0.15579	0.47631	32	80	80
0.31126	0.61126	0.02520	32	81	81
0.00596	0.91831	0.43609	32	82	82

S9.3 Silicon-Slab xyz Files

S9.3.1 Si.db-monolayer (oP10)

$\rho = 0.2110 \text{ \AA}^{-2} = 1.364 \text{ ML}$, $E - E_{\text{bulk}} = 430 \text{ meV/at.}$

7.40937	0.00000	0.00000				
0.00000	35.75410	0.00000				
0.00000	0.00000	6.39543				
10 atoms						
0.01913	0.00000	0.81934	14	1	1	
0.48087	0.00000	0.81934	14	2	2	
0.51913	0.00000	0.18066	14	3	3	
0.98087	0.00000	0.18066	14	4	4	
0.25000	0.03788	0.67701	14	5	5	
0.25000	0.96212	0.67701	14	6	6	
0.75000	0.96212	0.32299	14	7	7	
0.75000	0.03788	0.32299	14	8	8	
0.25000	0.00000	0.37407	14	9	9	
0.75000	0.00000	0.62593	14	10	10	

S9.3.2 Si.iso-II-2.5

$\rho = 0.3851 \text{ \AA}^{-2} = 2.489 \text{ ML}$, $E - E_{\text{bulk}} = 322 \text{ meV/at.}$

15.01360	0.00000	0.00000				
0.00000	10.72374	0.00000				
0.00000	0.00000	24.81168				
62 atoms						
0.00530	0.00000	0.00000	14	1	1	
0.36693	0.00000	0.11410	14	2	2	
0.36693	0.00000	0.88590	14	3	3	
0.50034	0.00000	0.16477	14	4	4	
0.50034	0.00000	0.83523	14	5	5	
0.76091	0.00000	0.04838	14	6	6	
0.76091	0.00000	0.95162	14	7	7	
0.91223	0.00000	0.07669	14	8	8	
0.91223	0.00000	0.92331	14	9	9	
0.49346	0.00000	0.05520	14	10	10	
0.49346	0.00000	0.94480	14	11	11	
0.24599	0.11233	0.00000	14	12	12	
0.24599	0.88767	0.00000	14	13	13	
0.55251	0.16366	0.10837	14	14	14	
0.55251	0.83634	0.89163	14	15	15	
0.55251	0.16366	0.89163	14	16	16	
0.55251	0.83634	0.10837	14	17	17	
0.31244	0.18904	0.07990	14	18	18	
0.31244	0.81096	0.92010	14	19	19	
0.31244	0.18904	0.92010	14	20	20	

0.31244	0.81096	0.07990	14	21	21
0.94147	0.19531	0.11305	14	22	22
0.94147	0.80469	0.88695	14	23	23
0.94147	0.19531	0.88695	14	24	24
0.94147	0.80469	0.11305	14	25	25
0.09512	0.18183	0.00000	14	26	26
0.09512	0.81817	0.00000	14	27	27
0.69757	0.19292	0.07633	14	28	28
0.69757	0.80708	0.92367	14	29	29
0.69757	0.19292	0.92367	14	30	30
0.69757	0.80708	0.07633	14	31	31
0.06053	0.30706	0.07633	14	32	32
0.06053	0.69294	0.92367	14	33	33
0.06053	0.30706	0.92367	14	34	34
0.06053	0.69294	0.07633	14	35	35
0.66301	0.31816	0.00000	14	36	36
0.66301	0.68185	0.00000	14	37	37
0.81674	0.30459	0.11295	14	38	38
0.81674	0.69541	0.88705	14	39	39
0.81674	0.30459	0.88705	14	40	40
0.81674	0.69541	0.11295	14	41	41
0.44568	0.31096	0.07990	14	42	42
0.44568	0.68904	0.92010	14	43	43
0.44568	0.31096	0.92010	14	44	44
0.44568	0.68904	0.07990	14	45	45
0.20560	0.33635	0.10836	14	46	46
0.20560	0.66365	0.89164	14	47	47
0.20560	0.33635	0.89164	14	48	48
0.20560	0.66365	0.10836	14	49	49
0.51214	0.38767	0.00000	14	50	50
0.51214	0.61233	0.00000	14	51	51
0.25778	0.50000	0.16477	14	52	52
0.25778	0.50000	0.83523	14	53	53
0.26467	0.50000	0.05519	14	54	54
0.26467	0.50000	0.94481	14	55	55
0.39120	0.50000	0.11411	14	56	56
0.39120	0.50000	0.88589	14	57	57
0.75282	0.50000	0.00000	14	58	58
0.84591	0.50000	0.07668	14	59	59
0.84591	0.50000	0.92332	14	60	60
0.99722	0.50000	0.04837	14	61	61
0.99722	0.50000	0.95163	14	62	62

S9.3.3 Si.equi-II-3

$\rho = 0.5032 \text{ \AA}^{-2} = 3.253 \text{ ML}$, $E - E_{\text{bulk}} = 280 \text{ meV/at.}$

10.27433	-0.00034	0.00000			
-5.13746	8.89766	-0.00000			
0.00001	-0.00000	26.09222			
46 atoms					
0.33334	0.04309	0.27406	14	1	1
0.95693	0.29027	0.27407	14	2	2
0.70976	0.66667	0.27406	14	3	3
0.71884	0.05218	0.27250	14	4	4
0.33333	0.28116	0.27251	14	5	5
0.94782	0.66666	0.27251	14	6	6
0.95693	0.29027	0.02445	14	7	7
0.33334	0.04309	0.02445	14	8	8
0.70976	0.66667	0.02445	14	9	9
0.33333	0.28116	0.02601	14	10	10
0.71884	0.05218	0.02601	14	11	11
0.94782	0.66666	0.02601	14	12	12
0.54259	0.45614	0.07488	14	13	13
0.54385	0.08644	0.07488	14	14	14
0.91356	0.45741	0.07488	14	15	15
0.75311	0.87719	0.22364	14	16	16
0.12407	0.24689	0.22364	14	17	17
0.12280	0.87592	0.22363	14	18	18
0.00001	0.00000	0.10469	14	19	19
0.66667	0.33334	0.19382	14	20	20
0.54259	0.45614	0.22363	14	21	21
0.54386	0.08644	0.22364	14	22	22
0.91356	0.45741	0.22364	14	23	23
0.75311	0.87718	0.07488	14	24	24
0.12407	0.24689	0.07488	14	25	25
0.12281	0.87593	0.07488	14	26	26
0.00001	0.00000	0.19382	14	27	27
0.66667	0.33334	0.10469	14	28	28
0.46565	0.53450	0.14926	14	29	29
0.46550	0.93115	0.14926	14	30	30
0.06885	0.53434	0.14926	14	31	31
0.59782	0.79884	0.14926	14	32	32
0.20101	0.40218	0.14926	14	33	33
0.20117	0.79898	0.14926	14	34	34
0.10121	0.43454	0.34567	14	35	35
0.13149	0.66665	0.32727	14	36	36
0.33332	0.46483	0.32727	14	37	37
0.33333	0.89878	0.34565	14	38	38
0.56544	0.66667	0.34565	14	39	39
0.53517	0.86850	0.32727	14	40	40
0.10121	0.43454	0.95284	14	41	41
0.13150	0.66665	0.97125	14	42	42
0.33332	0.46483	0.97125	14	43	43
0.33333	0.89878	0.95286	14	44	44
0.56544	0.66667	0.95286	14	45	45
0.53517	0.86850	0.97125	14	46	46

S9.3.4 Si.iso-II-4 $\rho = 0.6056 \text{ \AA}^{-2} = 3.915 \text{ ML}$, $E - E_{\text{bulk}} = 232 \text{ meV/at.}$

10.62542	0.00000	0.00000				
0.00000	14.91779	0.00000				
0.00000	0.00000	34.35054				
96 atoms						
0.25000	0.51535	0.23141	14	1	1	
0.75000	0.48465	0.23141	14	2	2	
0.25000	0.11281	0.95396	14	3	3	
0.75000	0.88719	0.95396	14	4	4	
0.25000	0.12141	0.87777	14	5	5	
0.75000	0.87859	0.87777	14	6	6	
0.13684	0.63142	0.14602	14	7	7	
0.86316	0.36858	0.14602	14	8	8	
0.36316	0.63142	0.14602	14	9	9	
0.63684	0.36858	0.14602	14	10	10	
0.13684	0.86858	0.99724	14	11	11	
0.86316	0.13142	0.99724	14	12	12	
0.36316	0.86858	0.99724	14	13	13	
0.63684	0.13142	0.99724	14	14	14	
0.05522	0.56261	0.91432	14	15	15	
0.94478	0.43739	0.91432	14	16	16	
0.44478	0.56261	0.91432	14	17	17	
0.55522	0.43739	0.91432	14	18	18	
0.06192	0.56696	0.08724	14	19	19	
0.93808	0.43304	0.08724	14	20	20	
0.43808	0.56696	0.08724	14	21	21	
0.56192	0.43304	0.08724	14	22	22	
0.06162	0.56646	0.20451	14	23	23	
0.93838	0.43354	0.20451	14	24	24	
0.43838	0.56646	0.20451	14	25	25	
0.56162	0.43354	0.20451	14	26	26	
0.06764	0.71671	0.99726	14	27	27	
0.93236	0.28329	0.99726	14	28	28	
0.43236	0.71671	0.99726	14	29	29	
0.56764	0.28329	0.99726	14	30	30	
0.06763	0.78329	0.14600	14	31	31	
0.93237	0.21671	0.14600	14	32	32	
0.43237	0.78329	0.14600	14	33	33	
0.56763	0.21671	0.14600	14	34	34	
0.06161	0.93353	0.93876	14	35	35	
0.93839	0.06647	0.93876	14	36	36	
0.43839	0.93353	0.93876	14	37	37	
0.56161	0.06647	0.93876	14	38	38	
0.06191	0.93304	0.05602	14	39	39	
0.93809	0.06696	0.05602	14	40	40	

0.43809	0.93304	0.05602	14	41	41
0.56191	0.06696	0.05602	14	42	42
0.05523	0.93739	0.22893	14	43	43
0.94477	0.06261	0.22893	14	44	44
0.44477	0.93739	0.22893	14	45	45
0.55523	0.06261	0.22893	14	46	46
0.05633	0.31849	0.94166	14	47	47
0.94367	0.68151	0.94166	14	48	48
0.44367	0.31849	0.94166	14	49	49
0.55633	0.68151	0.94166	14	50	50
0.05362	0.31807	0.05335	14	51	51
0.94638	0.68193	0.05335	14	52	52
0.44638	0.31807	0.05335	14	53	53
0.55362	0.68193	0.05335	14	54	54
0.08304	0.32564	0.22620	14	55	55
0.91696	0.67436	0.22620	14	56	56
0.41696	0.32564	0.22620	14	57	57
0.58304	0.67436	0.22620	14	58	58
0.08305	0.17437	0.91707	14	59	59
0.91695	0.82563	0.91707	14	60	60
0.41695	0.17437	0.91707	14	61	61
0.58305	0.82563	0.91707	14	62	62
0.05362	0.18193	0.08991	14	63	63
0.94638	0.81807	0.08991	14	64	64
0.44638	0.18193	0.08991	14	65	65
0.55362	0.81807	0.08991	14	66	66
0.05633	0.18151	0.20160	14	67	67
0.94367	0.81849	0.20160	14	68	68
0.44367	0.18151	0.20160	14	69	69
0.55633	0.81849	0.20160	14	70	70
0.25000	0.38114	0.96221	14	71	71
0.75000	0.61886	0.96221	14	72	72
0.25000	0.37950	0.03194	14	73	73
0.75000	0.62050	0.03194	14	74	74
0.25000	0.38720	0.18930	14	75	75
0.75000	0.61280	0.18930	14	76	76
0.25000	0.37859	0.26550	14	77	77
0.75000	0.62141	0.26550	14	78	78
0.25000	0.53273	0.94144	14	79	79
0.75000	0.46727	0.94144	14	80	80
0.25000	0.53248	0.05212	14	81	81
0.75000	0.46752	0.05212	14	82	82
0.25000	0.62605	0.99685	14	83	83
0.75000	0.37395	0.99685	14	84	84
0.25000	0.87395	0.14640	14	85	85
0.75000	0.12605	0.14640	14	86	86
0.25000	0.12050	0.11132	14	87	87
0.75000	0.87950	0.11132	14	88	88
0.25000	0.11887	0.18105	14	89	89

0.75000	0.88113	0.18105	14	90	90
0.25000	0.98466	0.91187	14	91	91
0.75000	0.01534	0.91187	14	92	92
0.25000	0.96752	0.09113	14	93	93
0.75000	0.03248	0.09113	14	94	94
0.25000	0.96728	0.20182	14	95	95
0.75000	0.03272	0.20182	14	96	96

S9.3.5 Si.iso-II-5

$\rho = 0.8272 \text{ \AA}^{-2} = 5.347 \text{ ML}$, $E - E_{\text{bulk}} = 186 \text{ meV/at.}$

10.57224	0.00000	0.00000			
0.00000	14.86573	0.00000			
0.00000	0.00000	43.59367			
130 atoms					
0.25000	0.62159	0.21259	14	1	1
0.25000	0.62159	0.78741	14	2	2
0.75000	0.37841	0.78741	14	3	3
0.75000	0.37841	0.21259	14	4	4
0.25000	0.48433	0.18583	14	5	5
0.25000	0.48433	0.81417	14	6	6
0.75000	0.51567	0.81417	14	7	7
0.75000	0.51567	0.18583	14	8	8
0.25000	0.61260	0.15253	14	9	9
0.25000	0.61260	0.84747	14	10	10
0.75000	0.38740	0.84747	14	11	11
0.75000	0.38740	0.15253	14	12	12
0.25000	0.03275	0.83797	14	13	13
0.25000	0.03275	0.16203	14	14	14
0.75000	0.96725	0.16203	14	15	15
0.75000	0.96725	0.83797	14	16	16
0.63655	0.63102	0.11807	14	17	17
0.86345	0.63102	0.88193	14	18	18
0.13655	0.36898	0.88193	14	19	19
0.36345	0.36898	0.11807	14	20	20
0.36345	0.36898	0.88193	14	21	21
0.13655	0.36898	0.11807	14	22	22
0.86345	0.63102	0.11807	14	23	23
0.63655	0.63102	0.88193	14	24	24
0.63592	0.86935	0.00000	14	25	25
0.86408	0.86935	0.00000	14	26	26
0.13592	0.13065	0.00000	14	27	27
0.36408	0.13065	0.00000	14	28	28
0.58265	0.32544	0.18156	14	29	29
0.91735	0.32544	0.81844	14	30	30
0.08265	0.67456	0.81844	14	31	31
0.41735	0.67456	0.18156	14	32	32

0.41735	0.67456	0.81844	14	33	33
0.08265	0.67456	0.18156	14	34	34
0.91735	0.32544	0.18156	14	35	35
0.58265	0.32544	0.81844	14	36	36
0.56182	0.56654	0.16429	14	37	37
0.93818	0.56654	0.83571	14	38	38
0.06182	0.43346	0.83571	14	39	39
0.43818	0.43346	0.16429	14	40	40
0.43818	0.43346	0.83571	14	41	41
0.06182	0.43346	0.16429	14	42	42
0.93818	0.56654	0.16429	14	43	43
0.56182	0.56654	0.83571	14	44	44
0.55537	0.93719	0.18366	14	45	45
0.94463	0.93719	0.81634	14	46	46
0.05537	0.06281	0.81634	14	47	47
0.44462	0.06281	0.18366	14	48	48
0.44462	0.06281	0.81634	14	49	49
0.05537	0.06281	0.18366	14	50	50
0.94463	0.93719	0.18366	14	51	51
0.55537	0.93719	0.81634	14	52	52
0.56699	0.71656	0.00000	14	53	53
0.93301	0.71656	0.00000	14	54	54
0.06699	0.28344	0.00000	14	55	55
0.43301	0.28344	0.00000	14	56	56
0.56726	0.78317	0.11800	14	57	57
0.93274	0.78317	0.88200	14	58	58
0.06726	0.21683	0.88200	14	59	59
0.43274	0.21683	0.11800	14	60	60
0.43274	0.21683	0.88200	14	61	61
0.06726	0.21683	0.11800	14	62	62
0.93274	0.78317	0.11800	14	63	63
0.56726	0.78317	0.88200	14	64	64
0.56200	0.93286	0.04673	14	65	65
0.93800	0.93286	0.95327	14	66	66
0.06200	0.06714	0.95327	14	67	67
0.43800	0.06714	0.04673	14	68	68
0.43800	0.06714	0.95327	14	69	69
0.06200	0.06714	0.04673	14	70	70
0.93800	0.93286	0.04673	14	71	71
0.56200	0.93286	0.95327	14	72	72
0.56201	0.56710	0.07162	14	73	73
0.93799	0.56710	0.92838	14	74	74
0.06201	0.43290	0.92838	14	75	75
0.43799	0.43290	0.07162	14	76	76
0.43799	0.43290	0.92838	14	77	77
0.06201	0.43290	0.07162	14	78	78
0.93799	0.56710	0.07162	14	79	79
0.56201	0.56710	0.92838	14	80	80
0.55344	0.18209	0.07366	14	81	81
0.94656	0.18209	0.92634	14	82	82

0.05344	0.81791	0.92634	14	83	83
0.44656	0.81791	0.07366	14	84	84
0.44656	0.81791	0.92634	14	85	85
0.05344	0.81791	0.07366	14	86	86
0.94656	0.18209	0.07366	14	87	87
0.55344	0.18209	0.92634	14	88	88
0.55322	0.31790	0.04458	14	89	89
0.94678	0.31790	0.95542	14	90	90
0.05322	0.68210	0.95542	14	91	91
0.44678	0.68210	0.04458	14	92	92
0.44678	0.68210	0.95542	14	93	93
0.05322	0.68210	0.04458	14	94	94
0.94678	0.31790	0.04458	14	95	95
0.55322	0.31790	0.95542	14	96	96
0.55621	0.18155	0.16191	14	97	97
0.94379	0.18155	0.83809	14	98	98
0.05621	0.81845	0.83809	14	99	99
0.44379	0.81845	0.16191	14	100	100
0.44379	0.81845	0.83809	14	101	101
0.05621	0.81845	0.16191	14	102	102
0.94379	0.18155	0.16191	14	103	103
0.55621	0.18155	0.83809	14	104	104
0.25000	0.88108	0.14556	14	105	105
0.25000	0.88108	0.85444	14	106	106
0.75000	0.11892	0.85444	14	107	107
0.75000	0.11892	0.14556	14	108	108
0.25000	0.12585	0.11829	14	109	109
0.25000	0.12585	0.88170	14	110	110
0.75000	0.87415	0.88170	14	111	111
0.75000	0.87415	0.11829	14	112	112
0.25000	0.87951	0.09067	14	113	113
0.25000	0.87951	0.90933	14	114	114
0.75000	0.12049	0.90933	14	115	115
0.75000	0.12049	0.09067	14	116	116
0.25000	0.03268	0.07463	14	117	117
0.25000	0.03268	0.92537	14	118	118
0.75000	0.96732	0.92537	14	119	119
0.75000	0.96732	0.07463	14	120	120
0.25000	0.46758	0.04376	14	121	121
0.25000	0.46758	0.95624	14	122	122
0.75000	0.53243	0.95624	14	123	123
0.75000	0.53243	0.04376	14	124	124
0.25000	0.62067	0.02753	14	125	125
0.25000	0.62067	0.97247	14	126	126
0.75000	0.37933	0.97247	14	127	127
0.75000	0.37933	0.02753	14	128	128
0.25000	0.37468	0.00000	14	129	129
0.75000	0.62532	0.00000	14	130	130

S9.4 Ge-Clathrate/InN

S9.4.1 Thinner Ge Clathrate Film on InN (initial configuration)

See Figure S6.2.

10.89643	0.00000	-0.00000				
-5.44821	9.43658	0.00000				
0.00000	0.00000	26.29850				
95 atoms						
0.26262	0.13131	0.17022	32	1	1	
0.86869	0.13131	0.17022	32	2	2	
0.86869	0.73738	0.17022	32	3	3	
0.66667	0.33333	0.21704	32	4	4	
0.33333	0.66667	0.21710	32	5	5	
0.41997	0.20999	0.24593	32	6	6	
0.79002	0.20999	0.24593	32	7	7	
0.79002	0.58003	0.24593	32	8	8	
0.20999	0.41997	0.24594	32	9	9	
0.20999	0.79002	0.24594	32	10	10	
0.58003	0.79002	0.24594	32	11	11	
0.39163	0.99998	0.28812	32	12	12	
0.39163	0.39165	0.28812	32	13	13	
0.60835	0.99998	0.28812	32	14	14	
0.60835	0.60837	0.28812	32	15	15	
0.00002	0.39165	0.28812	32	16	16	
0.00002	0.60837	0.28812	32	17	17	
0.00052	0.38429	0.04618	32	18	18	
0.00052	0.61623	0.04618	32	19	19	
0.38377	0.38429	0.04618	32	20	20	
0.38377	0.99948	0.04618	32	21	21	
0.61571	0.61623	0.04618	32	22	22	
0.61571	0.99948	0.04618	32	23	23	
0.41845	0.20923	0.09415	32	24	24	
0.79077	0.20923	0.09415	32	25	25	
0.79077	0.58155	0.09415	32	26	26	
0.20914	0.41829	0.09469	32	27	27	
0.20914	0.79086	0.09469	32	28	28	
0.58171	0.79086	0.09469	32	29	29	
0.66667	0.33333	0.12381	32	30	30	
0.33333	0.66667	0.12389	32	31	31	
0.13090	0.26180	0.17048	32	32	32	
0.13090	0.86910	0.17048	32	33	33	
0.73820	0.86910	0.17048	32	34	34	
-0.77000	0.00000	0.35200	32	35	35	
-0.76077	0.23947	0.35200	32	36	36	
-0.23989	0.76044	0.35200	32	37	37	
-0.23989	0.00000	0.35200	32	38	38	

-0.03003	0.76052	0.35200	32	39	39
-0.03003	0.23956	0.35200	32	40	40
0.00000	0.00000	0.30200	32	41	41
0.66667	0.33333	0.73784	49	42	42
0.33333	0.66667	0.73561	49	43	43
0.00000	0.00000	0.73969	49	44	44
0.00385	0.33274	0.72373	49	45	45
0.00385	0.67111	0.72373	49	46	46
0.32889	0.33274	0.72373	49	47	47
0.32889	0.99615	0.72373	49	48	48
0.66726	0.67111	0.72373	49	49	49
0.66726	0.99615	0.72373	49	50	50
0.43857	0.21928	0.83677	49	51	51
0.78072	0.21928	0.83677	49	52	52
0.78072	0.56143	0.83677	49	53	53
0.11075	0.22151	0.84237	49	54	54
0.11075	0.88925	0.84237	49	55	55
0.77850	0.88925	0.84237	49	56	56
0.11170	0.55585	0.83822	49	57	57
0.44415	0.55585	0.83822	49	58	58
0.44415	0.88830	0.83822	49	59	59
0.56097	0.12193	0.94440	49	60	60
0.56097	0.43903	0.94440	49	61	61
0.87807	0.43903	0.94440	49	62	62
0.22710	0.45421	0.95022	49	63	63
0.22710	0.77290	0.95022	49	64	64
0.54580	0.77290	0.95022	49	65	65
0.21562	0.10781	0.95497	49	66	66
0.89219	0.10781	0.95497	49	67	67
0.89219	0.78438	0.95497	49	68	68
0.11198	0.22396	0.75643	7	69	69
0.11198	0.88802	0.75643	7	70	70
0.77604	0.88802	0.75643	7	71	71
0.43990	0.21995	0.75028	7	72	72
0.78005	0.21995	0.75028	7	73	73
0.78005	0.56010	0.75028	7	74	74
0.10927	0.55463	0.75192	7	75	75
0.44537	0.55463	0.75192	7	76	76
0.44537	0.89073	0.75192	7	77	77
0.55592	0.11184	0.86040	7	78	78
0.55592	0.44408	0.86040	7	79	79
0.88816	0.44408	0.86040	7	80	80
0.22427	0.11213	0.86930	7	81	81
0.88787	0.11213	0.86930	7	82	82
0.88787	0.77573	0.86930	7	83	83
0.22254	0.44508	0.86554	7	84	84
0.22254	0.77746	0.86554	7	85	85
0.55492	0.77746	0.86554	7	86	86
0.33884	0.00024	0.97522	7	87	87

0.33884	0.33860	0.97522	7	88	88
0.66140	0.00024	0.97522	7	89	89
0.66140	0.66116	0.97522	7	90	90
0.99976	0.33860	0.97522	7	91	91
0.99976	0.66116	0.97522	7	92	92
0.00000	0.00000	0.98093	7	93	93
0.66667	0.33333	0.97516	7	94	94
0.33333	0.66667	0.98001	7	95	95

S9.4.2 Thicker Ge Clathrate Film on InN (initial configuration)

See Figure S6.6.

10.89643	0.00000	-0.00000				
-5.44821	9.43658	0.00000				
0.00000	0.00000	50.00000				
129 atoms						
1.00700	1.00700	0.36991	32	1	1	
0.34644	0.06187	0.16999	32	2	2	
-0.04787	0.29157	0.16999	32	3	3	
-0.27757	-0.33244	0.16999	32	4	4	
-0.27757	0.06187	0.16999	32	5	5	
0.34644	0.29157	0.16999	32	6	6	
-0.04787	-0.33244	0.16999	32	7	7	
-0.04176	0.28546	0.03126	32	8	8	
0.33423	0.05576	0.03126	32	9	9	
-0.27146	-0.32023	0.03126	32	10	10	
0.33423	0.28546	0.03126	32	11	11	
-0.27146	0.05576	0.03126	32	12	12	
-0.04176	-0.32023	0.03126	32	13	13	
-0.37510	-0.38120	0.21851	32	14	14	
0.00089	0.38910	0.21851	32	15	15	
0.39520	0.01311	0.21851	32	16	16	
0.00089	-0.38120	0.21851	32	17	17	
0.39520	0.38910	0.21851	32	18	18	
-0.37510	0.01311	0.21851	32	19	19	
-0.45167	0.46567	0.05657	32	20	20	
-0.45167	0.08966	0.05657	32	21	21	
-0.07566	0.46567	0.05657	32	22	22	
0.21500	-0.20100	0.24382	32	23	23	
0.21500	0.42299	0.24382	32	24	24	
-0.40899	-0.20100	0.24382	32	25	25	
-0.24367	-0.11834	0.14468	32	26	26	
0.13234	0.25767	0.14468	32	27	27	
0.13234	-0.11834	0.14468	32	28	28	
0.00700	0.00700	0.07722	32	29	29	
-0.32633	0.34033	0.26447	32	30	30	

-0.32633	0.34033	0.12403	32	31	31
-0.44907	0.46307	0.14127	32	32	32
-0.44907	0.09486	0.14127	32	33	33
-0.08086	0.46307	0.14127	32	34	34
-0.23847	-0.11574	0.05998	32	35	35
0.12974	0.25247	0.05998	32	36	36
0.12974	-0.11574	0.05998	32	37	37
0.42819	0.21760	0.24723	32	38	38
-0.20360	-0.41419	0.24723	32	39	39
-0.20360	0.21760	0.24723	32	40	40
0.00700	0.00700	0.12893	32	41	41
-0.32633	0.34033	0.07232	32	42	42
0.34033	-0.32633	0.25957	32	43	43
0.47177	-0.45777	0.09958	32	44	44
0.47177	-0.06346	0.09958	32	45	45
0.07746	-0.45777	0.09958	32	46	46
0.13844	-0.12444	0.28683	32	47	47
0.13844	0.26987	0.28683	32	48	48
-0.25587	-0.12444	0.28683	32	49	49
-0.39679	-0.19490	0.10167	32	50	50
0.20890	0.41079	0.10167	32	51	51
0.20890	-0.19490	0.10167	32	52	52
0.01311	0.39520	0.35723	32	53	53
-0.38120	-0.37510	0.35723	32	54	54
0.38910	0.00089	0.35723	32	55	55
0.38910	0.39520	0.35723	32	56	56
0.01311	-0.37510	0.35723	32	57	57
-0.38120	0.00089	0.35723	32	58	58
0.42299	0.21500	0.33193	32	59	59
-0.20100	-0.40899	0.33193	32	60	60
-0.20100	0.21500	0.33193	32	61	61
0.34033	-0.32633	0.31128	32	62	62
0.21760	-0.20360	0.32852	32	63	63
0.21760	0.42819	0.32852	32	64	64
-0.41419	-0.20360	0.32852	32	65	65
-0.32633	0.34033	0.31618	32	66	66
0.26987	0.13844	0.28892	32	67	67
-0.12444	-0.25587	0.28892	32	68	68
-0.12444	0.13844	0.28892	32	69	69
0.76744	1.76743	0.39949	32	70	70
0.76744	1.00700	0.39949	32	71	71
1.00700	1.76743	0.39949	32	72	72
1.00700	1.24656	0.39949	32	73	73
0.24656	1.00700	0.39949	32	74	74
0.24656	1.24656	0.39949	32	75	75
0.66667	0.33333	-0.13789	49	76	76
0.33333	0.66667	-0.13906	49	77	77
0.00000	0.00000	-0.13692	49	78	78
0.00385	0.33274	-0.14531	49	79	79
0.00385	0.67111	-0.14531	49	80	80

0.32889	0.33274	-0.14531	49	81	81
0.32889	0.99615	-0.14531	49	82	82
0.66726	0.67111	-0.14531	49	83	83
0.66726	0.99615	-0.14531	49	84	84
0.43857	0.21928	-0.08586	49	85	85
0.78072	0.21928	-0.08586	49	86	86
0.78072	0.56143	-0.08586	49	87	87
0.11075	0.22151	-0.08291	49	88	88
0.11075	0.88925	-0.08291	49	89	89
0.77850	0.88925	-0.08291	49	90	90
0.11170	0.55585	-0.08509	49	91	91
0.44415	0.55585	-0.08509	49	92	92
0.44415	0.88830	-0.08509	49	93	93
0.56097	0.12193	-0.02925	49	94	94
0.56097	0.43903	-0.02925	49	95	95
0.87807	0.43903	-0.02925	49	96	96
0.22710	0.45421	-0.02618	49	97	97
0.22710	0.77290	-0.02618	49	98	98
0.54580	0.77290	-0.02618	49	99	99
0.21562	0.10781	-0.02368	49	100	100
0.89219	0.10781	-0.02368	49	101	101
0.89219	0.78438	-0.02368	49	102	102
0.11198	0.22396	-0.12811	7	103	103
0.11198	0.88802	-0.12811	7	104	104
0.77604	0.88802	-0.12811	7	105	105
0.43990	0.21995	-0.13134	7	106	106
0.78005	0.21995	-0.13134	7	107	107
0.78005	0.56010	-0.13134	7	108	108
0.10927	0.55463	-0.13049	7	109	109
0.44537	0.55463	-0.13049	7	110	110
0.44537	0.89073	-0.13049	7	111	111
0.55592	0.11184	-0.07343	7	112	112
0.55592	0.44408	-0.07343	7	113	113
0.88816	0.44408	-0.07343	7	114	114
0.22427	0.11213	-0.06875	7	115	115
0.88787	0.11213	-0.06875	7	116	116
0.88787	0.77573	-0.06875	7	117	117
0.22254	0.44508	-0.07072	7	118	118
0.22254	0.77746	-0.07072	7	119	119
0.55492	0.77746	-0.07072	7	120	120
0.33884	0.00024	-0.01303	7	121	121
0.33884	0.33860	-0.01303	7	122	122
0.66140	0.00024	-0.01303	7	123	123
0.66140	0.66116	-0.01303	7	124	124
0.99976	0.33860	-0.01303	7	125	125
0.99976	0.66116	-0.01303	7	126	126
0.00000	0.00000	-0.01003	7	127	127
0.66667	0.33333	-0.01307	7	128	128
0.33333	0.66667	-0.01051	7	129	129